ROLE OF AMMONIA IN THE ACTIVATION

OF METHANOL DEHYDROGENASE/CYTOCHROME C_L

ENZYME

by

Ancy Kunjumon, B. Tech.

A Dissertation Presented in Partial Fulfillment
of the Requirements for the Degree
Doctor of Philosophy

COLLEGE OF ENGINEERING AND SCIENCE
LOUISIANA TECH UNIVERSITY

November 2011

LOUISIANA TECH UNIVERSITY

THE GRADUATE SCHOOL

09/27/2011
_____
Date

We hereby recommend that the thesis prepared under our supervision

by Ancy Kunjumon
_____

entitled_____

Role of Ammonia in the Activation of

Methanol Dehydrogenase/Cytochrome cL Enzyme

_____

_____

be accepted in partial fulfillment of the requirements for the Degree of

Doctor of Philosophy
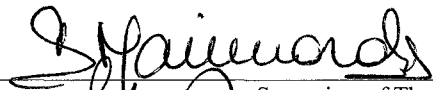
_____
Supervisor of Thesis Research
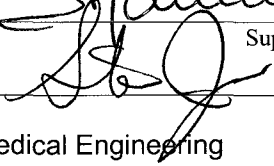
_____
Head of Department

Biomedical Engineering
_____
Department

Recommendation concurred in:
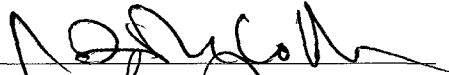
Advisory Committee

Approved:
_____
Director of Graduate Studies

_____
Dean of the College

Approved:
_____
Dean of the Graduate School
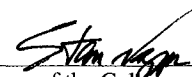
ABSTRACT

Recent advancement in enzyme catalysis has opened ways to design efficient bio-catalysts, bio-sensors and bio-fuel cells. An in-depth knowledge about the mechanism of the reaction taking place within the enzymes is of great importance to achieve these goals. In this dissertation, various computation methods are applied to investigate the mechanism behind enzyme catalysis in the presence of compounds called activators.

Methanol dehydrogenase (MDH) is a well-known bio-catalyst that can oxidize excess of methanol from the environment to formaldehyde. The enzyme works well within the bacterial environment, but under *in vitro*, it loses activity. Ammonia is used as an activator to restore the activity of MDH. The Monte Carlo search using simulated annealing metaheuristic method is conducted to explore the binding of MDH with its natural electron acceptor Cytochrome c_L in varying concentration of ammonia. The main aim behind this is to explore the interaction energy between the enzymes under the influence of its activator. The concentration of ammonia is varied from 0 to 5 ammonia molecules.

Moving deeper into the active site of MDH, molecular mechanics and dynamics calculations were performed to investigate the position and effect of ammonia in the active site amino acids of MDH. The concentration of ammonia was varied from 0 to 55.39 mM. It was proposed that ammonia may form a complex conjugate with the cofactor of MDH (Pyrroloquinoline quinone) to assist in the oxidation of methanol. Two

of the most debated methanol oxidation mechanisms, Addition-Elimination reaction and Hydride-Transfer mechanism, were used to investigate the role of ammonia in the oxidation of methanol. Density functional theory (DFT) was applied to explore the methanol oxidation mechanism in the presence of ammonia. Models of varying size that best represent the active site of MDH were tested for this purpose.

The interaction energy obtained after the docking of MDH and Cytochrome c_L (C_L) indicate that the presence of a single ammonia molecule increased the binding between the enzymes by 108.50 kcal/mol. The presence of ammonia at the active site of MDH affected the diffusivity of various components of the active site, such as the Ca^{2+} ion, Glu177, Asn261 and probable catalytic base Asp303. Rise in the concentration of ammonia increased the diffusivity coefficient of active site components. At ammonia concentration of 20 mM to 35 mM, the distance among Pyrroloquinoline quinine (PQQ), Ca^{2+} and Asp303 decreased, which assisted in the oxidation of methanol. Excess of ammonia caused instability in the amino acids of the active site and increased the distance between the cofactor and Asp303, thereby reducing the affinity of MDH towards methanol.

Based on the transition states obtained, it is observed that ammonia does not form any complex with PQQ of MDH during the oxidation mechanism. Instead, ammonia assisted in the re-oxidation of PQQ by abstracting a proton from the reduced form of PQQ ($PQQH_2$). Re-oxidation of PQQ was important as it allowed the oxidation of subsequent methanol molecule, thus increasing the activity and efficiency of the enzyme. The free energy barriers of the rate determining step indicated that the ammonia reduced the activation energy involved in the dissociation of the methanol molecule by 6.2

kcal/mol in the case of Addition-Elimination reaction and 6.8 kcal/mol in the case of

Hydride-Transfer mechanism.

APPROVAL FOR SCHOLARLY DISSEMINATION

The author grants to the Prescott Memorial Library of Louisiana Tech University the right to reproduce, by appropriate methods upon request any or all portions of this Thesis It is understood that "proper request" consists of the agreement on the part of the requesting party, that said reproduction is for his personal use and that subsequent reproduction will not occur without written approval of the author of this Thesis Further, any portions of the Thesis used in books papers and other works must be appropriately referenced to this Thesis

Finally, the author of this Thesis reserves the right to publish freely, in the literature, at any time, any or all portions of this Thesis

Author _____

Date _____ 11 / 02 / 20 11 _____

DEDICATION

I dedicate this work to my dear parents Thankamony Kunjumon (Mother), Kunjumon Kochukoshy (Father) and my husband Kiran Joseph Kuncheria for their immense support and encouragement. Above all I thank God Almighty for giving me privilege and strength in my endeavors.

TABL E OF CONTENTS

LIST OF TABLES

LIST OF FIGURES

ACKNOWLEDGMENTS

When I take this opportunity to relish the fruit of all my endeavors, I would stand with a grateful heart at the feet of God almighty. During my time in Louisiana Tech University, many people have imparted their support in building my professional life. First of all, I would like to thank my advisor Dr. Daniela Mainardi for instilling in me the qualities of being a good researcher and guiding me through the project. Her enthusiasm and expert advice have been the major driving force for completion of this project. I want to thank Dr. Mark A. DeCoster for being on my dissertation committee and giving me a privilege to be associated with his project. Dr. Steven A. Jones who is the member of my dissertation committee has been the instructor of several courses and I extend my thanks for providing me with immense support in my project. I would like to thank Dr. Ramu Ramachandran and Dr. June Feng for being a part of my dissertation committee and teaching me various computational and experimental techniques involved in my project.

I want to thank my colleagues Dr. Phani Dathar, Fernando Soto, Purnima Khal and all my group members for the support they have lent me over all these years. I also express my gratitude to Dr. Tom J. John and Dr. Bobby Mathew for supporting me in various stages of my research. Finally, I would like to conclude this section by thanking my dear husband Mr. Kiran Joseph for providing me with whole-hearted support during the entire course of my research.

CHAPTER 1

INTRODUCTION

1.1   Enzymes as Biocatalyst

Enzymes are remarkable proteins that have catalytic properties for transforming various sets of substrates to specific products [1]. They catalyze the inter conversion of a vast number of molecules ranging from the fixing of nitrogen from the atmosphere to the building of large and complex atomic structures. These catalysts are highly energy efficient and environment friendly [2]. It is this nature of the enzyme that has guided to great advancements in the biocatalyst research. Enzymes are highly chemo-selective and stereo-specific catalysts. The rate of reaction varies from as slow as one catalytic reaction per minute to 10^5 in a second. The variability in enzymes has led to the investigation of structural and functional properties of enzymes in chemical synthesis [1].

The first couple of enzymes were discovered by Payen, Persoz and Schwann in 1830's. Payen and Persoz discovered diastase that breaks starch to maltose, and Schwann explored pepsin that splits the big proteins to smaller peptide molecules [3]. By the 1920's, many of the known enzymes were discovered, but it was only in the 1960's and 70's the enzymes were used for commercial applications. The use of enzymes started off in food processing industries with the use of carbohydrate processing enzymes in corn, potato and other carbohydrates. Later, the enzymes were used in textile industry. With the

development of deoxyribonucleic acid (DNA) recombinant and enzyme immobilization techniques, enzymes were used as biocatalyst, biosensors, biomedical devices and implants [3].

In the past couple of decades, scientists have been investigating the mechanism behind various enzyme catalysis reactions. One of the most common methods is the protein-engineering-based, site-directed mutagenesis approach. Researchers have obtained a great deal of understanding on the mechanism behind enzyme catalysis using this method. Understanding the mechanism behind enzyme catalysis is of great significance, as it can be used to increase the activity of the enzyme, or to develop enzyme variants with modified physical and chemical properties to suit the required application [4]. Developments in molecular genetics techniques have enabled researchers to alter the metabolic or biosynthetic pathways in enzymes. These methods have allowed the production of primary and secondary metabolites which include aromatic compounds, antibiotics, non-ribosomal peptides, etc. [4].

Unlike conventional chemical catalyst, enzymes produce few by-products. These features have led to the use of enzymes in various fields such as biomedical, chemical industries, food, and pharmaceuticals [5].

1.1.1   Applications of Biocatalysts

Enzymes can be used for developing bio-selective electrodes or biosensors in combination with suitable mediators. These mediators are enzyme-based biocatalysts. The biocatalysts can convert the substrate to be measured to another compound or ion that can be sensed by the electrodes. For example, for the detection of glutamate, enzymes from squash plant tissues are used as biocatalysts to reduce glutamate to CO_2

and other compounds. This CO_2 can be measured using a gas sensor, which in turn gives the concentration of glutamate in the sample [6].

Enzymes can be reacted with imaging compounds such as fluorophores to alter their physical property and increase quantum yield. This further helps in improving analytical sensitivity and obtaining high temporal and spatial sampling capability. They have proved to be of great advantage in enzyme linked immune assays such as Enzyme-linked immunosorbent assay (ELISA), testing of cell viability, and the detection of DNA and ribonucleic acid (RNA). Highly sensitive requirements of *in vivo* imaging techniques make use of fluorophoric probes for detection and visualization of various bio-molecules [7]. Enzymes such as Lipases are excellent biocatalysts for the synthesis of chiral compounds, such as, nikkomycin-B, non-steroidal drugs such as naproxen, ibuprofen, suprofen and ketoprofen, anti-viral agent lamivudine, etc. which are of great importance in the biomedical industry. In addition to this, they are also used for the production of anti-tumor drugs, alkaloids, and antibiotics [8].

Some enzymes and proteins present in the surface of the cell or bacterial membranes act as tools to display other recombinant enzymes and are called auto-transporter enzymes. This can be of great advantage for the development of whole cell biocatalysis or bioremediation, vaccination or virus inactivation. For example, the display of heme-containing P450 enzymes are of great medical importance as they synthesize various bio-chemical compounds, which can be used for degradation of toxic compounds present within the human body. Hence, they can be used for enzyme coated applications for P450 mediated drug metabolism studies [9].

Biocatalysts have found great application in the continuous resolution process of bio-transformations. The pH at which the reaction takes place is neither too acidic nor too

basic. The enzymes can be recycled, hence providing maximum utility. Cross-linked enzyme crystals of laccase have been tested to induce biotransformation of pyrogallol to purpurogallin, which is a compound with high antioxidant property. It also has anti-bacterial activity against gram positive bacteria and hence is an important compound in the pharmaceutical industry [10-11]. Extensive research is being done in various countries on fuel cells with enzymes as catalysts instead of transition metal. They are termed as bio-fuel cells and have some advantages over regular fuel cells. Enzymes oxidize alcohols at low over potential and do not release harmful gases such as carbon monoxide. In addition to that, they can be operated at low temperatures [12]. However, there are some limitations with bio-fuel cells. The power produced by them is limited to run small applications such as mobile phones. Researchers are looking for ways to amplify the power produced by bio-fuel cells to run bigger applications.

1.1.2   Stabilization and Activation of Free Enzymes

Earlier, the enzymes present in the cell surface had greater benefits as they were freely available for reactions with substrates, binding with its electron acceptors, or studying cross-linking properties. They display great stability when they are connected to a matrix compared to when they are free molecules. Under normal conditions, the enzymes are present with the cell which acts as a natural matrix and hence are chemically stable [9].

With the improvement in recycling and immobilization techniques, the use of free enzymes proved to be of better advantage. Free enzymes can be recycled to increase the utility and decrease the cost of the catalysis process. In the case of microorganisms, the population may vary with time, thereby effecting the concentration of enzymes used in

the bio-catalytic process. This issue of fluctuating enzyme concentration can be eliminated by the use of free enzymes [10].

Scientists are developing multiphase bioconversion technology with the focus on biocatalyst. With the help of catalyst engineering and gene-shuffling techniques, the yield, selectivity and stability of free enzymes can be increased so that they will be functional in both aqueous and non-aqueous mediums. Increase in enzyme activity and stability will help in the development of nanomaterials to be used in proteomics, functional genomics and micro-fluidic biocatalysts. It will also help in the advancement of miniaturized bio-devices for screening certain unknown compounds [5].

The stability of the enzymes can also be achieved by immobilizing them using various techniques. The two ways by which immobilization of enzymes are carried out are physical and chemical. Physical methods involve the capture of enzymes in natural or synthetic gel matrices such as alginates, κ-carrageenan and polyacrylaminde gel. In the case of chemical methods, the enzymes are cross-linked or covalently bound to a chemically inert material [10].

Though many stabilization techniques have been developed in the past, many of the enzymes display less or no catalytic activity under *in vitro* conditions. Extensive study is being done in the biocatalyst process design to make the enzymes functional under *in vitro* conditions [1]. There are a few enzymes that have similar activity both *in vivo* and *in vitro*. On the other hand, many of the enzymes get deactivated once they are taken out of the bacteria or cell.

In the past few years, there is growing interest in enzyme activation assays, where the presence of certain compounds called 'activators' can turn on the activity of the enzymes. These molecules can take the role of ligands that can replace biological ligands

to enhance enzymatic activity [13]. The association between the activator and enzymes is very complex. It is possible that there can be a specific requirement by the active site of the enzyme which is compensated by the activator ions. Recent developments have shown that the addition of kosmotropic salts can stabilize and preserve the folded structures of the enzymes. This has led to higher enzymatic activity outside the cell environment. Activation of enzymes has also been obtained by adding crown ethers, transition state analogs, substrates or substrate mimics [5].

In this work the activation of Methanol dehydrogenase/Cytochrome c_L complex using ammonia is investigated. This particular enzyme oxidizes methanol to formaldehyde. The structure and function of these enzymes will be explained in detail in the subsequent sections. As in the case of many enzymes, Methanol dehydrogenase (MDH) functions normally when it is inside the bacteria, but it loses its activity once it is removed from the cell body. It regains activity once small concentration of ammonia is added to the free enzymes [14].

1.2   Brief Overview of Following Chapters

In Chapter 2, the purpose of this research and a detailed description of the enzymes MDH and Cytochrome c_L (C_L) will be given. The present knowledge about the effect of ammonia in MDH will also be discussed. Chapter 3 deals with the theory behind the computational methods used in this research.

In Chapter 4, the interaction of MDH and C_L is investigated in the presence of ammonia. In Section 4.4.2, effect of ammonia in the active site of MDH is presented. In Chapters 5 and 6, the oxidation of methanol is investigated in the presence of ammonia. The two most debated methanol oxidation mechanisms in MDH are Addition-Elimination

and Hydride-Transfer reaction. The role ammonia is explored based on these two mechanisms. Finally, the results will be concluded in Chapter 7 and recommendations for future work will be discussed.

CHAPTER 2

OBJECTIVE AND LITERATURE REVIEW

2.1   Research Objective

Methane is one of the highly potent greenhouse gases. Though the concentration of methane is less than carbon dioxide, it is ten times more effective in absorbing and re-radiating infrared energy. Technological developments and urbanization have resulted in an increase in production, resource consumption and intensity of waste production and emission in the form of methane [15]. A large amount of methane reaches the atmosphere through the plant vascular system, especially from the rice fields. Due to growth in human population, demand for the production of rice has increased and the climate soil characteristics and growth methods have further increased the level and intensity of methane production [15].

The soil of rice fields contains methylotrophic bacteria that contain an enzyme called Methane mono-oxygenase (MMO). It converts atmospheric methane to methanol. MMO coexists with various other enzymes such as Methanol dehydrogenase (MDH), Cytochrome c_L (C_L), etc. The methanol released by MMO is further oxidized to formaldehyde by MDH. The formaldehyde is further reduced to simpler compounds and gets assimilated in the soil. The production of methanol by MMO is much more than the

oxidation of methanol to formaldehyde. This increases the concentration of methanol in the soil and changes its chemistry [16].

The main objective of this research is to explore the effect of ammonia on MDH surface and the active site. Apart from that, the mechanism of oxidation of methanol by MDH in the presence of ammonia is also explored. By investigating the mechanism of activation of the MDH enzyme, artificial biocatalysts can be designed to obtain higher activity and overcome environmental damage caused by human practices.

It is known that MDH is activated by ammonia for oxidation of methanol and the rate of oxidation depends on the concentration of ammonia [14]. Therefore, stability of the enzyme at varying concentrations of ammonia is also inspected. This application can be applied for the development of micro bio-sensors, which can be used to detect ammonia concentration during hyperammonemic syndrome caused due to an excess of concentration of ammonia in the human blood [17].

The MDH enzyme can also act as anodic catalyst in a bio-fuel cell. A bio-catalytic fuel cell that uses a bacterial MDH enzyme immobilized on N,N,N',N'-tetramethyl-p-phenylenediamine (TPMD)-functionalized carbon paste electrode as the anodic catalyst. It can produce a continuous power output of 0.25 mW/cm^2 for 30 days [18]. Efficiently using ammonia to increase the activity of the enzyme can help in increasing the output of MDH based bio-fuel cells.

2.2 Methanol Dehydrogenase Enzyme

MDH is an enzyme that oxidizes methanol to formaldehyde. In nature, methanol is formed by the degradation of methyl esters and ethers found in pectin and lignin of plant components. Methylotrophic microorganisms grow on methanol and oxidize them

through special metabolic pathways. In the process, it generates energy and forms compounds with carbon-carbon bonds. Methylotrophic microorganisms that contain MDH include both Gram-negative and Gram-positive bacteria. Since most of the fast growing microorganisms come under Gram-negative bacteria, it is widely used for isolation techniques [19].

Some of the bacteria used for isolation of MDH are *Hyphomicrobium X, Methylophilus methylotrophus, Methylobacterium extorquens,* etc. [20-21]. One of the most extensively studied bacteria is *Methylobacterium extorquens.* Some of the main reasons for using this bacterium are the simple and inexpensive requirements for its cultivation, availability of high-cell-density fermentation protocols and presence of known genome sequence and genetic tools for its study. In fact, the *Methylobacterium* species naturally produces components such as vitamin B12, Pyrroloquinoline quinine, and carotids, which are of commercial importance [22]. The X-Ray crystallographic structure of MDH from *Methylobacterium extorquens* is well described by Gosh et al. and updated by Williams et al. at a resolution of 1.2 Å [23-24]. *M. extorquens* grows on single carbon compounds such as methanol, methylamine and formulate along with multicarbon compounds such as pyruvate and succinate [21].

MDH is soluble quinoprotein, which is found in the periplasm of the methylotrophic bacteria. It was the first quinoprotein containing enzyme whose structure was determined using X-Ray crystallographic method (Fig. 2.1). The basic structure of the enzyme is in the form of $\alpha_2\beta_2$ tetramer [25]. The α subunit is the bigger unit with 66 kDa, and the smaller β subunit has a weight of 8 kDa; α subunit is shaped in the form of propeller fold composed of four stranded eight β sheets. It is arranged about an eightfold pseudo symmetric axis. The structure is stabilized due to the presence of tryptophan

residues at regular intervals. Tryptophan residues from one of the β sheets form

hydrophobic and polar interactions with amino acids present in the adjacent β sheet. The

smaller β subunit consists of α helical structure that partially covers a part of α subunit

[24].

Figure 2.1: Structure of MDH obtained from protein data bank (call no 1w6s) [23-24].

In the entire enzyme structure there is a small part of the enzyme where the actual

reaction takes place called the active site. In the case of MDH, the active site is located in

the inner compartment of the α subunit. Some of the amino acids present at the surface of

α subunit form a funnel shaped depression. These residues are hydrophobic in nature and

are listed as follows: 100-AVACCDL; 420-PFMLP; 430-FFV; 540-WPGVGLVFDLA;

551-DPTAGL [23].

2.2.1   Active Site of MDH

The active site of MDH (Fig. 2.2 a) and b)) consists of the prosthetic group Pyrroloquinoline quinine (PQQ), Ca^{2+} ion, Asp303 and 12 other amino acids surrounding the PQQ. The active site was stabilized by the tryptophan residue (Trp243) at the bottom and a disulphide bridge on the top. The protein structure keeps the Ca^{2+} ion coordinated to PQQ and neighboring amino acids. PQQ is also known as methoxatin. It acts as a cofactor for the oxidation mechanism of methanol.
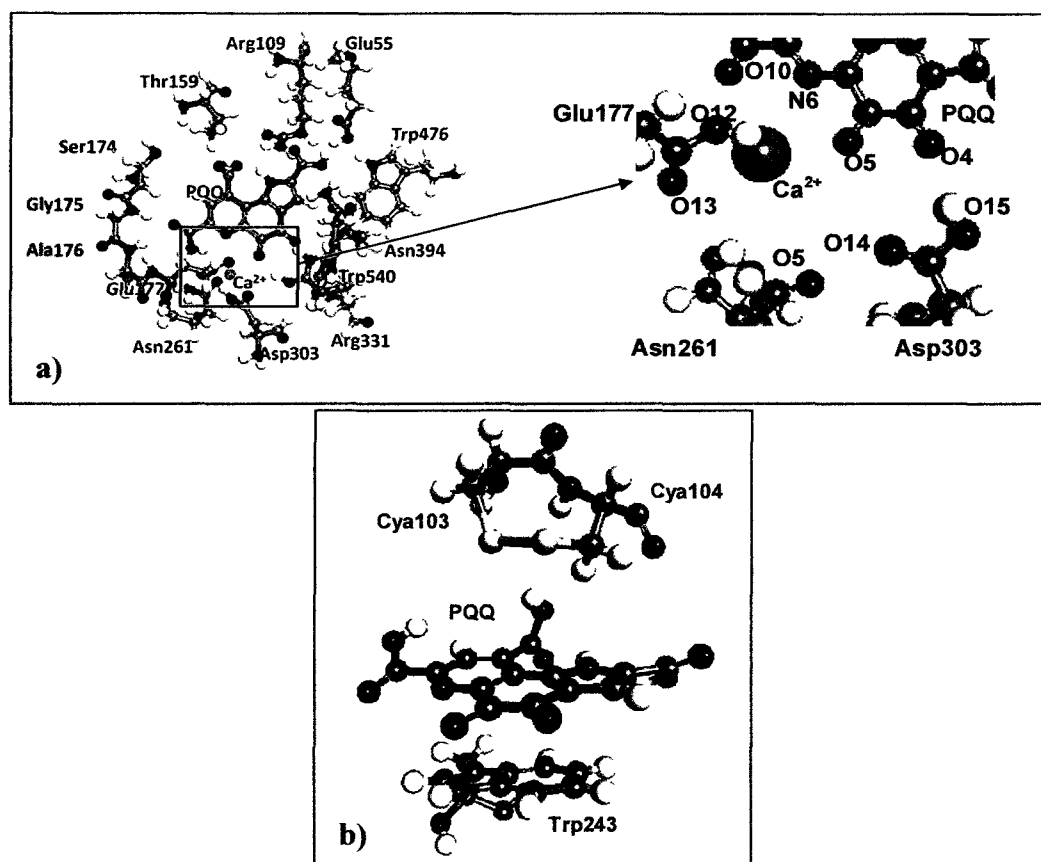
Figure 2.2: a) Active site of MDH with PQQ at the center, radially surrounded by 13 residues. A closer view shows the Ca^{2+} and the atoms it forms coordinate bonds with, b) PQQ sandwiched between tryptophan residue and disulphide bridge formed by cysteine residue.

2.2.2   Structure and Function of PQQ as the Cofactor

Many of the experimental and theoretical studies show that PQQ is a tri-cyclic ring structure which is planar in shape. It is hard to say if the structure of PQQ is planar by itself or if it is due to the crystallographic packing forces [24, 26]. Crystal structures show that PQQ is a planar structure. On the other hand, some *ab initio* molecular studies show that PQQ may not be completely planar. The O4 and O5 oxygen atoms are not coplanar to the tri-cyclic ring. They are bent in opposite direction to reduce the repulsive force as both are negatively charges. Also, some of the carboxylic groups were planar with the ring whereas others were slightly bent. It was also suggested that the carboxylic group are attached to PQQ via C-C single bond. Due to this reason, there will not be much difference between the potential energies of twisted or coplanar carboxylic group. Hence, both forms can exist depending on the environmental conditions [26].

PQQ has a high midpoint redox potential of 100 mV. Therefore, apart from alcohols, it can also reduce flavins and reduce neucleotides. PQQ is mostly found in the enzymes of Gram-negative bacteria. Its presence in the eukaryotes is not known [27]. PQQ has a similar orientation in the case of both alcohol and glucose dehydrogenases. The binding characteristics of PQQ are similar in both sub-units. There is a slight difference in the geometry of PQQ between them. In the case of glucose dehydrogenase, PQQ is non planar with all the three carboxylate groups twisted out of plane with respect to the ring. The O4 and O5 oxygen atom (Fig. 2.2) lies on the plane with the cofactor. The repulsive force between atoms do not force them to lie on the opposite side of the same plane due to its interaction with the side chain of proteins and coordinate bond with Ca^{2+} ion [28].

Structural parameters indicate that the C4 and C5 carbonyl groups are tightly bound with neither pyrrole nor pyridine ring structures. Being adjacent to pyrrole ring, the electron density at the carbonyl ends decreases and their reactivity increases. Under basic and neutral conditions C5 carbonyl is more reactive, whereas C4 is more reactive under acidic conditions due to resonance activity at N1 nitrogen of PQQ. Theoretical studies using HF/6-31g(d) theory level on the energy of C5 and C4 carbonyl groups show that C5 adduct is structurally favored by 0.9 kcal/mol when compared to that of C4 [26].

Ca^{2+} is the only metal ion found in MDH and plays an important role in holding the PQQ in its position. Ca^{2+} bound PQQ is also found in ethanol and glucose dehydrogenase such as *Pseudomonas aeruginosa* and *Acinetobacter calcoaceticus*, respectively [29]. The presence of Ca^{2+} is confirmed by the fact that it is the strongest binding alkaline metal. The size of Ca^{2+} ion best fits the active site of MDH. Possibility of Sr^{2+} or Ba^{2+} is negated as the presence of these ions can cause strain in the active site due to the large size. The presence of Ma^{2+} is also nullified due to its very small size [29]. It forms coordinate bonds with six atoms which are O5, N6 and O10 atoms of PQQ, O11 of Asn261 and O12-13 oxygen atoms of Glu177. Asn261 in turn form hydrogen bonds with the proposed catalytic base Asp303. Hence, Ca^{2+} plays a very important role in maintaining structural stability of the active site of MDH (Fig. 2.2) [24-25, 30-31]. The binding constant K_m of Ca^{2+} with PQQ trimethyl ester was found to be $1.9 \times 10^3 M^{-1}$ [29].

Richardson et al. conducted experiments on mutant MDH which was devoid of Ca^{2+} ion. An active enzyme was reconstituted when the mutant MDH was incubated in the presence of Ca^{2+}. It showed once the Ca^{2+} ion is restored, PQQ becomes available for reduction [32]. Apart from the structural stability, it also has catalytic properties. It acts as a Lewis acid by facilitating the attack on the electrophilic C5 carbonyl group during

the oxidation of methanol [31]. Molecular dynamics calculations by Reddy et al. show that Ca^{2+} may polarize the double bond between C5 and O5 atoms which may cause higher reactivity to C5 carbonyl group [33]. It also stabilizes the hemiacetal PQQ-Methanol complex formed during the oxidation of methanol [30].

The disulphide bridge present above the PQQ is formed by two cysteine residues (Cys103-104) bound together with a non-planar peptide bond. This is one of the unique structural features found in an active enzyme; therefore, it might play a specific role in the active sight. Experimental studies have shown that reduction of the peptide bond can temporarily deactivate the enzyme. This suggests that the disulphide bridge may not be directly involved in an electron transfer path, but it assists in stabilizing the intermediate free radical form of MDH. Experiments involving mutation of MDH with altered cysteine residues show that the enzyme loses its ability to oxidize methanol [25-26]. Molecular dynamics calculations done by Reddy et al. shows that methanol resides in the hydrophobic cavity surrounded by tryptophan and leucine residues. The disulphide cysteine residues assist in holding the substrate at the active site of MDH and protect it from the bulk water molecules. The orientation of methanol is further stabilized by the surface water and might act as a channel for methanol to enter the active site of MDH [34].

2.2.3 Oxidation of Methanol in MDH

The oxidation of methanol involves a ping-pong reaction at the active site of MDH. Methanol gets oxidized to give formaldehyde as the by-product. In this reaction PQQ initially gets reduced to form a semiquinone structure PQQH, and then it is completely reduced to $PQQH_2$. Asp303 is suggested to be the catalytic base that instigates the abstraction of hydrogen from methanol [25]. Various mechanisms have

been proposed for the oxidation of methanol. The two most debated methanol oxidation mechanisms by MDH are Addition-Elimination (A-E) and Hydride-Transfer (H-T). The difference between these two mechanisms is as follows: In the case of addition-elimination reaction, methanol forms a covalent hemiketal structure with PQQ and releases formaldehyde in the subsequent steps. Hydride transfer method involves direct transfer of hydrogen by methanol to PQQ. The sections below gives further details about both the mechanisms [35-38].

2.2.3.1   *Addition-Elimination Reaction*

Experimental studies conducted by Xia et al. specify that the distance between the hydroxyl oxygen of methanol is 3.1Å from oxygen (O15) atom of Asp303. This position is well suited for Asp303 to act as the catalytic base. The hydroxyl oxygen of methanol faced C5 carbonyl group of PQQ with a distance of 3.2Å. Whereas the methyl group of methanol is positioned away from PQQ. This orientation supports the formation of hemiketal intermediate with PQQ [35]. Spectroscopic analysis done by Itoh et al. also showed the formation of C5 hemiketal intermediate suggesting A-E mechanism is the probable mechanism involved in the oxidation of methanol [29-30]. A-E mechanism consists of three steps to oxidize methanol. The first step involves abstraction of hydrogen (H16) from methanol to O14 atom of Asp303 along with formation of covalent hemiketal intermediate (Fig. 2.3). The covalent bond is formed due to the attraction between O16 oxyanion of methanol and C5 carbonyl of PQQ. In the second step, the H16 proton is eliminated from Asp303 and transferred to O5 of PQQ. The third step involves the release of formaldehyde and the transfer of H17 proton to O4 oxygen of PQQ [37, 39].
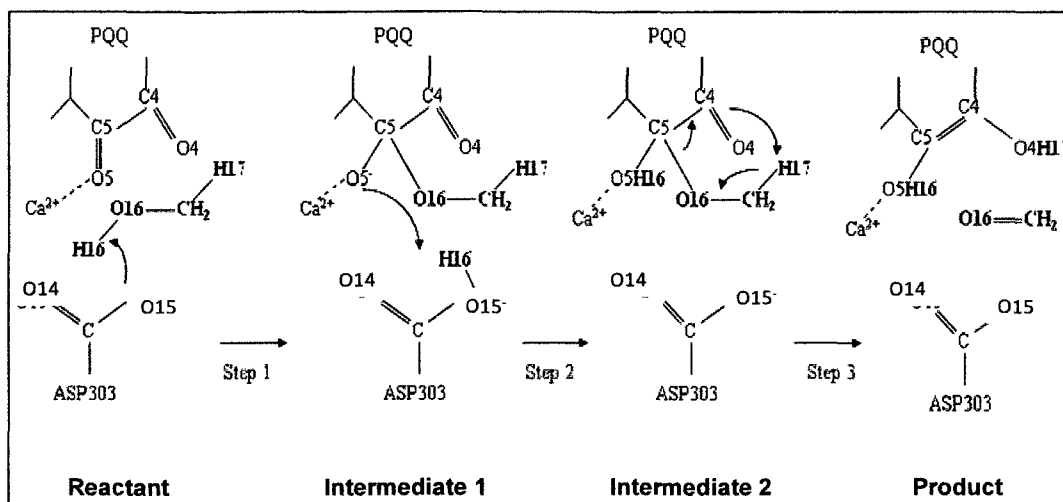
Figure 2.3: Schematic representation of A-E reaction mechanism for oxidation of methanol by MDH.

MDH has normal activity when it is inside the bacterial cell. But once the enzyme is removed from the cell body, it loses its functionality. Spectrophotometric studies on MDH have shown that the addition of ammonium chloride to the enzyme can reactivate the enzyme. The rate at which MDH oxidizes methanol depends on the concentration of ammonia and the pH of the solution. Apart from ammonium chloride, other salts of ammonia can also activate the enzyme, namely, ammonium salts of sulfate, sulfamate, phosphate, formate, etc. The most suitable pH for the oxidation of methanol to take place is a 9 [14].

2.2.3.2   *Hydride-Transfer Reaction*

Oubrie et al. and Zheng et al. investigated the structure of PQQ from methanol and glucose dehydrogenases using both experimental and computational methods inorder to examine the most favorable mechanism for the oxidation [28, 40]. Detailed study on the conformation of PQQ shows that C5 carbonyl group is the most reactive group of PQQ. Therefore, formation of PQQ-methanol complex or direct transfer of hydride from

methanol to PQQ most probably takes place at the C5 position [28]. Some of the quantum mechanical studies showed planarity in the semiquinone form of PQQ, but higher resolution X-Ray crystallographic studies on MDH from *Methylophilus methylotrophus* W3A1 showed contradictory results. The C5 position of PQQ showed notable distortions from planarity and tetrahedral structure. PQQ and methanol complex at C5 center can give a tetrahedral structure, but it is not compatible with the electron density map. Theoretical and crystallographic studies done by Zheng et al. favors the presence of hydride at the C5 position [40]. Therefore, a second mechanism was proposed for the oxidation of methanol called a Hydride-Transfer.

Experimental studies show the breaking of C-H bond at the C5 center of PQQ. This suggests that there is no formation of hemiketal intermediate, instead a hydrogen is attached directly to C5 during the oxidation of substrate [41]. Theoretical studies by Zheng et al. also showed that the transition state for the formation of PQQ-methanol adduct varies from that of direct hydride transfer from methanol. The transition state supports direct hydride transfer and the energy barrier for the same reaction was found to be 10 kcal/mol [26].

The H-T follows a four step mechanism. In the case of the H-T mechanism, by-product formaldehyde is formed at the first step (Fig.2.4). Methanol dissociates in such a way that hydride H16 moves towards O14 atom of Asp303 and methyl hydride H17 attaches to C5 carbonyl group of PQQ leading to the formation of formaldehyde. The second step involves the transfer of hydride H16 from O14 of Asp303 to carbonyl oxygen O5 of PQQ. This leads to the formation of semiquinone or a partially reduced form of PQQ. The third step is followed by the detachment of H17 from C5 of PQQ and

association with O14 of Asp303. In the fourth step, PQQ is completely reduced by the transfer of H17 from Asp303 to O4 carbonyl oxygen of PQQ [40-41].
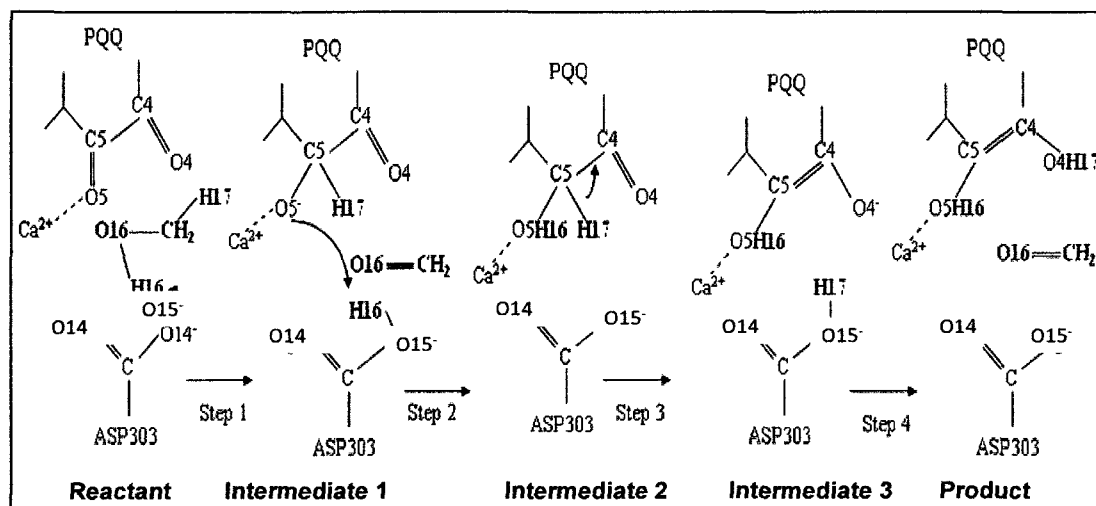
Figure 2.4: Schematic representation of H-T reaction mechanism for oxidation of methanol by MDH.

2.3 Electron Acceptor Cytochrome c_L

Under *in vitro* conditions, many researchers use phenazine methosulphate as an electron acceptor for MDH. For this reaction to take place, ammonia or methylamine is required as enzyme activators [42]. Cytochrome c_L (C_L) is the natural electron acceptor for MDH, which is found only in methylotrophic bacteria. The properties of C_L are similar to a few other c-type cytochromes of Class 1 but differ in the amino acid sequence [25]. C_L transfers the electrons to Cytochrome c_H which further transfers electrons to cytochrome oxidase followed by the release of oxygen [25]. MDH, C_L and Cytochrome c_H, are water soluble and exists at the periplasm of the gram negative bacteria. This property and location is of great advantage to study intra-molecular and intermolecular electron transfer pathways. X-Ray crystallographic studies reveal (Fig. 2.5) that it consists of six α-helical regions. Three of the six α helixes surround the heme molecule

providing a small opening to one side of the heme. The rest of the helixes provide further structural support.
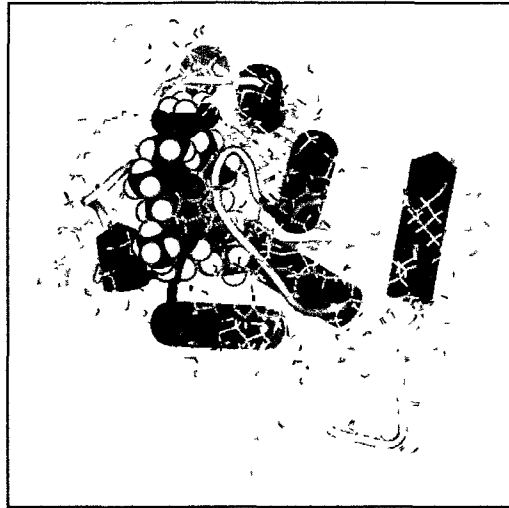
Figure 2.5: Structure of C_L obtained from protein data bank (Call No. 2c8s) [43].

Some of the cross-linking studies show that carboxylate group of C_L interacts with lysine groups of MDH. The same carboxylate group interacts with its natural electron acceptor Cytochrome c_H. One of the common features in c-type cytochrome is the presence of heme molecule. C_L also has a heme molecule, but its arrangement of amino acids is very different from other c-type cytochromes. The only other cytochrome which has close resemblance to C_L is cytochrome c_{551i}. Size of C_L is comparatively larger with 19 kDa. It constitutes 1133 protein atoms and 173 water molecules. Some of the main components of C_L enzyme are the heme prosthetic group, Ca^{2+} ion, disulphide bridge and the residues coordinated to them. The heme group is covalently bound to the rest of the enzyme through Cys65 and Cys68 residues. It also forms a hydrogen bond with Tyr88.

The center of the heme molecule consists of Fe ion with 3+ oxidized states which is coordinated to His69 and His112 residues. His69 is surrounded by hydrophobic residues which induce high redox potential that may assist in attracting electrons from MDH. The midpoint redox potential of this group is 256 mV. Most of the heme group is covered by the protein residues, but a part of the heme is exposed to the bulk solvent. The residues immediately surrounding the heme group is hydrophobic in nature. There is a similar hydrophobic surface found in MDH which is right above the active site [23]. Hence, there is a possibility that this may be the site where electron transfer takes place between MDH and C_L.

The Ca^{2+} ion is present close to the inner heme propionate near to the disulphide bridge. It is bound to seven oxygen ligands provided by carbonyl groups of Gly80, Tyr85, Asp83, and a couple of water molecules. Generally, in the c-type cytochromes, the oxidized state of Fe^{3+} is stabilized by Arginine residues. In the case of C_L, Ca^{2+} ion stabilizes the oxidized state of the enzyme and increases the redox potential. Another important feature of this enzyme is the disulphide bridge which is formed by cysteine residues Cys53 and Cys167. The main function of this bridge is to provide structural stability to the enzyme.

2.3.1   Ammonia as an Activator

Patel et al. conducted spectrophotometric studies on MDH to study the effect of ammonium chloride on the enzyme. In their investigation they used methanol, ethanol, and various other alcohols to compare their activity. Once ammonium chloride was added, the enzyme retained its activity. Ammonium salts of sulfate, sulfamate, phosphate, formate, thiocynate, molybdate, and acetate can also act as an activator for MDH. They also found that the activity depended on the concentration of ammonium chloride and the

pH of the system. As the concentration of ammonium chloride was increased from 0 to 40 µM, the activity of the enzyme increased steadily. The ideal condition for the oxidation was found to be at a pH of 9. The experiments were conducted using artificial electron acceptors such as PMS, phenazine ethosulphate, ethylphenazinium ethosulphate, and 5-methyl phenazinium methylsulfate [14].

Isotopic studies showed that ammonia acts as an activator for MDH and plays a significant role in the rate limiting step of the removal of hydrogen from the methyl group of methanol. An increase in the concentration of NH_4Cl from 0.25 mM to 15 mM increased the activity of MDH, but high concentration of ammonia has inhibitory affects on the enzyme. It is believed that both methanol and ammonia may have similar binding site; therefore, high concentration of ammonia can reduce the affinity of methanol to the binding site and hence decrease the oxidation of methanol [25]. Experimental studies were conducted in which MDH was incubated with electron acceptor and activator in the absence of the substrate. It was observed that a large amount of electron acceptor was reduced. On the other hand, if it is continued to react in the absence of the substrate, it becomes inactivated. The possible reason for this inactivation might be the presence of unidentified substrate [42]. This phenomenon is found in all the MDH from various different methylotrophic bacteria [44]. Ammonia is not used up during the reaction mechanism [42].

Harris et al. showed that ammonia is vital for both endogenous and substrate dependent reactions. In the absence of ammonia enzyme remained inactive. The highest methanol dependent activity of 7.2 units/mg was observed at an ammonia concentration of 6 mM with Wurster's blue as the electron acceptor. Maximum activity was also

observed in endogenous reaction at an ammonia concentration of 6 mM. Furthermore, increase in ammonia concentration led to a decrease in enzyme activity [44].

Though it is known for the last couple of decades that ammonia acts as an activator for MDH, the exact mechanism by which ammonia affects the oxidation of methanol is still not well understood. It has been suggested that ammonia may bring some chemical transformation in PQQ, which may result in oxidation of methanol under *in vitro* conditions. Ammonia may bind to C4, C5 carbonyl groups, or it may attach to C10 carboxylic group of PQQ. Since the addition of NH_4Cl to MDH does not cause notable change in the spectrographic analysis, there can be other possibilities. There is a likelihood that ammonia may react with the protein residues instead of PQQ and cause chemical change in the active site environment [45].

CHAPTER 3

MOLECULAR MODELING AND
COMPUTATIONAL METHODS

3.1 Introduction

X-Ray crystallographic studies may not provide a clear differentiation between oxidized and reduced forms of enzymes. Under these circumstances molecular modeling and theoretical studies play a very crucial role in giving a clear understanding on how the atoms and molecules behave. They also offer clear visualization of reactions taking place in the active site of the enzymes [33].

Molecular modeling deals with imitation of the behavior of atoms and molecules in the real system. It started off by the use of balls and sticks or space models to visualize a molecular system in three dimensions. This method is still being practiced for teaching and research purposes. Apart from the physical models, molecular modeling involves abstract models that predict the position of electrons or atoms in a system. This was done using quantum mechanics. Nowadays, with the development of highly intelligent computer systems, molecular modeling is associated with computational chemistry [46].

Computational chemistry involves molecular visualization tools, quantum mechanics, molecular mechanics, energy minimization, simulations, and conformational predictions. In this chapter, the theory behind our computational calculations of this work will be discussed.

3.2 Quantum Mechanics

Quantum mechanical methods form the foundation for the prediction of energies and other physical and chemical properties of an atomic system [47]. Those calculations are based on solving Schrödingers equation shown in Eq. 2.1.

$$\hat{H}\psi_i\left(\vec{r}_1,\vec{r}_2...\vec{r}_n,\vec{R}_1,\vec{R}_2,...\vec{R}_M\right) = E_i\psi_i\left(\vec{r}_1,\vec{r}_2...\vec{r}_n,\vec{R}_1,\vec{R}_2,...\vec{R}_M\right) \qquad 2.1$$

In Eq. 2.1, $\hat{H}$ is the Hamilton operator for an atomic system with M number of nuclei and N number of electrons, E_i is the spatial energy of the system and ψ_i is the wave function. The wave function depends on 3 M spatial coordinates of nuclei and 3 N spatial and N spin coordinates of electrons, which is collectively described by the term $\vec{r}_i$. The Hamiltonian operator $\hat{H}$ is in turn the sum of the kinetic energy of electrons and nuclei, potential energy of attractive forces between nuclei and electrons, electron-electron repulsive force, and nucleus-nucleus repulsive force shown in Eq. 2.2.

$$\hat{H} = -\frac{1}{2}\sum_{i=1}^{N}\nabla_i^2 - \frac{1}{2}\sum_{A=1}^{M}\frac{1}{M_A}\nabla_A^2 - \sum_{i=1}^{N}\sum_{A=1}^{M}\frac{Z_A}{r_{iA}} + \sum_{i=1}^{N}\sum_{j>i}^{N}\frac{1}{r_{ij}} + \sum_{A=1}^{M}\sum_{B>A}^{M}\frac{Z_AZ_B}{R_{AB}} \qquad 2.2$$

∇^2 is the Laplace operator, M_A is the mass of the nucleus A, Z is the charge and r is the distance between the particles. The exact solution for Schrödinger's equation is obtained only for one electron system like the hydrogen atom [48].

One of the major approximations considered in the quantum mechanics method is the Born-Oppenheimer or clamped nuclei approximation [46]. Born-Oppenheimer also known as adiabatic approximation helps in simplifying calculations dealing with multi scale molecular system [49]. If the nucleus of an atom is considered fixed in space, the kinetic energy is zero and the resulting potential energy due to the nucleus-nucleus

repulsion is a constant [50]. Therefore, Eq. 2.2 reduces to electronic Hamiltonian as shown in Eq. 2.3.

$$\hat{H}_{elec} = -\frac{1}{2}\sum_{i=1}^{N}\nabla_i^2 - \sum_{i=1}^{N}\sum_{A=1}^{M}\frac{Z_A}{r_{iA}} + \sum_{i=1}^{N}\sum_{j>i}^{N}\frac{1}{r_{ij}} = \hat{T} + \hat{V}_{Ne} + \hat{V}_{ee} \qquad 2.3$$

The solution for the electronic Hamiltonian is written as the product of electronic wave function ψ_{elec}, and electronic energy E_{elec} (Eq. 2.4). Ψ_{elec} term mainly depends on the electron coordinates. The total energy (E_{tot}) of the system will be the sum of electronic energy and the nuclear repulsion (E_{nuc}) and is shown in Eq. 2.5.

$$\hat{H}_{elec}\psi_{elec} = E_{elec}\psi_{elec} \qquad 2.4$$

$$E_{tot} = E_{elec} + E_{nuc}, \qquad 2.5$$

where the term E_{nuc} is given by Eq. 2.6:

$$E_{nuc} = \sum_{A=1}^{M}\sum_{B>A}^{M}\frac{Z_A Z_B}{R_{AB}}. \qquad 2.6$$

The wave function ψ term by itself is not of much significance, but the square of the wave function can represent the probability of finding electrons within a certain volume and is represented by Eq. 2.7.

$$\left|\psi(\vec{x}_1, \vec{x}_2, ..., \vec{x}_N)\right|^2 d\vec{x}_1 d\vec{x}_2 ... d\vec{x}_N \qquad 2.7$$

Electrons are fermions with a spin equal to ½; therefore, anti-symmetric wave function is applied with respect to interchange of the spatial and spin coordinates of any two electrons (Eq. 2.8).

$$\psi(\vec{x}_1, \vec{x}_2, ...x_i, x_j, ..., \vec{x}_N) = -\psi(\vec{x}_1, \vec{x}_2, ...x_i, x_j, ..., \vec{x}_N) \qquad 2.8$$

The electronic structure methods are of two types, namely, *ab initio* methods and semi-empirical methods. The major difference in these two types of method is the level

of approximation used to solve the electronic Hamiltonian Eq. 2.4. Examples of *ab initio* methods are Hartree-Fock, configuration interaction (CI), and density functional theory (DFT) [50]. The Hartree-Fock (HF) approximation forms the basis for all wave function based quantum mechanical methods. It is based on the independent particle model where each electron is considered to move on the mean field of all other particles. If the coordinates of two electrons are interchanged, the sign of the wave function changes. HF method satisfies the condition that the square of the wave function ($|\psi|^2$) is not affected with the exchange of any two electrons by considering the wave function anti symmetric [50]. In this method, the many-electron wave function is represented using Slater determinant. It considers a system with N number of electrons as N one-particle problem and is shown in Eq. 2.9 [51].

$$\hat{F}\chi_i = \varepsilon_i \chi_i \qquad\qquad 2.9$$

In Eq. 2.9, $\hat{F}$ is the Fock operator, ε_i are the orbital energies. The Fock operator is an effective one electron operator and is defined by Eq. 2.10 [50].

$$\hat{F}_i = -\frac{1}{2}\nabla_i^2 - \sum_A^M \frac{Z_A}{r_i A} + V_{HF}(i) \qquad\qquad 2.10$$

In the case of CI methods, wave function (ψ) cannot be written as a single determinant. Instead, it builds other determinants by replacing one or more occupied orbitals with a virtual orbital. The virtual orbital is equivalent to exciting an electron to a higher energy orbital [50]. In this research, DFT methods have been used to predict energies of our system which is discussed in detail in the subsequent section.

3.3 Density Functional Theory

During the last few decades, DFT approach to the electronic structures of atoms have gained great amount of interest. This method is being extensively used by quantum chemists and physicists to efficiently compute ground state energies of clusters, bulk models and surfaces [46, 50]. As in the case of HF method, DFT also considers single electron functions. HF method calculates the full N-electron wave function, but the approach of DFT method is to calculate the total electronic energy and the overall electronic density distribution. In 1964, Kohn and Hohenberg proved a theory that the complicated wave functions can be replaced by the electron density [52]. They showed that the total energy of a non-degenerate ground state is a unique functional of the electron density $(E=E[\rho(r)])$. The energy functional can be written as the sum of two terms shown in Eq. 2.11.

$$E[\rho(r)] = \int V_{ext}(r)\rho(r)dr + F[\rho(r)]$$ 2.11

The first term in Eq. 2.11 represents the interaction of the electron with an external potential $V_{ext}(r)$. The external potential is due to the Coulombic interaction with the nuclei. Second term $F[\rho(r)]$ is the sum of the kinetic energy of the electrons and inter-electronic interactions. Further development was made in the DFT by Kohn and Sham by suggesting a method to solve Hohenberg and Kohn theorem for a set of interacting electrons. According to Kohn and Sham, $F[\rho(r)]$ can be written as the sum of three terms, as shown in Eq. 2.12.

$$F[\rho(r)] = E_{KE}[\rho(r)] + E_H[\rho(r)] + E_{XC}[\rho(r)]$$ 2.12

$E_{KE}[\rho(r)]$ is the kinetic energy of a system of non-interacting electrons with the same density $\rho(r)$ as the real system, $E_H[\rho(r)]$ is the electron-electron Coulombic energy,

also known as Hartree electrostatic eenergy, and $E_{XC}[\rho(r)]$ contains contributions from exchange and correlation. $E_{KF}[\rho(r)]$ and $E_H[\rho(r)]$ can also be written as Eq. 2.13 and Eq. 2.14.

$$E_{KL}[\rho(r)] = \sum_{i=1}^{N} \int \psi_i(r) \left(-\frac{\nabla^2}{2} \right) \psi_i(r) dr \qquad 2.13$$

$$E_H[\rho(r)] = \frac{1}{2} \int \int \frac{\rho(r_1)\rho(r_2)}{|r_1 - r_2|} dr_1 dr_2 \qquad 2.14$$

Therefore, the full expression for the energy of an N-electron system within the Kohn-Sham scheme is shown in Eq. 2.15.

$$E[\rho(r)] = \sum_{i=1}^{N} \int \psi_i(r) \left(-\frac{\nabla^2}{2} \right) \psi_i(r) dr + \frac{1}{2} \int \int \frac{\rho(r_1)\rho(r_2)}{|r_1 - r_2|} dr_1 dr_2$$

$$- \sum_{A=1}^{M} \frac{Z_A}{|r - R_A|} \rho(r) dr$$

$$2.15$$

There are various DFT methods available in which the kinetic energy term and exchange correlation terms are described differently [53-54]. It uses general functionals of the electron density to calculate the electron correlation in the molecular system [55-56]. Three types of functionals are used for the computational calculations, which are local spin density approximation (LSDA), generalized gradient approximation (GGA) functional and hybrid functionals. LSDA uses the electron spin density values to calculate the electron correlation terms. In the case of GGA functional, electron spin density and its gradient is included in the calculations. In the case of hybrid functionals, exchange function is described as a linear combination of Hartree-Fock, local and gradient corrected exchange term [55-56]. The exchange term is eventually combined with local or gradient corrected correlation term [50, 55-56].

The three most extensively used GGA exchange-correlation combinations in various atomic calculations are BP86, BLYP and BPW91 [57-58]. In the case of DMOL^3 module of Materials Studio® software BLYP exchange-correlation functional is used to perform optimization and transition state calculations in this project [59-60]. In this functional Becke's (B) GGA exchange correlation function is combined with correlation function of Lee, Yang and Parr (LYP). The LYP GGA correlation functional can take care of the self-interaction error in multi-electron systems in an improved manner and hence is considered very efficient in molecular systems [57-58].

3.4 Basis Sets

A mathematical expression that can represent the atomic orbitals is called a basis set [58]. An atomic or molecular orbital represents a particular region in space where there is probability of finding an electron. In order to express the unknown molecular orbitals, quantum mechanical calculations use basis set expansions. They are expressed as linear combination of atomic orbitals as shown in Eq. 2.16 [58, 61].

$$\Psi_i = \sum_{\mu=1}^{K} C_\mu \varphi_\mu$$

2.16

In Eq. 2.16, Ψ_i is a spatial molecular orbital (MO), and φ_μ is one of K atomic orbitals, and $C\mu$ are the atomic coefficients. The basis functions φ_μ are generally H-like functions, but it need not be the same in all the cases. The orbitals are more accurately represented by larger basis sets. This is because it imposes fewer restrictions on the locations where an electron can be present. The limitation associated with larger basis sets are that they require higher computational resources, longer durations, and are difficult to use in systems with a large number of atoms [58, 61].

When the basis sets are defined as analytical functions, they are called as Gaussian-type basis sets. On the other hand, when they are represented as numerical functions, they are known as numerical functions. A numerical basis function consists of a table of the values that an atomic orbital wavefunction has at many points around the nucleus, with empirical functions fitted to pass through these points. In most calculations, empirical functions are used instead of the analytical Gaussian-type functions. This is because the molecule can be dissociated exactly to its constituent atoms. It minimizes the basis set superposition effects and result in accurate descriptions even if the bonds are weak [61-62].

One of the most efficient basis set is double numerical plus polarization (DNP), which is used in this dissertation [61-62]. In the case of DNP, heavy atoms are represented by polarization d function and the hydrogen atoms are considered by polarization p function. This basis set can be considered to one of the Gaussian basis sets 6-31G** in size but it is more accurate when compared to the Gaussian basis set of the same size. This basis set is most suitable in atomic systems consisting of free ions in combination with Density functional theory calculations [59-60].

3.5 Transition State Theory and Reaction Rates

In this dissertation the reaction mechanism involved in MDH enzyme in the presence of ammonia is investigated. In order to do so, a process involving continuous chemical and potential energy changes is considered and characterized by reaction rates. The rate of a reaction depends on how readily the reactant of the system changes into products. Figure 3.1a and b shows a schematic representation of free energy profile of various chemical reactions taking place in a molecular system.
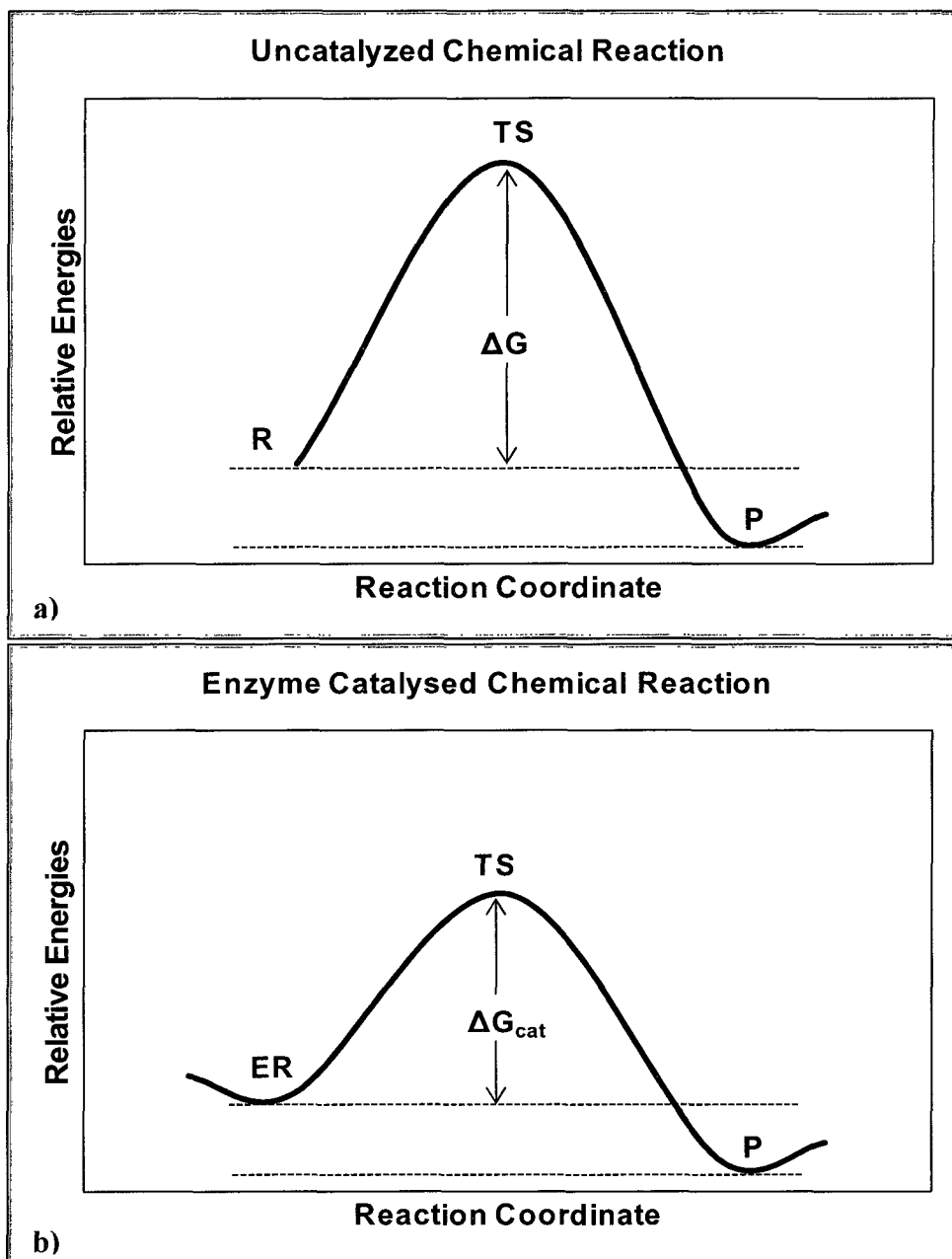
Figure 3.1: Schematic representation of free energy profile for a) uncatalayzed and b) enzyme catalyzed chemical reactions.

In the case of uncatalyzed reaction, ΔG represents the reaction barrier. It is also the relative free energy of the transition state (TS) to the reactant (R). On the other hand, the first step in enzyme catalyzed reaction is the binding of the reactant to the enzyme

forming and enzyme-reactant complex (ER). The reaction is followed by one (or several) transition state(s) resulting in an enzyme-product complex (EP). In the final step, the product (P) is released and the enzyme is released to be used to catalyze the next available reactant. ΔG_{cat} is the reaction barrier for the enzyme catalyzed reaction. It is represented as the relative energy between the ER complex and the transition state. The advantage of enzyme catalyzed reaction is that it reduces the energy barrier which speeds up the rate of reaction [63].

Reaction rates of a reactant are determined using experimental methods, but to compute potential energy surfaces and relative energies between them, quantum chemistry is being widely used. A very powerful way to connect these two concepts is in terms of classical transition state theory (TST). TST assumes that once a reaction passes through its reaction barrier it cannot go back again. Its postulates an equilibrium (Boltzmann) energy distribution at all stable and unstable states along the reaction coordinates. The expression for the rate constant is given by Eq. 2.17.

$$k = \frac{k_B T}{h} \exp\left(-\frac{\Delta G}{RT} \right)$$ 2.17

In Eq. 2.17, k is the first order rate constant (s^{-1}), k_B is the Boltzmann's constant (1.38×10^{-23} J/K), h is the Planck's constant (6.626×10^{-34}J s), T is the absolute temperature (298.15 K at room temperature), R is the universal gas constant (8.314 J K^{-1} mol^{-1}) and ΔG is the Gibbs free energy of activation. Gibbs free energy is calculated using the formula, $\Delta G = \Delta H - T\Delta S$ [63].

Transition state calculations conducted as a part of this dissertation work are performed using the DMOL^3 module of the Materials Studio® [59-60] software using synchronous transit methods (Linear Synchronous Transit, LST and Quadratic

Synchronous Transit, QST [64-65]). Appropriate optimized geometries of reactants and products involved in each reaction step are considered for defining atom pairing as shown in Eq. 2.18.

$$r'_{ab}(f) = (1 - f)r^{R}_{ab} + fr^{P}_{ab}$$

2.18

A 3D trajectory file representing the reaction path is generated using the Reaction Preview tool of the Materials Studio® software [64-65]. In Eq. 2.18, r^{R}_{ab} and r^{P}_{ab} are the inter-nuclear distances between the pair of atoms a and b in the reactant and the product respectively and f is an interpolation parameter which varies between 0 and 1 [64-65]. For molecule with N atoms, the number of distinct inter-nuclear separations is N(N-1)/2, which is greater than 3N Cartesian degrees of freedom of the system by which the interpolation equation over specifies the geometry.

Once these trajectory files are obtained, they are used as inputs to obtain the corresponding transition states, using the linear synchronous transit and quadratic synchronous transit (LST/QST) calculation with conjugate gradient (CG) minimization using the transition state search tool in DMOL³. This methodology starts with a LST/optimization (bracketing the maximum between the reactant and product and performing energy minimization of the obtained maximum in the reaction pathway). The transition state hence obtained is used as starting point for performing a finer search with the QST/optimization followed by a conjugate gradient (CG) minimization [64-65]. This cycle is repeated until a stationary point with only one imaginary frequency is found. Then this imaginary mode is selected to perform transition state optimization. But in some cases, several imaginary frequencies were found by the end of LST/QST/CG. In such situation, the corresponding (imaginary) modes of vibrations are animated in order

to visualize the mode that would eventually follow the intended step from a particular reactant to product. That particular mode is then selected to perform the transition state optimization to verify whether the obtained geometry is indeed a transition state.

The transition state finally obtained by the LST/QST/CG method may not be the transition state connecting the intended reactant and product for a particular reaction step. Therefore, in order to thoroughly investigate the reaction paths, the intrinsic reaction coordinate (IRC) analysis is performed. In $DMOL^3$, the IRC calculations are included in the Transition State Confirmation tool. This tool starts at the transition state and locates successive minima in the direction of the reactant and product paths. This path is known as the minimum energy path, which should connect the supposed transition state to the presumed reactants and products. It uses the nudged elastic band method to validate a transition state by introducing a fictitious spring force which connects the neighboring points to ensure continuity of the path, and then it projects the force so that the system converges to the minimum energy path [64-65].

3.6   Monte Carlo Search

Monte Carlo searches the configurational space of the enzyme system as the temperature is slowly decreased according to a simulated annealing schedule. Simulated annealing method is a metaheuristic algorithm for precisely calculating the global minimum along a large search space [66-67]. In order to reduce the number of defects in the crystal lattice, a microcrystalline material is heated and then cooled slowly and in a controlled manner. Similar concept is used in the simulated annealing method. Various kinds of structures can be minimized using this concept. The enzyme structure to be minimized plays a role equivalent to the energy of the crystal. The function variables of

the enzyme correspond to the atom configurations, where the global minimum configuration is considered as the ground state. To control the algorithm to solve for the minimum, a parameter equivalent to the temperature in physical annealing is being used. Hence, the simulated annealing method uses a canonical Monte Carlo sampling of the search space during which the temperature is gradually decreased. The temperature range selected for these MDH/C_L studies (298.15 K to 323.15 K) is consistent to the temperature range methanotropic bacteria-where these enzymes are exposed in nature [68]. Each step of the Monte Carlo sampling will attempt to change the current configuration n of the system into a randomly chosen configuration m, with a probability $\rho_{n\to m}$, that in the canonical ensemble, is given by Eq. 2.19 [69].

$$\rho_{n\to m} = C \exp(-\beta\Delta E) \qquad\qquad 2.19$$

In Eq. 2.19, C is an arbitrary normalization constant, $\beta = 1/(k_B T)$ is the reciprocal temperature, k_B is the Boltzmann constant, T is the absolute temperature, and $\Delta E \equiv E_m - E_n$ is the total energy difference between the energies of configuration m and n, respectively.

Initially, in the simulated annealing method, when the temperature is high, large energy increases are acceptable, allowing the system to explore a broad region of the search space, whilst ignoring small ripples in the energy surface. As the temperature decreases, steps that lead to an increase in energy are increasingly disfavored, thereby steering the system to step to neighboring states with a lower energy. Eventually, when the temperature is low enough, the system is forced to evolve to the local minimum in the current region of the search space. At the end of an annealing simulation, the system will have reached a state corresponding to a local minimum of the object function in an area of the search space. This state is an approximation to the global minimum in the search

space. Repeating the temperature cycles can give solutions that are closer to the global minimum solution [43].

3.7 Molecular Mechanics

Quantum mechanics deals with the electronic motion present in the system where the calculations are long and computationally expensive. Therefore, while dealing with bigger systems with large number of atoms this method may not be feasible. Molecular mechanics (MM) method ignores the electronic motion of a system. Instead, it considers the position of the nucleus on an atom to calculate the energy of a large atomic system. It is also known as the force field method. Since it ignores the position of electrons we cannot obtain the properties that deal with electronic configuration of an atom or molecular system. There are cases in which MM can give results as accurate as high level quantum mechanics calculations.

MM considers interactions such as bond stretching, angle bending and rotations about single bonds. It consist of functions that can describe the energy changes in bonded parts of the system and also force fields that can describe the non-bonded interactions of the system [46]. Molecular modeling uses force fields that are designed to give structural and in some cases spectral properties of a molecular system. Since MM is an empirical method, force fields can obtain various functional forms depending on the system. Some of the most common functional forms taken into account for accurate prediction of properties are bond stretching, angle bending, bond rotation, non-bonded electronic and Van der Waal's Interactions as shown in Eq. 2.20.

$$f(r^N) = \sum_{bonds} \frac{k_i}{2}(l_i - l_{i,0})^2 + \sum_{angles} \frac{k_i}{2}(\theta_i - \theta_{i,0})^2 + \sum_{torsions} \frac{V_n}{2}(1 + \cos(n\omega - \gamma))$$

$$+ \sum_{i=1}^{N} \sum_{j=i+1}^{N} \left(4\varepsilon_{ij} \left[\left(\frac{\sigma_{ij}}{r_{ij}}\right)^{12} - \left(\frac{\sigma_{ij}}{r_{ij}}\right)^{6} \right] + \frac{q_i q_j}{4\pi\varepsilon_0 r_{ij}} \right)$$

2.20

Generally, a force-field energy calculation reports a strain energy, which is the deviation of internal molecular coordinates from its equilibrium position. It also reports sum of strain energy and non-bonded interaction energies and heats of formation of atomic systems [47]. The force fields used in this research is COMPASS (Condensed phase optimized *ab initio* forcefield). COMPASS forcefield used while running these calculations. It is one of the advanced forcefields with very accurate predictions of structural, vibrational, and thermo-physical properties at various experimental conditions [70-72]. In the case of MS4.4, the minimization is done using Smart Minimizer which uses Steepest descent algorithm, followed by Conjugate gradient method, and finally quasi-Newton methods for optimizing the enzyme models [73-75].

3.8   Molecular Dynamics

Molecular dynamics (MD) calculations were carried out using DISCOVER module of MS 4.4 [43]. It uses classical force-field based MD using empirical potentials of inter-atomic interactions [76-77]. In the molecular system as the atomic position changes force on each particle also changes. In order to generate molecular dynamics trajectories with continuous potential models, finite difference technique is used. The integral terms are broken in such a way that each stage is separated by a fixed time 'δt'. Various algorithms are available to integrate the equations of motion using finite difference method. Velocity-verlet method is used in this project. This algorithm uses the

position, acceleration and velocities at time 't' to compute the position, acceleration and velocities at time 't + δt'. Even though this algorithm is computationally expensive, it is more precise than other algorithms [77]. The forcefield involved in the calculations are COMPASS.

The DISCOVER module consists of ensembles such as micro-canonical NVE (constant energy and constant volume) and canonical ensemble NVT (constant temperature and constant volume) which is being used in this dissertation work [59-60]. NVT ensemble is used for the MD calculations in this work at a constant temperature of 298 K. It is an isothermal ensemble where heat is exchanged with a temperature bath to maintain a constant thermodynamic temperature. These ensembles can be used to calculate various structural, energetic, and dynamic properties of the systems under study [59-60].

CHAPTER 4

PHYSICAL AND CHEMICAL EFFECTS
AMMONIA ON MDH

4.1   Introduction

Researchers have demonstrated that the ammonia acts as an activator for MDH [14, 78-79]. The need for an activator arises when the enzymes are extracted from the methylotropic bacteria. Loss of enzyme activity can be due to the change in environmental conditions outside the cell body. Other possibility is that during the extraction process the structure of the enzyme might gets altered or there can be a possibility of another unknown component involved in the oxidation of methanol. The enzyme regains its activity in the presence of small concentration of ammonia [14, 78-79].

Though it is known that ammonia acts as an activator, but the process by which it activates the enzyme is still not clear. The knowledge of the role of activator in the enzymes is of great importance as it can be used to design and develop efficient artificial bio-catalysts which can be used for biomedical, environmental and chemical industries. In this chapter, the effect of ammonia on free MDH and C_L enzymes is investigated.

In order to investigate the behavior of MDH and C_L in the presence of ammonia, the binding energy between the two enzymes was explored. This helped in the

understanding of the effect of ammonia at the surface of the enzymes. Researchers have detected the presence of ammonia inside the enzyme structure, too. Therefore, the physical changes happening within the enzymes were also inspected.

4.2   Enzyme Modeling

The structures for examining the binding energy of MDH and C_L were obtained from protein data bank (PDB) (Call No. 1w6s and 2c8s for MDH and C_L respectively) [23-24, 43, 80]. Two approaches were used for running the simulations of MDH and C_L. In the case of Approach 1 (Fig. 4.1), the entire enzyme structure along with the water molecules present within and at the surface of the enzyme were considered for calculations.
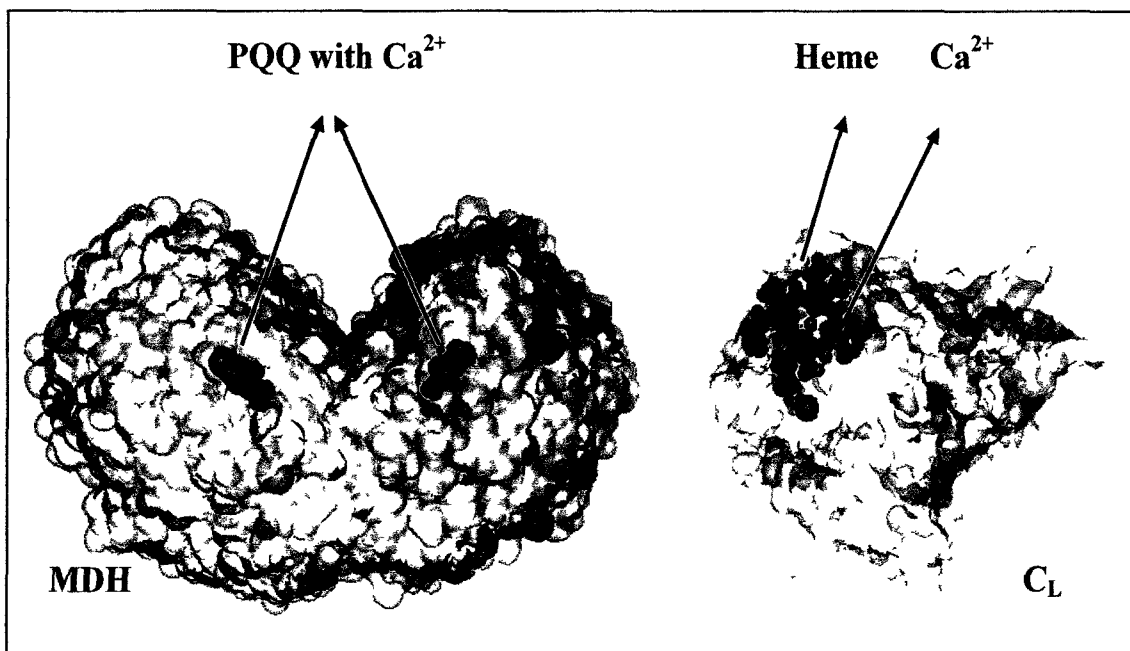
Figure 4.1: Approach 1 of MDH and C_L obtained from PDB (Call No. 1w6s and 2c8s) [23-24, 43].

The main aim in Approach 2 was to scale down the enzyme structure. The bulk enzyme structure was reduced in such a way that the active site of MDH and the amino

acids surrounding the active site was included. The model for MDH consisted of PQQ, Ca^{2+} and the possible catalytic base Asp303 (Fig. 1.2) [23]. Asn261 forms hydrogen binds with Asp303 and stabilizes its orientation in the active site and hence was used in the second approach [24].

The model consists of disulphide bridge formed by cysteine residues (Cys103-104). The cysteine residues provide stability to the semiquinone form of PQQ and also protect it from the solvent molecules [23]. In some quinohaemoproteins alcohol dehydrogenases, such as *C. Testosteroni* and *P. Putida*, it has been implicated that the disulphide bridge assists in electron transfer during the re-oxidation process [24]. MDH has a funnel shaped depression just above the active site formed by hydrophobic residues, which is also incorporated in the model (Fig. 4.2).
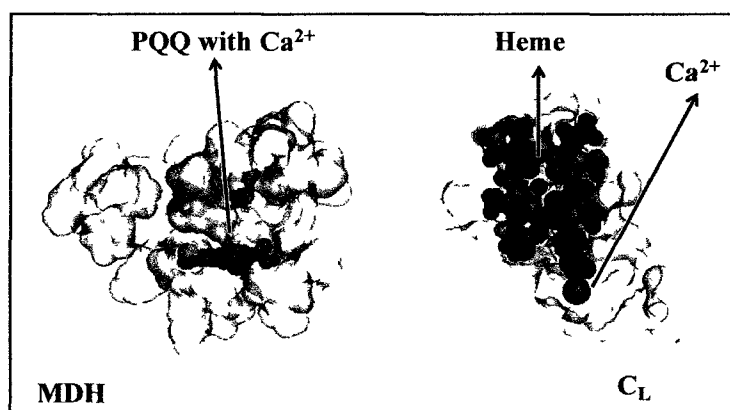
Figure 4.2: Approach 2 of MDH and C_L obtained from PDB (Call No. 1w6s and 2c8s) [23-24, 43] edited using Materials Studio 4.4 [70].

The amino acids forming the funnel are 100-AVACCDL; 420-PFMLP; 430-FFV; 540-WPGVGLVFDLADPTAGL [23]. The model is built using the initial coordinates from the crystal structure. In the case of C_L heme group along with Fe^{3+} metal ion and amino acids surrounding, the heme was taken into account. The amino acids surrounding

Heme are 62F; 67-CH; 76-LGPGL; 84-YWTY; 108-MG; 112H; 128I; 138D. The Ca^{2+} ion present close to the Heme group stabilizes the oxidized state of the enzyme and increases the redox potential thereby attracting electrons [43].

4.3   Computational Details

All the simulations were performed using DISCOVER module of Materials Studio 4.4 (MS4.4) software of Accelrys, Inc. [70]. Before calculating the binding energy between MDH and C_L, the enzyme structures were optimized using MM techniques. The minimization is done using smart minimizer, which uses steepest descent algorithm, followed by conjugate gradient method and finally quasi-Newton methods for optimizing the enzyme models [73-75].

COMPASS forcefield was used while running these calculations. It is one of the advanced forcefields with very accurate predictions of structural, vibrational, and thermo-physical properties at various experimental conditions [70-72]. The docking of optimized MDH and C_L was first investigated using the adsorption locator module of MS4.4 [70]. Adsorption locator uses an approach where possible docking configurations are identified by carrying out Monte Carlo searches of the configurational space of the MDH/C_L system. During the search, the temperature is slowly decreased according to a simulated annealing schedule. [66-67]. Once the MDH/C_L configuration is obtained the system is re-optimized. The interaction energy is calculated using Eq. 4.1.

$$IE_{MDH\text{-}cL} = E_{MDH\text{-}cL} - (E_{MDH} + E_{cL} + E_{(NH3)n}) \qquad 4.1$$

Initially, MDH and C_L are docked without any ammonia molecules. In the subsequent simulations, the enzymes are docked in the presence of increasing

concentration of ammonia. The concentration of ammonia is increased from 1 to 5 molecules.

To further elucidate the behavior of the enzyme active site, Approach 2 of MDH and C_L was used. Based on the configurations obtained from adsorption calculations a series of orientations of MDH and C_L were constructed and optimized. The most stable MDH/C_L orientation was used for further calculations. MDH/ C_L system, in the presence of NH_3 is immersed in a water box and re-optimized. The concentration of NH_3 is increased by adding a molecule at a time. The water box was built using Amorphous Cell module of MS4.4 [70].

In order to simulate infinite systems effectively periodic boundary conditions were applied. This will result in interaction of atoms within the cell and also with that of the translated images of the system [81]. The system was relaxed using DISCOVER module of MS4.4. Molecular dynamics calculations were run using microcanonical ensemble NVT for a simulation time of 100 ps at time step of 0.5 fs.

4.4   Results and Discussion

4.4.1   Binding Energy of MDH and C_L

Distance measurements of the active site components of the optimized approaches are shown in Table 4.1. The results are compared with that of experimental values obtained from the X-Ray crystallographic studies [23-24, 43]. The values obtained through simulations are in close agreement with that of the experimental studies. Once the enzyme structures were optimized, Monte Carlo simulated MDH/C_L orientations were identified. MDH and C_L were adsorbed initially in the absence of NH_3 followed by

increasing the number of NH_3 molecules. Adsorption locator identified 30 probable orientations for each set of simulation where we focused on the most stable configuration.

Table 4.1: Refined distance between Ca^{2+} and neighboring active site residues minimized using DISCOVER module of MS4.4. Approach 1 represents the complete enzyme structure downloaded from PDB (Call No. 1w6s and 2c8s) and Approach 2 represents the reduced MDH and C_L model modified using MS4.4.

System	Length	X-Ray (Å) [24]	Approach 1 (Å)	Approach 2 (Å)
MDH	Ca^{2+} - O5	2.25	2.54	2.56
	Ca^{2+} - N6	2.32	2.54	2.57
	Ca^{2+} - O10	2.44	2.49	2.42
	Ca^{2-} - O11(Asn261)	3.13	3.18	3.23
	Ca^{2+} - O12(Glu177)	2.38	2.47	2.43
	Ca^{2+} - O13(Glu177)	2.81	2.61	2.74
	Ca^{2+} - O14(Asp303)	3.20	3.33	3.72
	Ca^{2+} - O15(Asp303)	4.60	4.95	4.71
C_L	Fe^{3+} - His69	2.00 - 2.05	2.43	2.48
	Fe^{3+} - His112	2.00 - 2.05	2.50	2.45

Figure 4.3 shows stable snapshots of MDH/C_L binding orientation at increasing concentration of NH_3. These snapshots depict that the NH_3 molecules concentrate at the surface interface of MDH/C_L. Based on the energy report from the adsorption and mechanics calculation, binding between MDH and C_L was assessed.
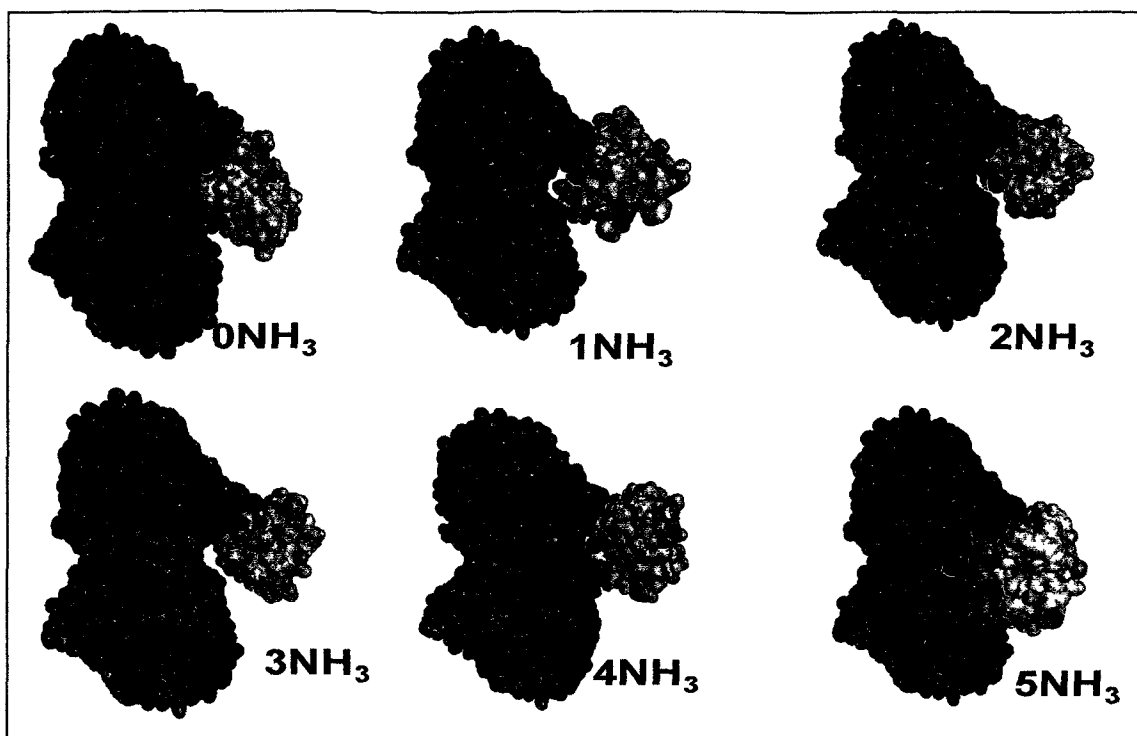
Figure 4.3: Figure shows adsorptive structures of MDH and C_L in the presence of increasing NH_3 concentration. MDH and C_L are represented in green and pink color respectively. NH_3 is represented in blue color.

The negative interaction energies (Fig. 4.4) show that the docking of MDH and C_L is thermodynamically favorable in all the cases. The simulated results show that the interaction energy between MDH and C_L is -106.83 kcal/mol in the absence of NH_3 and -215.33 kcal/mol in the presence of one molecule of NH_3. Clearly, the interaction energy of MDH and C_L is 108.50 kcal/mol lower in the presence of a NH_3 molecule when compared to that of no NH_3. As we increase the number of NH_3 molecules from 1 to 3, the interaction energy becomes more negative indicating increase of strength in the binding of MDH and C_L. Further increase in NH_3 molecules does lower the interaction energy, but the magnitude of change decreases.
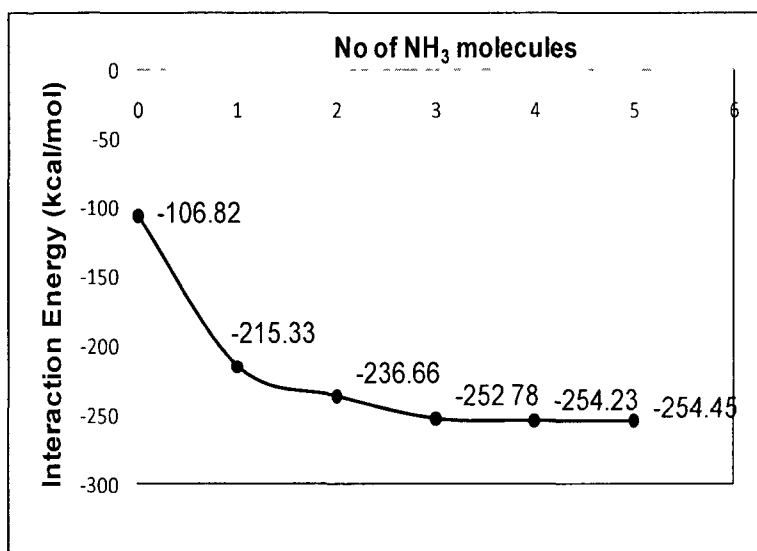
Figure 4.4: Interaction energy of MDH/C_L system at varying NH_3 concentration obtained using Adsorption locator and relaxed using molecular mechanics.

Isolating enzymes such as MDH from the bacteria can lead to the breaking of bonds or amino acids due to which enzymes lose their functionality or binding capacity. MDH enzyme structure downloaded from the PDB (entry 1w6s) [23-24, 80] shows broken amino acids at the surface of the enzyme. Most of the broken amino acids are the lysine residues, which is suggested to be responsible for the binding of MDH to C_L [43]. Therefore, it could be stated that the NH_3 molecules play a significant role in the initial docking of MDH and C_L and maintaining the stability of MDH/C_L complex.

4.4.2   Role of Ammonia in the Active Site of MDH

Experimental studies showed that NH_3 may play a significant role in the oxidation-reduction reaction taking place inside the active site of MDH [25, 82]. Therefore, the second approach of MDH and C_L was considered where models were constructed and optimized to better understand the behavior of various components of active site in the presence of NH_3.

Table 4.1 shows the bond lengths of active site amino acids with respect to Ca^{2+}. The data illustrate that the individually optimized structure of MDH and C_L are in close agreement with that of the experimental studies. The best candidate structure of MDH/C_L system is shown in Fig. 4.5, which also shows the schematic representation of the same.
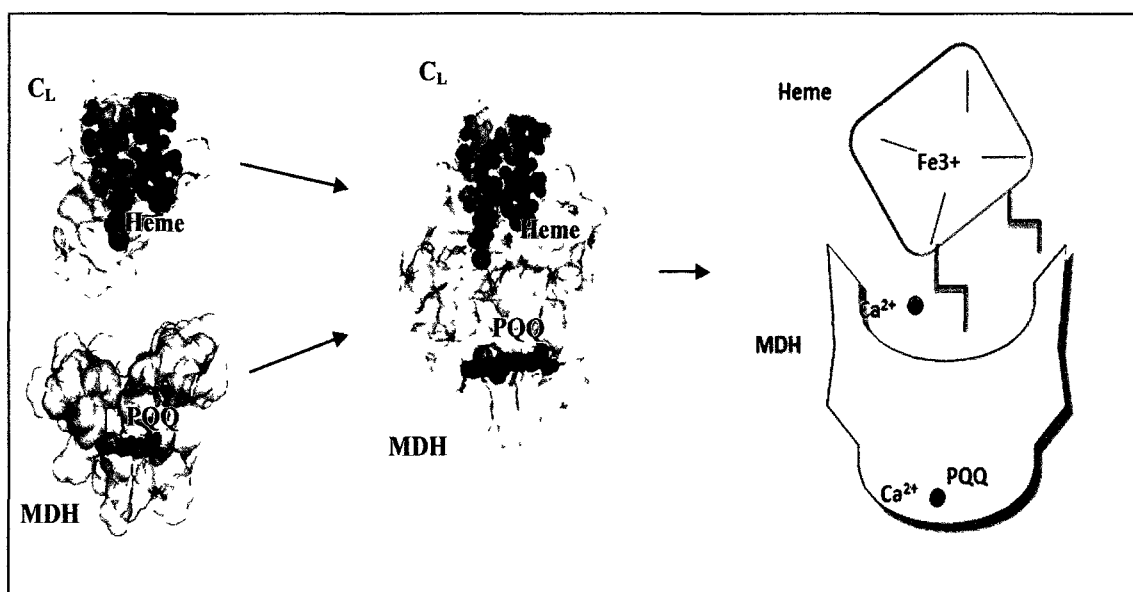
Figure 4.5: Orientation of reduced MDH and C_L minimized using DISCOVER module of MS4.4. Schematic representation of MDH/C_L complex.

The system shows that one of the propionates of the partially exposed heme molecule faces the amino acids forming the hydrophobic funnel of MDH. The active site of MDH is present right below the hydrophobic funnel [23]. The amino acids immediately surrounding the heme are also hydrophobic in nature. This favors the configuration obtained from the optimization calculation, as hydrophobic residues of C_L occupy the hydrophobic funnel of MDH [43]. Another significant factor about this orientation is that the Ca^{2+} ion of C_L is present near the entrance of cytochrome. Ca^{2+} is suggested to play a vital role in increasing the redox potential of C_L [43]. Therefore, the presence of Ca^{2+} can help in attracting electrons from MDH to C_L.

To further clarify the nature of MDH/C_L in the presence of NH_3, we explored the conformation of the various components present in the active site of MDH. Figure 4.6 shows schematic representations of the orientation of NH_3 molecule present within the MDH/C_L model. These stable energy conformations show that the relative energies are sensitive to the position of NH_3 molecules in the system.
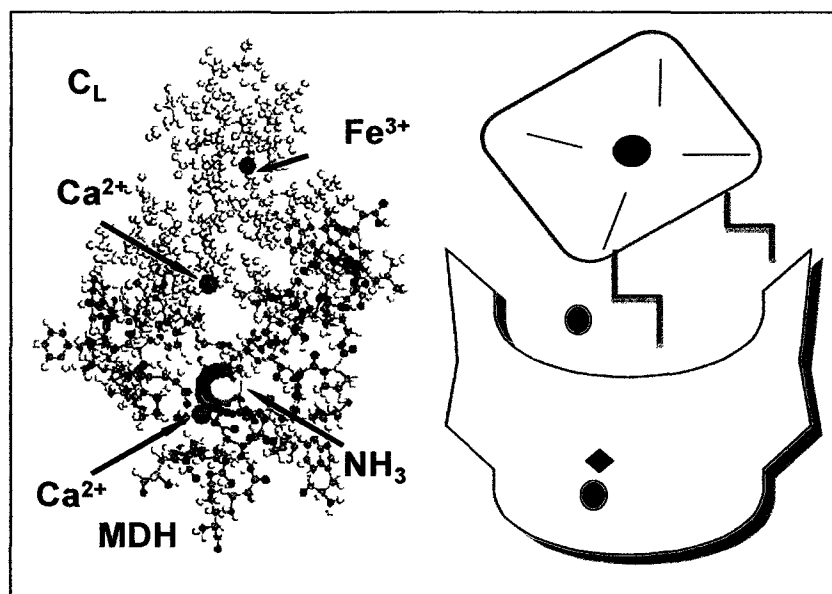
Figure 4.6: Orientation of ammonia molecule in MDH/C_L along with the schematic representation of the same.

Figure 4.7 shows the orientation of NH_3 molecules in the active site of MDH at varying concentration. When one molecule of NH_3 (equivalent to 5.54 mM) is added, it occupies a place close to the active site of MDH. The distance between Ca^{2+} ion and neighboring groups of active site do not show much alteration. Ca^{2+}-O5, Ca^{2+}-N6 and Ca^{2+}-O10 distances are 2.55 Å, 2.21 Å and 2.59 Å, respectively, which is within 0.22 Å of X-Ray crystallographic coordinates of MDH amino acids.
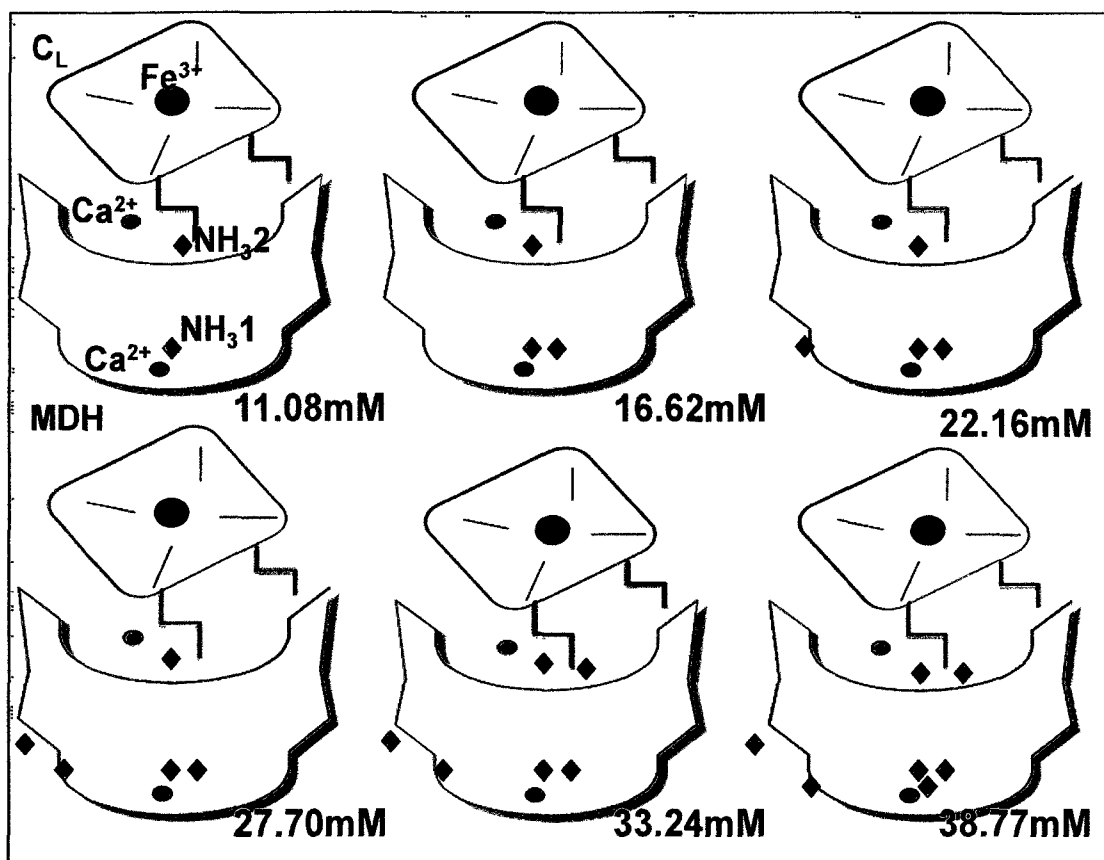
Figure 4.7: Schematic representation of orientation of NH_3 in MDH/C_L complex at increasing concentration. Molecular mechanics calculations were run using DISCOVER module of MS4.4.

The distance between Ca^{2+}-O12 and Ca^{2+}-O13 oxygen atom of Glu177 are 2.62 Å and 2.57 Å, respectively (Table 4.2). The distance between Ca^{2+} and O11 atom of Asn261 is the only active site amino acid that is 0.5 Å deviated from the experimental value. O14 oxygen atom of catalytic base Asp303 is 3.69 Å away from the MDH Ca^{2+}. NH_3 is close to O5 atom of PQQ and O13 atom of GLU177 at a distance of 3.49 Å and 3.52 Å, respectively (Table 4.3).

Distance between NH_3 and Ca^{2+} ion is 3.72 Å. The second NH_3 molecule is present at the interface of MDH and C_L and is at a distance of 11.17 Å from the first NH_3

molecule. Further addition (16.62 mM) increases the concentration of NH_3 to two molecules near the active site of MDH.

Table 4.2: Orientation of active site residues in the presence of increasing NH_3 concentration optimized using DISCOVER module of MS4.4.

NH₃ Conc (mM) →	0	5.54	11.08	16.62	22.16	27.70	33.2	38.77	44.31	49.85	55.39
Ca²⁺--O5	2 39	2 55	2 53	2 79	2 95	2 65	2 84	4 07	5 90	5 05	3 10
Ca²⁺--N6	2 32	2 21	2 51	2 66	2 89	2 64	2 43	3 05	5 49	4 18	4 50
Ca²⁺--O10	2 51	2 59	2 66	2 70	3 05	2 73	2 75	2 53	3 33	2 47	4 87
Ca²⁺--O11	2 64	3 71	3 65	4 08	3 29	3 32	3 22	5 99	5 09	5 97	5 87
Ca²⁺--O12	2 71	2 62	2 76	2 93	2 87	2 36	2 32	2 48	2 97	2 37	2 71
Ca²⁺--O13	2 62	2 57	2 61	3 02	2 96	2 34	2 56	2 45	2 44	2 59	2 08
Ca²⁺--O14	3 67	3 69	3 12	3 31	3 19	3 16	2 27	4 48	4 55	4 11	5 51
Ca²⁺--O15	4 53	4 48	3 86	3 47	3 00	3 18	2 86	4 69	4 87	5 48	5 52

The MDH Ca^{2+} ion moves closer towards NH_3 and Glu177 residue due to the negative charge upon the addition of NH_3. Prior studies have shown that Ca^{2+} forms coordinate bonds with the Asn261 [24]. Since Ca^{2+} moves closer towards NH_3 and Glu177 an alteration is seen in the position of Asn261. Asn261 forms coordinate bond with Ca^{2+} and also forms hydrogen bond with Asp303. The hydrogen bond helps in the positioning of Asp303 for effective electron transfer to take place [24].

Therefore, the distance between Asp303 and Ca^{2+} ion is also changed. O15 atom of Asp303 moves closer to Ca^{2+} atom and the distance is reduced from 4.53 Å to 3.47 Å (Tables 4.2 and 4.3). Figure 4.9 shows the variation of distance between Ca^{2+}-O11 (Asn261) and Ca^{2+}-O15 (Asp303) with an increase in the concentration of ammonia.

Further addition (33.24 mM) of NH$_3$ decreases the distance between Ca^{2+} and O15 atom

to 2.86 Å, as shown in the case of six NH$_3$ molecules.

Table 4.3: Configuration of active site residues with respect to NH$_3$ molecule. N1 and N2 are the two NH$_3$ molecules oriented close to active site optimized using DISCOVER module of MS4.4.

NH$_3$ (mM)	N1-O5	N1-Ca	N1-O13	N1-O14	N1-O15	N1-N2	N2-O14	N2-O15	N2-O13	N2-O5
0	-	-	-	-	-	-	-	-	-	-
5.54	3 49	3 72	3 52	3 91	4 66	-	-	-	-	-
11.09	2 35	3 41	2 92	4 13	3 56	11 17	-	-	-	-
16.62	2 74	3 08	3 2	4 82	4 59	3 72	4 63	4 99	5 17	5 97
22.16	4 12	3 97	2 31	4 4	3 38	4 4	5 8	7 67	5 89	3 65
27.70	3 47	3 05	2 35	3 38	3 3	4 12	6 47	4 87	5 59	2 92
33.24	3 58	2 39	3 02	3 62	3 17	3 5	5 43	5 24	5 19	3 47
38.77	4 09	2 68	2 73	5 46	5 05	3 81	8 36	6 98	6 49	4 16
44.31	3 37	3 34	3 29	5 91	5 26	4 18	8 57	9	6 2	5 31
49.85	3 19	2 38	3 49	5 14	5 95	4 32	8 74	8 89	7 23	5 69

In addition, the proximity of O5 atom of PQQ and O15 atom of Asp303 (Table 4.2) also changes from 3.42 Å to 3.03 Å. It is to be noted that Ca^{2+} acts as Lewis acids by facilitating hydride attack to C5 atom of PQQ during oxidation of methanol [37]. The close proximity of Ca^{2+}, O5 and O15 atoms are favorable orientations for electron and hydride transfer during the oxidation of methanol.

Later, the concentration of NH$_3$ is increased to 38.77 mM. The number of NH$_3$ molecules at the active site is increased to three. This causes a significant change in the orientation of active site residues. As the coordination between the NH$_3$ and Ca^{2+} tend to

increase, the distance between Ca^{2+} and Asn261 increases to 5.99 Å. This results in the drift of Asp303 away from Ca^{2+} and O5 oxygen atom of PQQ. The Ca^{2+}-O15 distance increases to 4.69 Å and O5-O15 goes up to 4.87 Å (Fig. 4.8). A further raise in the concentration of NH_3 leads to additional increase in distance between Asp303 and Ca^{2+}/O5. As the residues move apart, the interaction between them decreases which can result in a lower rate of oxidation of methanol. This might be the possible reason for the low rate of oxidation of methanol at high NH_3 concentration [25].
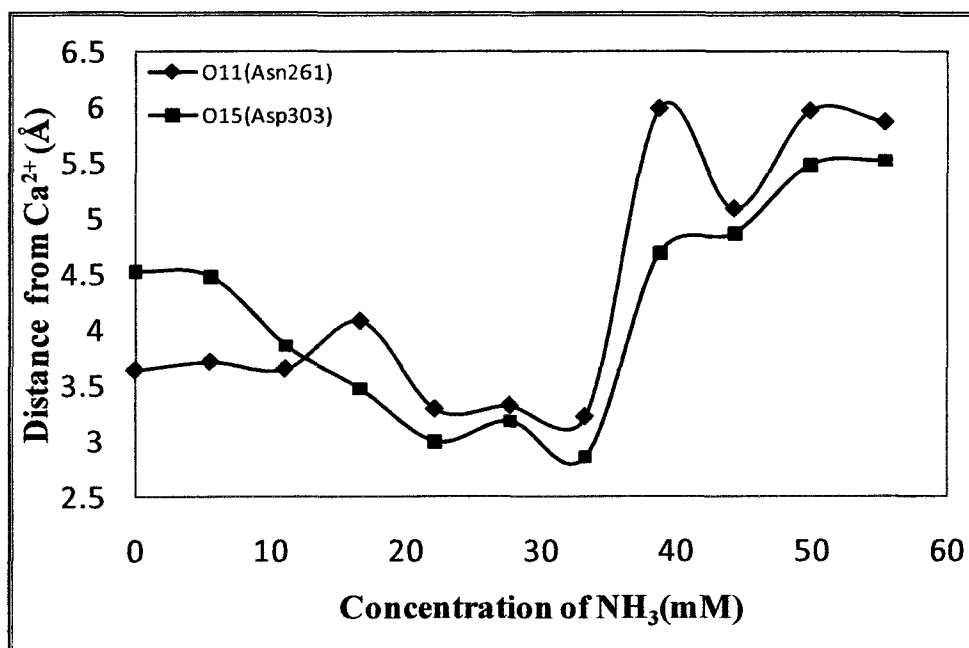
Figure 4.8: Distance of Asn261 and Asp303 from Ca^{2+} ion in varying concentration of ammonia.

The thermodynamic stability of each system is evaluated from the Molecular dynamics calculations and is shown in Fig. 4.9. Addition of NH_3 at a concentration of 5.54 mM does increase the overall stability of the system by 165.74 Kcal/mol compared to that of no NH_3. The system becomes more stable as the concentration of NH_3 increases. The system is most stable at a concentration of 33.24 mM of NH_3.
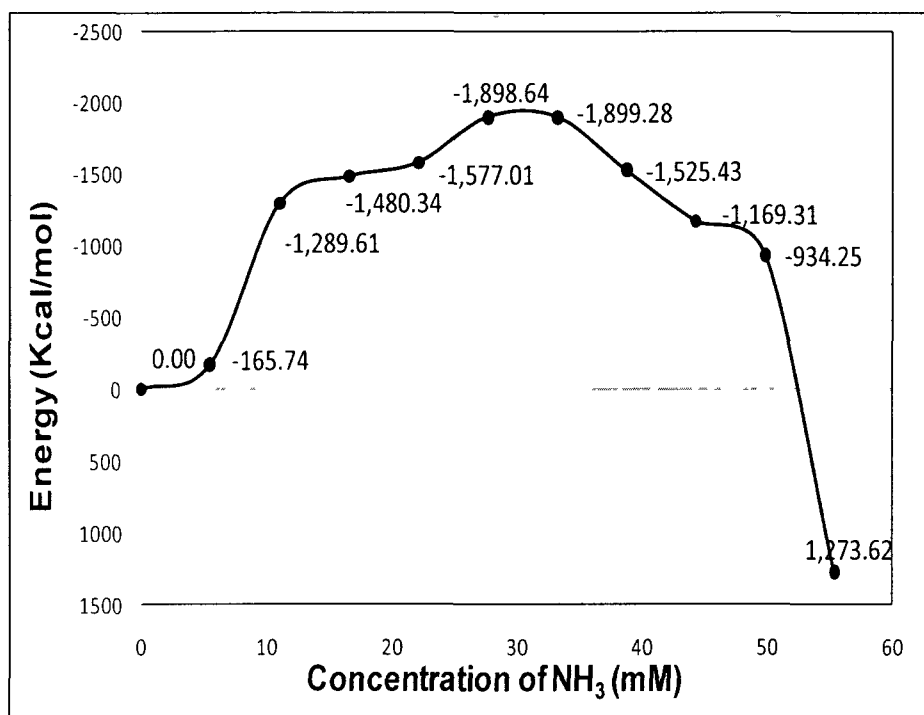
Figure 4.9: Thermodynamically stable energy of MDH/C$_L$/NH$_3$ system immersed in water. Energy was obtained using MD calculations at 298 K using COMPASS forcefield.

While comparing the orientation of the active site residues with the energy of the system at the same concentration, it is observed that it is at this concentration that the distance between Ca^{2+} and O15 oxygen atom of Asp303 are less. A further increase in concentration of NH$_3$ decreases the stability of the system. In addition to that, an increase in the distance between Ca^{2+} and Asn261/Asp303 was also observed (Table 4.2). When the concentration of ammonia is increased to 55.39 mM, the system becomes 1273.62 kcal/mol less stable than the system with no ammonia molecules.

In order to verify the active site residue further, activity diffusion coefficient values of each component was analyzed. The diffusion coefficients values of various components of the active site were obtained from the slope of Mean Square Displacement graphs and shown in Fig. 4.10. It is detected that as we increase the concentration of NH$_3$, the diffusivity of Ca^{2+} and ammonia molecule closest to the active site increases. The

increase is less prominent at low NH_3 concentrations, but rises rapidly at high concentration of NH_3. A similar trend is seen in the case active site amino acids such as Asn261, Asp303, and Glu177.
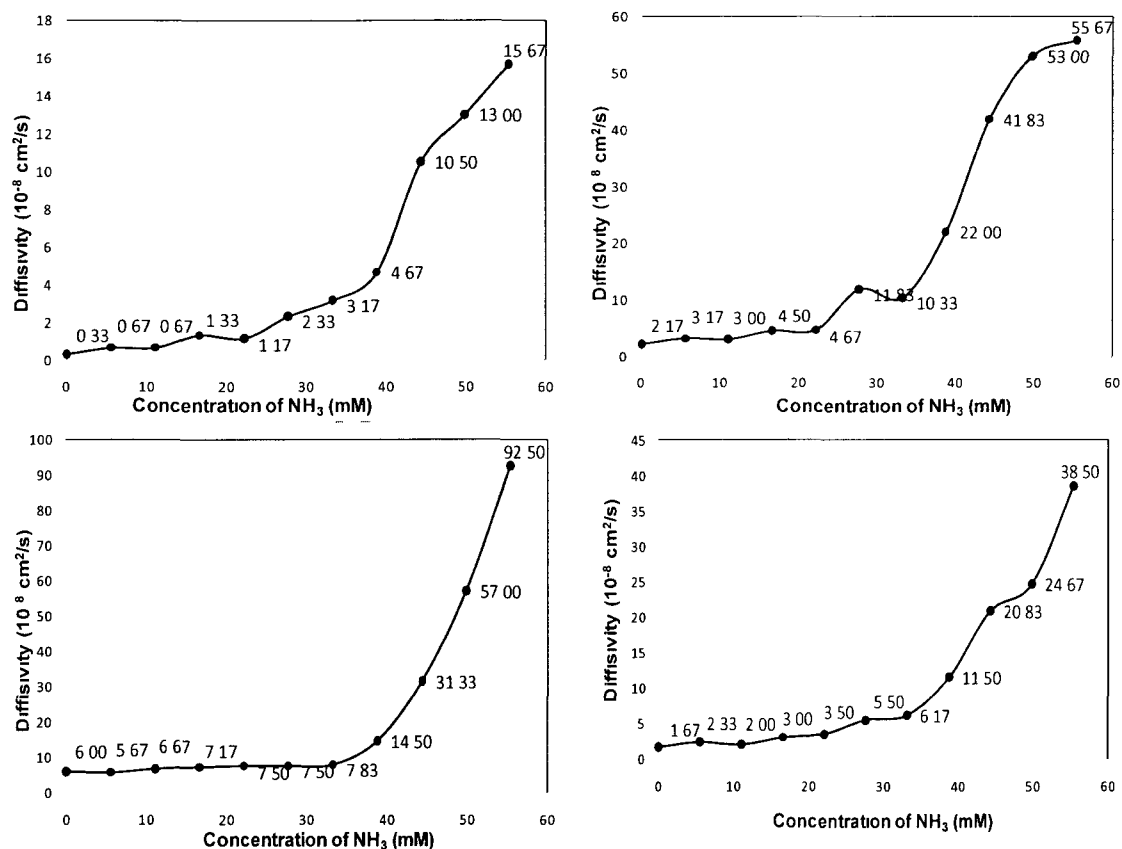
Figure 4.10: Diffusion coefficient values of a) MDH Ca^{2+}, b) Asn261, c) Glu177, and d) Asp303 at 298 K obtained from the MD calculations.

From Figure 4.11 the MDH Ca^{2+} ion has the least magnitude of diffusivity coefficient when compared to other amino acids present in the active site. This shows structural importance of Ca^{2+} ions. Ca^{2+} ion forms six coordinate bonds with the neighboring atoms such as O5, N6 and O10 atoms of PQQ, O11 oxygen atom of Asn261 and O12, O13 oxygen atoms of Glu177 [82].

A slight variation in the position of MDH Ca^{2+} can cause larger variation in the position of the active site amino acids. This shows that even though the magnitude of diffusivity is low in Ca^{2+}, it can cause larger magnitude of diffusion in the neighboring amino acids.
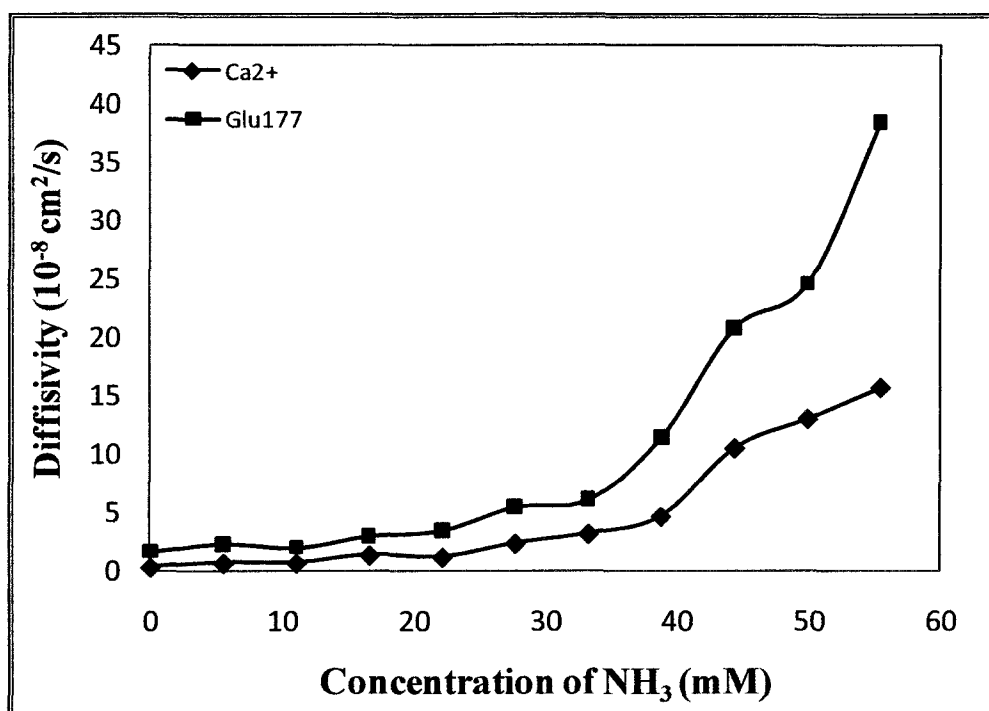
Figure 4.11: Figure compares the diffusivity coefficient of MDH Ca^{2+} and Glu177 in varying concentration of NH_3.

While comparing the magnitude of diffusivity coefficient of amino acids Asp303, Asn261, and Glu177 (Fig. 4.12) for a particular ammonia concentration, we do observe that Asp303 has the highest and Glu177 has the least diffusivity coefficient. The possible reason for this variation is because Glu177 has two coordinate bonds with Ca^{2+} ions, which restrict its mobility. Asn261 is bound to Ca^{2+} through a single coordinate bond, which also stabilizes the position of Asn261, but the stability is less than that of Glu177. Asp303 does not form any coordinate bond with Ca^{2+} ion. This allows Asp303 to have

less structural restrictions compared to Asn261 and Glu177. Due to this reason, the presence of hydrogen bond between Asn261 and Asp303 is very important to stabilize the position of Asp303 during the oxidation of methanol.
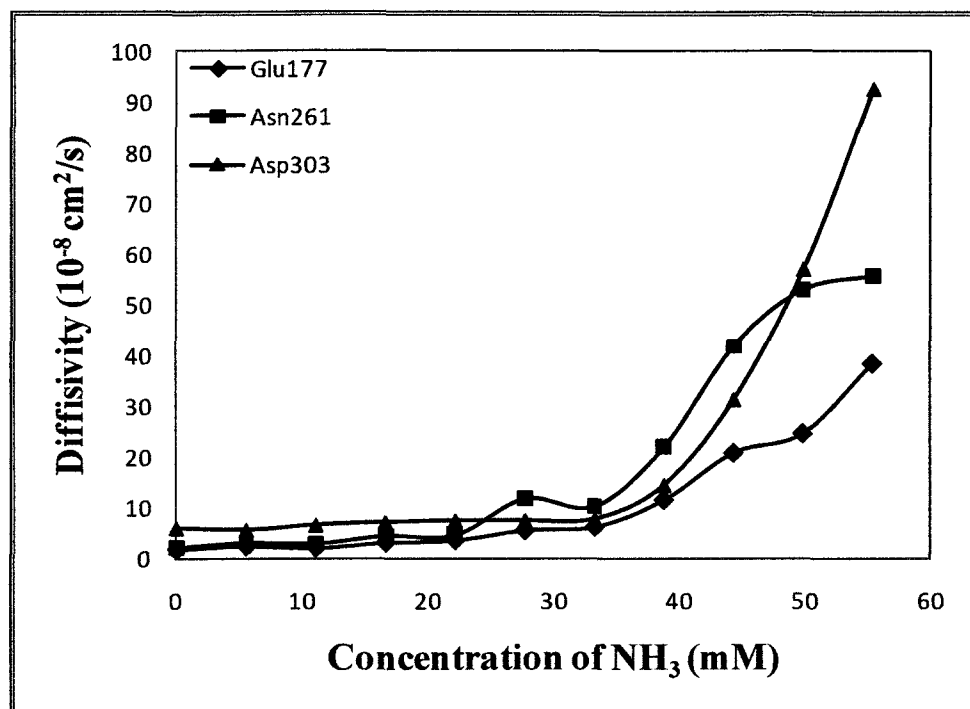
Figure 4.12: Figure compares the diffusivity of active site amino acids along with Glu177, Asn261 and Asp303 in varying concentration of ammonia.

Experimental studies done by Anthony et al. showed that the rate of reaction of MDH increases by increasing the concentration of methylammonium chloride from 0 to 30 mM at a pH of 9.0 [79]. Other studies with carbon electrode have shown that the activity of the enzyme increases linearly with an increase in concentration of NH_3 from 3 mM to 60 mM. A further increase in concentration of NH_3 did not increase the rate of reaction [83].

From the energy and diffusivity information obtained from the simulations, we do suggest that an increase in concentration beyond 33 mM of NH_3 does decrease the

stability of enzymes and affects the orientation of residues in the active side of MDH. This might be the possible reason for inhibition of MDH activity in the presence of excess of NH_3.

4.5 Conclusion

Monte Carlo adsorption calculations were run at 298 K to observe the docking of MDH and C_L in the presence of varying concentration of NH_3. It was observed that most of the NH_3 molecules oriented themselves at the interface between MDH and C_L. In addition, the interaction energy in the presence of NH_3 is stronger compared to the absence of ammonia. The negative interaction energy values suggest that the enzymes readily bind with each other. Once an ammonia molecule is added, the interaction energy between MDH and C_L becomes more stable by 108.5 kcal/mol. This suggests that ammonia may play a role of ligand that assists in binding MDH and C_L during the docking process.

Molecular mechanics calculations were then run to examine the effect of NH_3 inside the MDH/C_L system. Ca^{2+} ion of MDH, PQQ and Asp303 are nearest at a concentration of 33.24 mM of NH_3. Molecular dynamics simulations were run at 298 K using COMPASS forcefield to find the refined and thermodynamically stable configurations of NH_3 in MDH/C_L. The system was most stable at a concentration at the same concentration. As the concentration of ammonia increased at the active site of MDH, the diffusivity coefficient of MDH Ca^{2+}, Asn261 and Asp303 were also increased. All three of them showed a similar trend with varying magnitude.

There was a slight increase in the diffusivity coefficients of when the concentration of NH_3 was increased from 0 to 33.24 mM. Additional increases in

concentration of NH3 led to a rapid rise in the diffusivity coefficient of Ca^{2+}, Glu177, Asn261, and Asp303 and decrease in system stability. Ca^{2+} plays an important role in the stability of the active site of MDH. A slight variation in the position of Ca^{2+} can cause large variation in active site components. The magnitude of diffusivity coefficient for a particular concentration of ammonia is least in Ca^{2+} and maximum in Asp303. Ca^{2+} is coordinated to PQQ, Glu177, and Asn261 which limits the diffusivity of the ion. Small diffusivity in Ca^{2+} caused higher magnitude of diffusion in Asn261, which in turn increases the diffusivity coefficient of Asp303 as it forms hydrogen bond with the latter. The position of the closest NH_3 molecule in the active site of MDH obtained from MM calculations was further used in DFT simulations to investigate the role of NH_3 in the oxidation of methanol.

CHAPTER 5

EXTENDED ADDITION-ELIMINATION MECHANISM

5.1   Introduction

One of the most discussed methanol oxidation mechanism is the Addition-Elimination (A-E) reaction. This mechanism consists of three steps to oxidize methanol shown in Chapter 2. In the case of extended A-E mechanism, once the methanol is oxidized to formaldehyde and PQQ is completely reduced, re-oxidation of PQQ is initiated. H16 proton gets attracted to ammonia molecule and hence gets transferred from O5 carbonyl oxygen to the nitrogen of ammonia. In the final step, H16 hydrogen gets transferred to O13 oxygen atom of Glu177.

5.2   Computational Details

In order to investigate the role of ammonia in the oxidation of methanol, we consider the A-E reaction mechanism in this chapter. The reason for using this mechanism is the detection of hemiketal intermediate at the C5 carbonyl group of PQQ (See Fig. 2.2 from Chapter 1). This structure is the first intermediate formed during the A-E mechanism [29-30]. Two models were considered for investigating the mechanism of methanol oxidation in the presence of ammonia. Model 1 (Fig. 5.1) consists of PQQ, Ca^{2+} ion, ammonia, and the probable catalytic base Asp303. In this model, PQQ acts as

60

the cofactor for oxidation of methanol. Researchers have shown that Ca^{2+} ion facilitates attack on C5 and decreases the pKa of methanol substrate. Asp303 is the probable catalytic base which initiates the oxidation of the substrate [23-24, 26, 32].
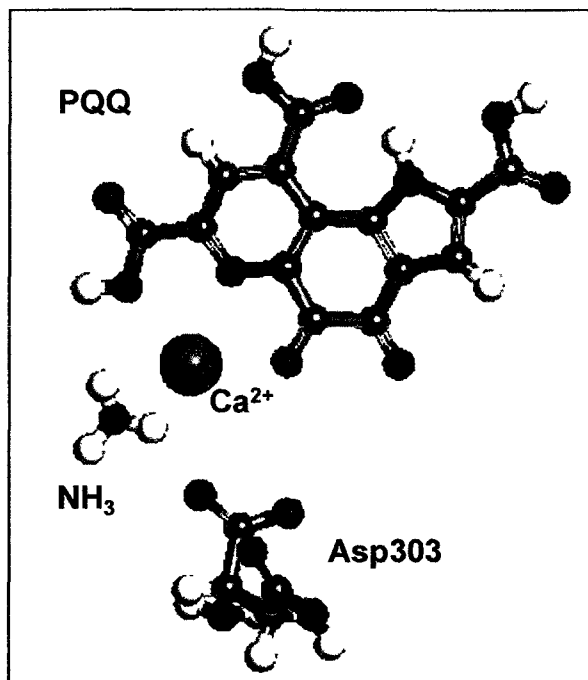
Figure 5.1: Model 1 of active site of MDH.

Model 2 (Fig.5.2) is comparatively bigger as we added two more amino acids and three water molecules to the system. Glu177 and Asn261 are the two amino acids introduced in Model 2. Crystallographic data shows that Asn261 forms hydrogen bond with Asp303, stabilizing the position of Asp303 to initiate the oxidation of methanol. Ca^{2+} ion forms coordinate bonds with both the oxygen atoms of Glu177. It is also suggested that the hydrogen atoms during re-oxidation are transferred to the periplasm via Glu177. Experimental studies also show the presence of water molecules in the active site of MDH; hence, three water molecules were added to the system [24]. The models are optimized using Density Functional Theory simulations. It is one of the most accurate

quantum mechanical methods to predict the properties of atoms and molecules within the active site of an enzyme. DFT methods are more cost and time efficient compared to Gaussian methods. Also, the computational cost increases at the rate of N^3 or lesser in the case of DFT, but in the case of *ab initio* method, the cost increases at the rate of N^4 or more. N represents the number of atomic orbitals [84].
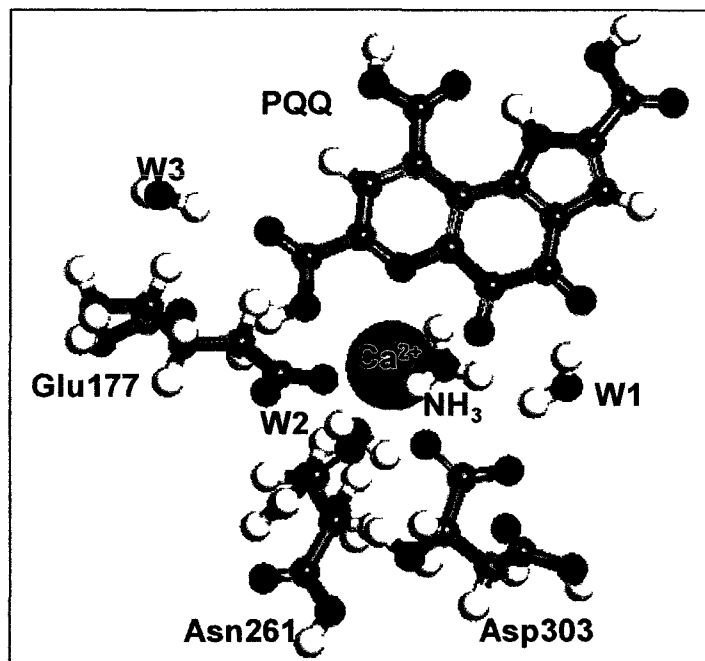
Figure 5.2: Model 2 of active site of MDH.

The numerical basis set used in DMOL^3 module is as accurate as the Gaussian bases in predicting the optimized geometry. In fact, the numerical basis set used by DMOL^3 can reduce or eliminate the basis set superposition error (BSSE) much more efficiently compared to Gaussian bases. The main reason for the low BSSE is because the DMOL^3 module uses the exact DFT-spherical atomic orbitals generated numerically. In the case of Gaussian, the orbitals are not numerically generated. Instead, linear combinations of multiple Gaussians are used to denote the electron density around the

nuclei [84]. The simulations were carried out using DMOL^3 module of Materials Studio4.4 [70]. Gradient Approximation Method (GGA) was employed with Becke exchange, plus Lee-Yang-Parr (BLYP) correlation functional and DNP basis set. In these simulations, Harmonic vibrational frequencies are also calculated in order to confirm that the stationary points on the potential energy surface are either all local minima or transition state. In the case of local minima, all the frequencies are real and transition state there is one imaginary frequency [36].

All the reactant, intermediates and product were optimized. Atom pairing of reactant and product involved in each step is done in order to generate a 3D trajectory file to represent the reaction path preview. Transition state calculations are obtained by using LST/OST conjugate gradient method. The transition state obtained are optimized and confirmed and the energies are reported.

5.3 Results and Discussion

Prior to finding the transition state, we optimize the reactant Models and compare the distance between the active site components with that of the X-Ray crystallographic structure.

Table 5.1 shows the distance measurements of both Models 1 and 2 along with the experimental values. The optimized active site models of MDH using the dielectric value of 4 shows that the distance measurements are in close agreement with the experimental values. Once measurements are confirmed, the structures that form the intermediates and the product are optimized and the transition states are obtained. Assessment on the movement of atoms, structural conformation and energies for each model are discussed in the following section.

Table 5.1: Refined distance between Ca^{2+} and neighboring active site residues in Models 1 and 2. The structures were optimized suing $DMOL_3$ module of MS4.4.

Length	X-Ray (Å) [24]	Model 1 (Å)	Model 2 (Å)
Ca^{2+}--O5	2.25	2.42	2.39
Ca^{2+}--N6	2.32	2.51	2.43
Ca^{2+}--O10	2.44	2.49	2.50
Ca^{2+}--O14(Asp303)	3.20	3.33	3.29
Ca^{2+}--O15(Asp303)	4.60	4.95	4.73
Ca^{2+}--O11(Asn261)	3.13	-	3.27
Ca^{2+}--O12(Glu177)	2.38	-	2.46
Ca^{2+}--O13(Glu177)	2.81	-	2.79

5.4 Reaction Profile of Model1

The components involved in Model 1 are PQQ, Ca^{2+} ion, Asp303, and ammonia. To initiate the oxidation reaction, a molecule of methanol was added to the system. The orientation of various components in the system was altered such that three reactant systems were built and optimized. The most stable orientation was used for further transition state calculations. A similar method was applied to the intermediate and product systems. The reaction path consists of reactant, three intermediates, and the product system. Co-ordinates of the reactant system were compared with that of the X-Ray crystallographic data. The configuration of methanol is such that the H16 is oriented towards Asp303 and O16 oxygen atom faces PQQ. The distance between H16 hydride of methanol from O15 oxygen of Asp303 is 2.81 Å and the distance between C5 carbonyl from O16 oxygen of methanol is 3.78 Å.

5.4.1   Formation of Hemiketal Structure

In the first step, the substrate methanol dissociates such that hydride H16 moves towards O15 atom of Asp303 and the rest of the methanol gets attached to C5 carbon atom of PQQ. This dissociation is confirmed from the distance measurements. The distance between O15 oxygen of Asp303 and H16 hydrogen of methanol decreases from 2.81 Å in the reactant to 2.01 Å in the transition state (Fig. 5.3).
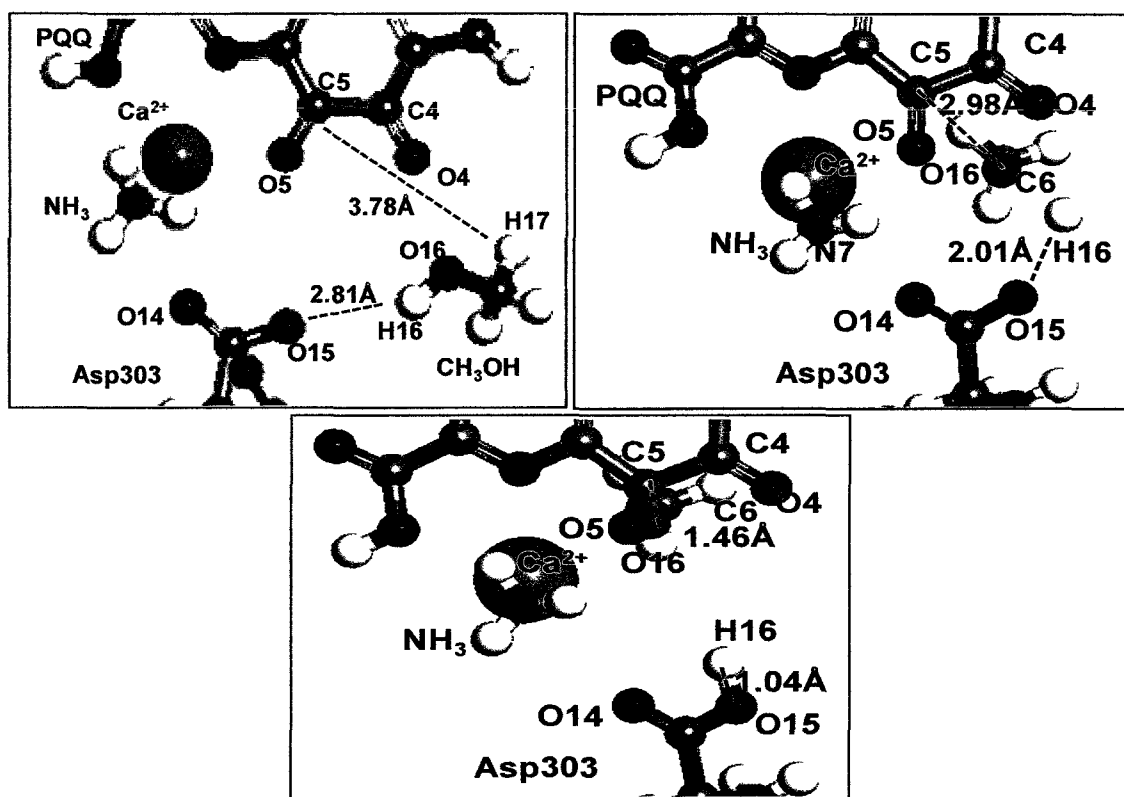
Figure 5.3: Figure shows orientation of active site components of Reactant, Transition state 1 and first intermediate system.

The distance further reduces 1.04 Å in the first intermediate indicating the bond formed between them. On the other hand, C5-O16 distance reduces from 3.78 Å to 2.98 Å in the transition state. C5 binds with O16 as the distance reduces to 1.46 Å and forms a hemiacetal complex with PQQ. The transition state is 13.9 kcal/mol less stable compared

to the reactant. Therefore, the activation energy for this step is 13.9 kcal/mol. First, intermediate formed is 8.8 kcal/mol less stable compared to the reactant. The single point imaginary frequency is -1752 cm^{-1} with an intensity of 1513, which corresponds to the stretching and contraction of H16-O16 bond.

5.4.2   Transfer of Hydride from Asp303 to PQQ

The second step involves the transfer of hydride from O15 oxygen of Asp303 to O5 carbonyl oxygen of PQQ. O15-H16 distance increases from 1.04 Å to 2.91 Å in the transition state (Fig. 5.4) indicating the detachment of O16 and H16 atoms.
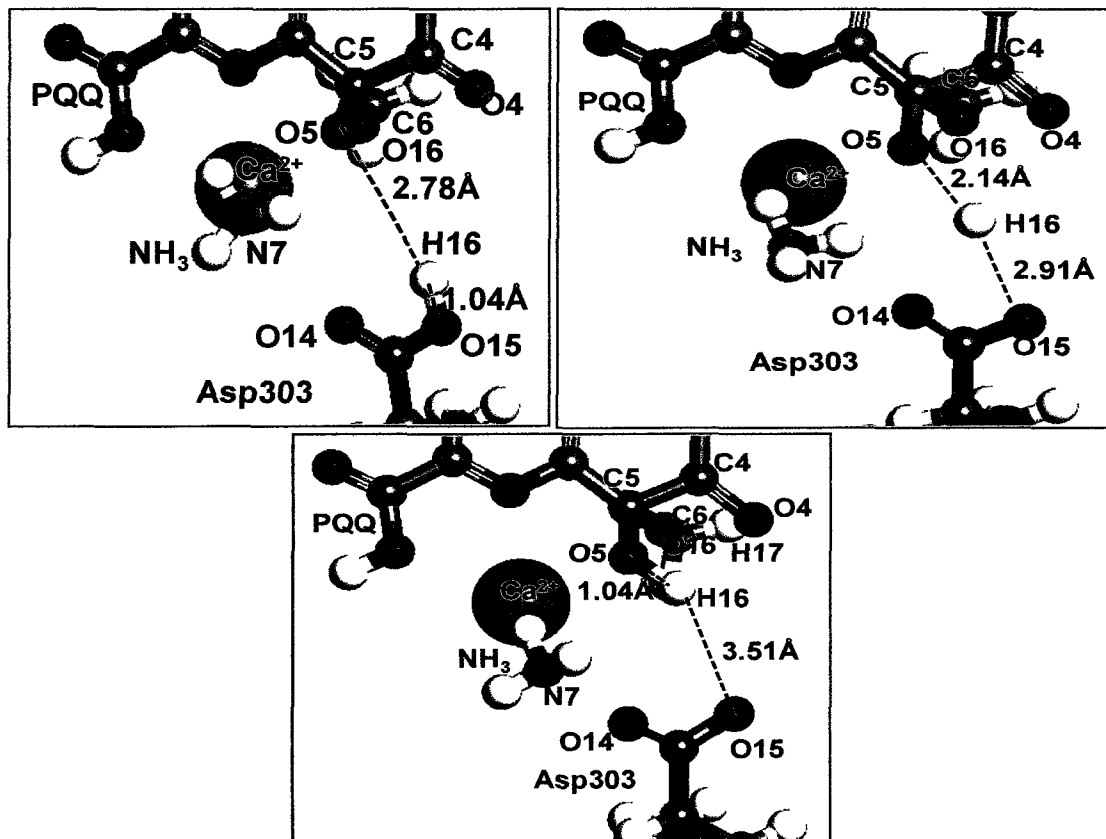
Figure 5.4: Figure shows orientation of active site components of first intermediate, Transition state 2, second intermediate.

H16 moves towards O5 as the distance between them reduces from 2.78 Å to 2.14 Å in the transition state. H16 binds with O5 as the distance further reduces to 1.04 Å. The energy barrier for the transfer of hydrogen is 7.8 kcal/mol. Transition state of this step is 16.5 kcal/mol less stable when compared to the reactant system. The second intermediate formed in this step is 3.2 kcal/mol more stable when compared to first intermediate. The imaginary frequency corresponding to this step is -60 cm^{-1} with an intensity of 420. The frequency is due to the stretching and contraction of bond between O16 and H16 atoms.

5.4.3   Reduction of PQQ and Formation of By-product

This step involves complete reduction of PQQ by transfer of hydride H17 to O4 carbonyl oxygen of PQQ and release of formaldehyde (Fig. 5.5).
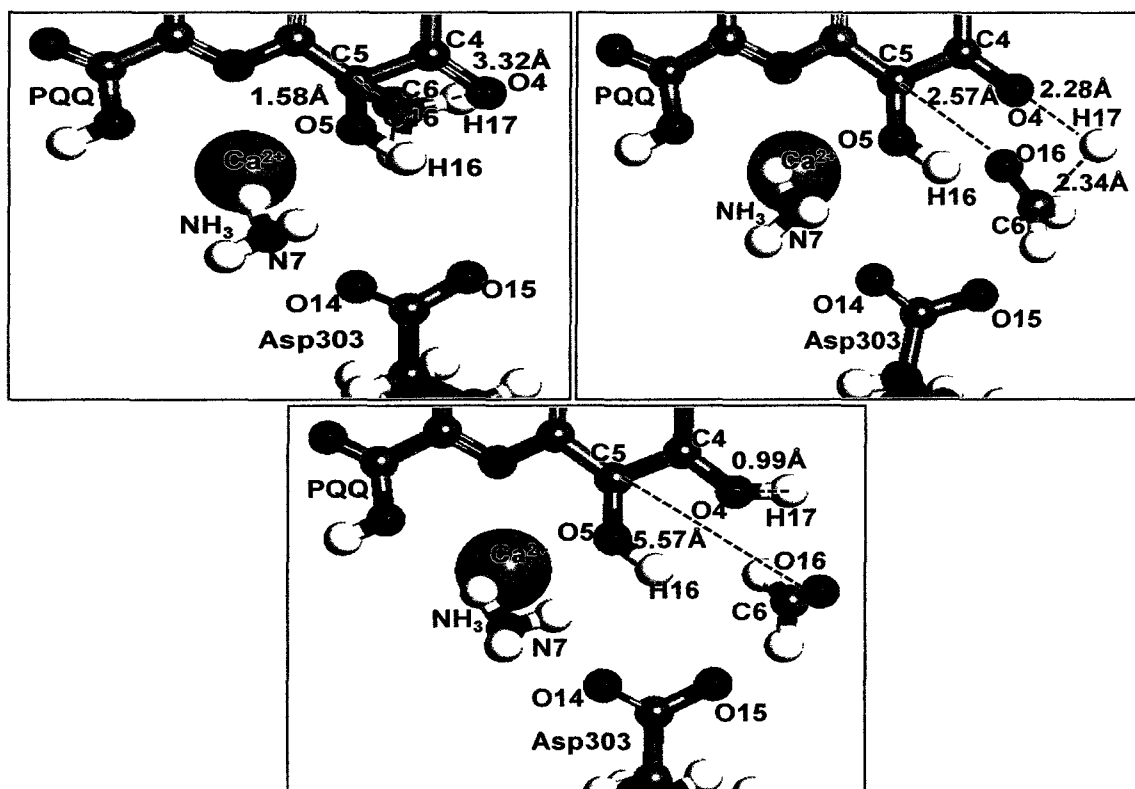
Figure 5.5: Figure shows orientation of active site components of second intermediate, Transition state 3 and third intermediate.

It is observed that the C6-H17 distance increases from 1.11 Å to 2.34 Å in the transition state verifying the detachment of hydrogen from the methyl group. The distance between them further increases to 4.36 Å. The distance between O4 and H17 decreases from 3.32 Å to 2.28 Å in the transition state. The distance finally reduces to 0.99 Å, confirming the binding of H17 with O4 carbonyl oxygen of PQQ. Simultaneously the C5-O16 distance increases from 1.58 Å in the second intermediate to 2.57 Å evidencing the breaking of bond. The distance settles at 5.57 Å leading to the release of formaldehyde.

The energy barrier for this step is 8.2 kcal/mol with an imaginary frequency of -790 cm^{-1}. The frequency corresponds to the stretching of bonds between C5-O16 and O4-H17. The system with reduced PQQ is 1.0 kcal/mol less stable compared to the reactant system and 4.6 kcal/mol more stable than the system with hemiacetal complex.

5.4.4   Partial Re-oxidation of PQQ

This step is followed after the A-E reaction and involves re-oxidation of PQQ. One of the hydride (H16) gets attracted to N7 nitrogen atom of ammonia leading to partial re-oxidation of PQQ. The distance measurement shows that the O4-H16 bond distance increases from 1.01 Å to 2.23 Å in the transition state. The distance finally increases to 4.98 Å. H16 moves towards N7 as the distance between these two atoms decreases from 2.63 Å to 2.07 Å in the transition state. H16 binds with N7 as the bond distance reduces to 1.11 Å, evidence of the binding of atoms (Fig. 5.6).
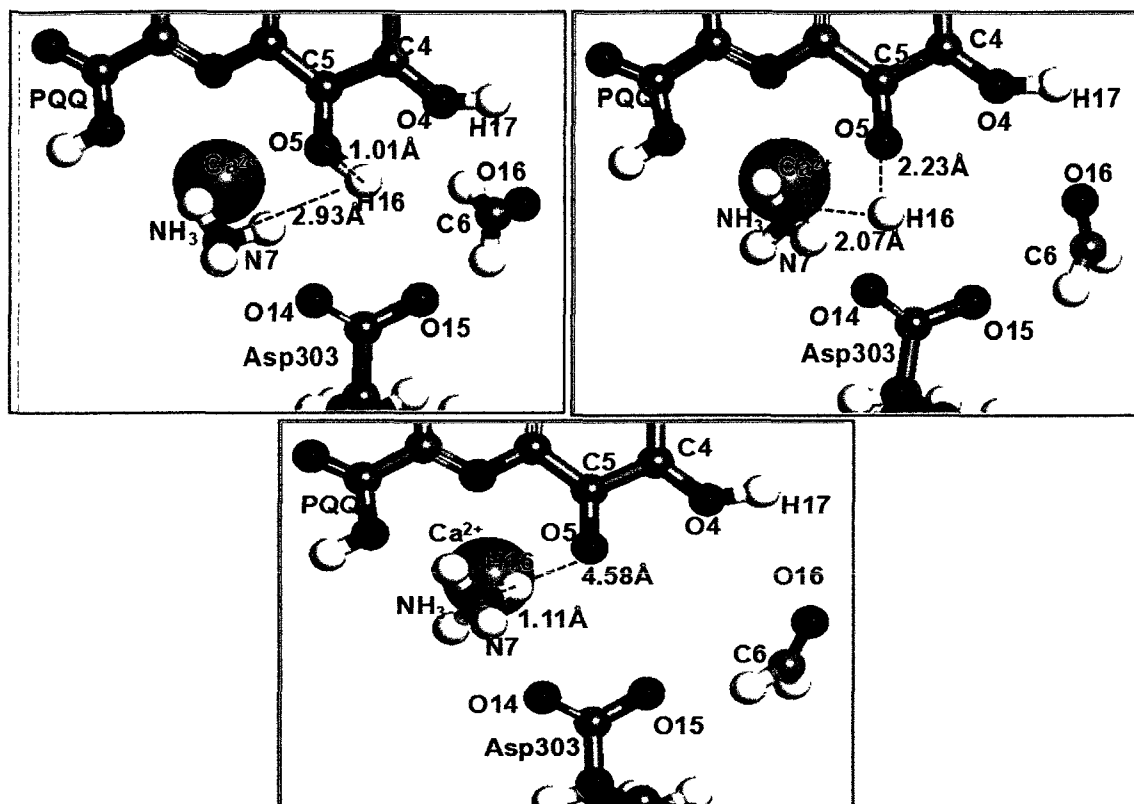
Figure 5.6: Figure shows orientation of active site components of third intermediate, Transition state 4 and Product.

The energy barrier for this step is 7.2 kcal/mol with an imaginary frequency of -5334 cm^{-1}. The imaginary frequency corresponds to bond stretching between O4 and H16 atoms. The partially oxidized PQQ system is 2.9 kcal/mol less stable compared to the system with completely reduced PQQ and 3.9 kcal/mol less stable compared to the reactant. Figure 5.7 shows the energy profile of the entire reaction mechanism.
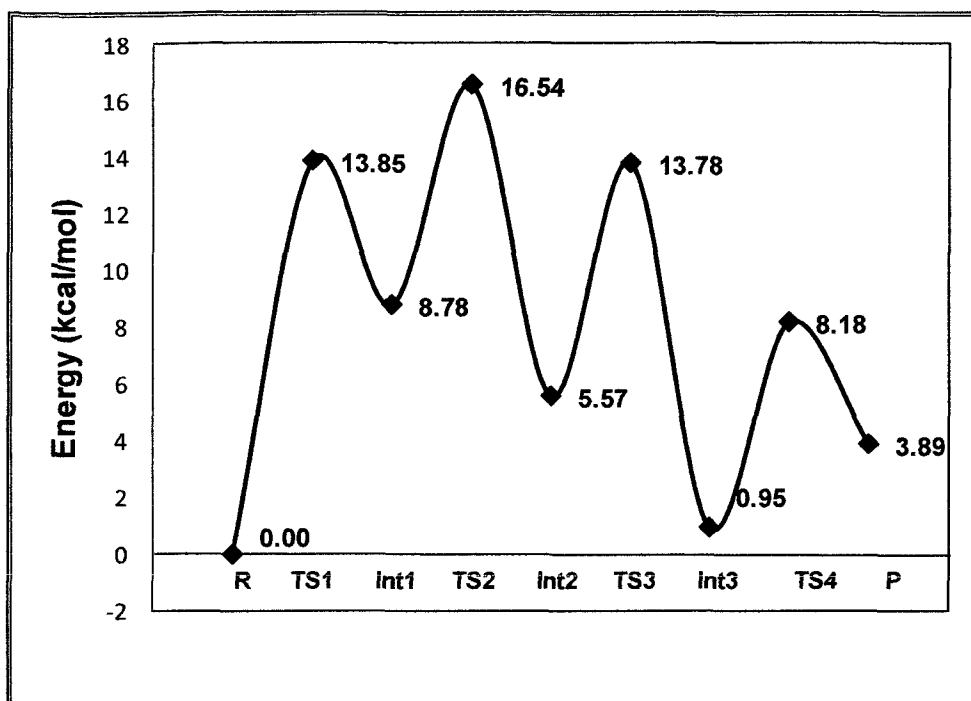
Figure 5.7: Energy profile of the extended A-E mechanism.

5.5   Reaction Profile of Model 2

Model 2 consists of the cofactor PQQ, Ca^{2+} ion, Asp303, Asn261, Glu177, and ammonia. To this system we added a single molecule of methanol. The orientation of various components was modified such that three reactant systems were built and optimized. The most stable reactant configuration was chosen for further simulation of the transition state. The same method was applied to the rest of the intermediate and product systems, too. The reaction path consists of reactant, four intermediates and product systems. In the reactant system, methanol orients itself in such a way that H16 faces towards Asp303 and O16 towards PQQ. The initial distance between O15 oxygen atom of Asp303 and H16 hydrogen of methanol is 2.70 Å, and the distance between C5 carbonyl group of PQQ and O16 of methanol is 3.85 Å.

5.5.1 Dissociation of Substrate

The mechanism Step 1 involves dissociation of methanol in such a way that the proton H16 binds with O15 atom of Asp303 and rest of the group gets attached to the C5 carbonyl atom of PQQ (Fig. 5.8). The O15-H16 was initially at 2.70 Å, which reduces to 2.54 Å in the transition state. The distance finally decreases to 1.04 Å indicating the bound state. The C5-O16 distance was 3.85 Å which reduced to 3.37 Å in the transition state. The bound state distance of C5-O16 is 1.51 Å. The product of Step 1 is the first intermediate.
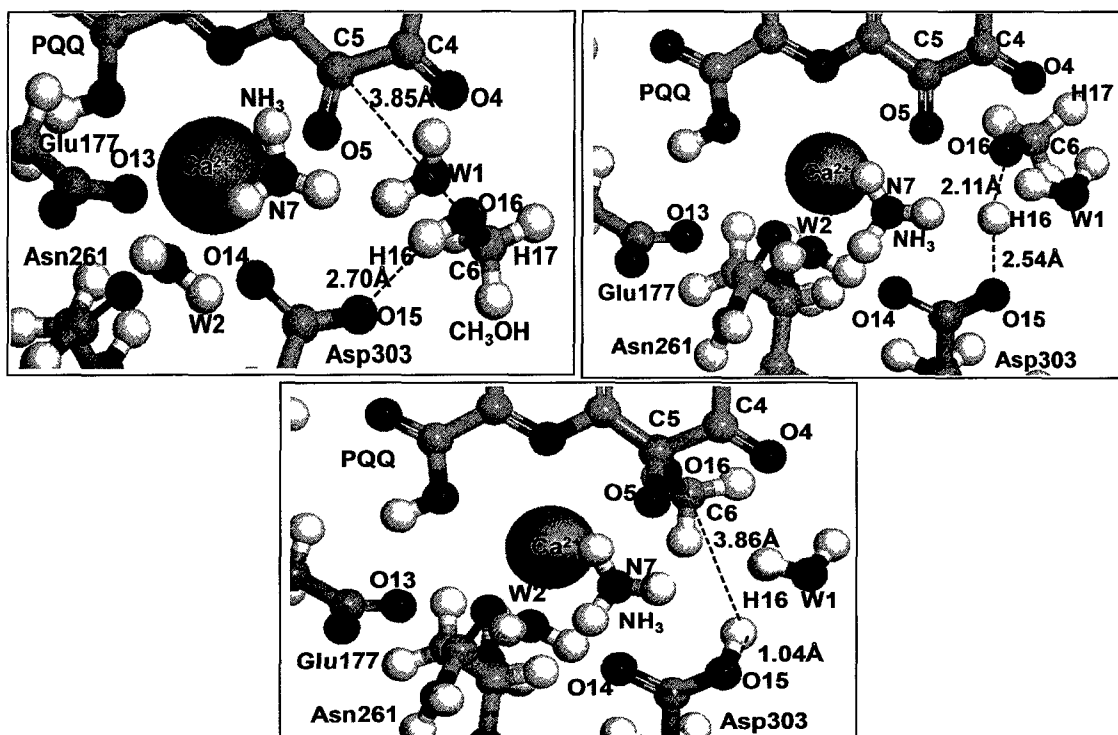
Figure 5.8: Figure shows orientation of reactant, Transition state 1 and first intermediate system.

Single point energy values show that the intermediate is 5.1 kcal/mol less stable compared to that of the reactant. The transition state between the reactant and first intermediate is 12.8 kcal/mol less stable than the reactant 4713 cm^{-1}. The imaginary

frequency of 4713 cm^{-1} corresponds to the dissociation of H16 from methanol group. Idupulapati et al. did computational studies on A-E reaction in the absence of ammonia and the energy barrier for the first step was found to be 28.0 kcal/mol [36]. The presence of ammonia molecule has greatly reduced the energy barrier in the abstraction of proton from methanol.

5.5.2   Formation of Semiquinone PQQ

In the second step, PQQ is partially reduced to form a semiquinone group. Hydride H16 is transferred from O15 oxygen atom of Asp303 to O5 oxygen atom of PQQ. The distance between O15 and H16 increases from 1.04 Å to 2.87 Å in the transition state (Fig. 5.9).
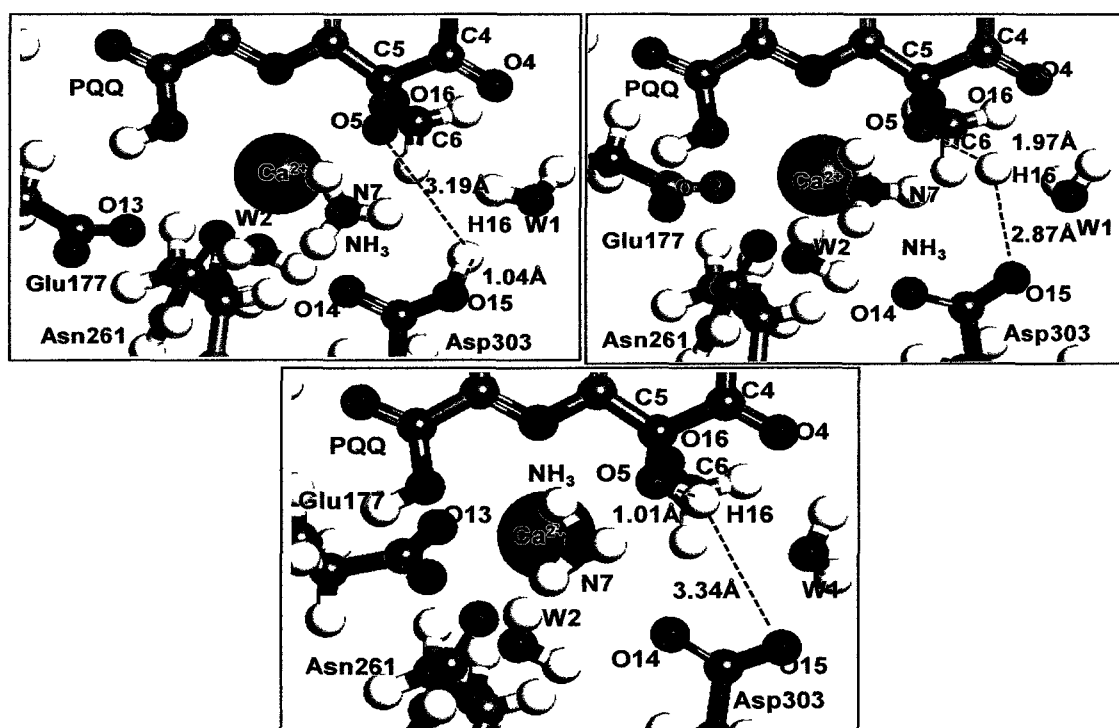
Figure 5.9: Figure shows orientation of first intermediate, Transition state 2 and second intermediate system.

The distance increases to 3.34 Å in the second intermediate, indicating dissociation of O15-H16 bond.The O5-H16 distance decreases from 3.08 Å in the first intermediate to 1.97 Å to 1.01 Å, indicating the association of O5-H16 bond. Second intermediate structure is 8.4 kcal/mol less stable when compared to the first intermediate and has an energy barrier of 7.2 kcal/mol. The imaginary frequency corresponding to the second transition state is 129 cm^{-1}, which represents the abstraction of H16 from O14 of Asp303 to O5 of PQQ.

5.5.3   Complete Reduction of PQQ

PQQ gets completely reduced to PQQH$_2$ in the third step. C5-O16 bond distance dissociates and H17 from the methyl group binds with O4 atom of PQQ (Fig. 5.10).
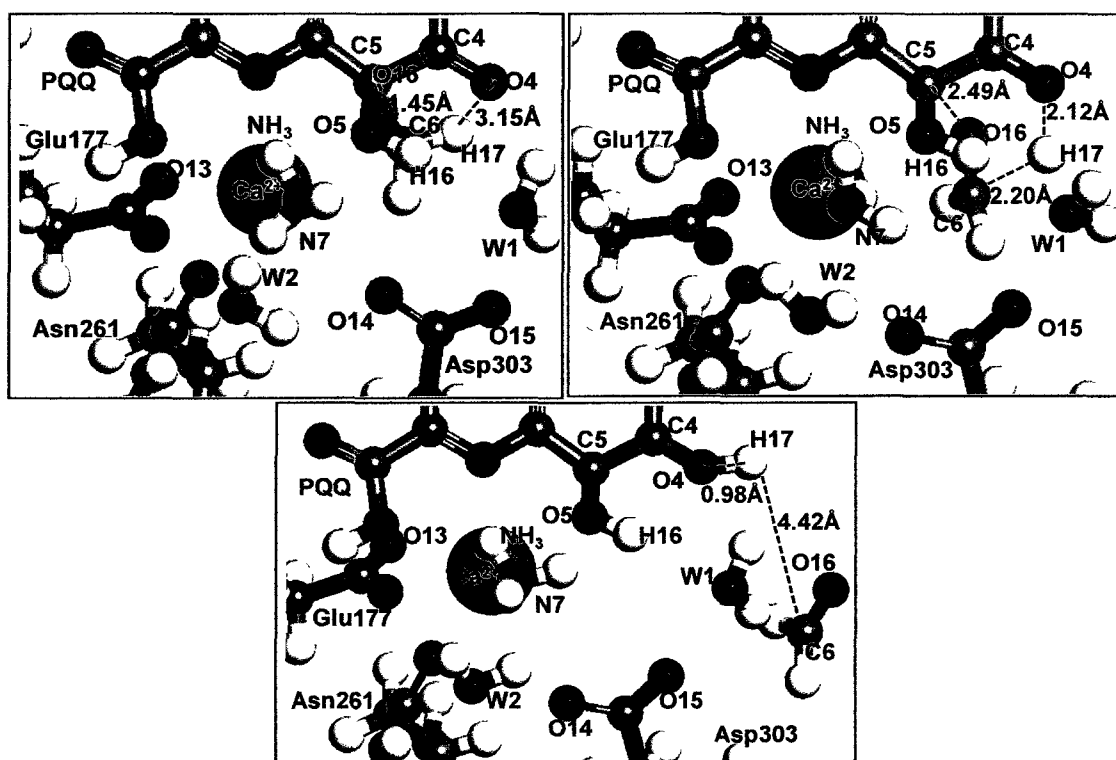
Figure 5.10: Figure shows orientation of second intermediate, Transition state 3 and third intermediate system.

O16 atom is initially at a distance of 1.45 Å from C5 carbonyl atom in the case of second intermediate. The distance between them increases to 2.49 Å in the transition state which further increases to 5.41 Å, indicating the release of formaldehyde and completion of oxidation of methanol. The distance between O4 and H17 decreases from 3.15 Å to 2.12 Å in the transition state. The distance between them finally reduces to 9.98 Å. The active site with reduced PQQ is 8.6 kcal/mol more stable compared to the partially reduced PQQ. The energy barrier for this step is 6.5 kcal/mol with an imaginary frequency of 1927 cm^{-1}. The frequency corresponds to the breaking of C5-O16 bond which results in the formation of formaldehyde.

5.5.4 Re-oxidation of PQQ

The reduction of PQQ is followed by re-oxidation of the same in step four. Proton H16 bound to O5 atom of PQQ gets attracted to ammonia molecule due to the negative charge of N7 nitrogen atom. The O5-H16 distance increases from 0.98 Å to 2.02 Å and to 2.67 Å indicating the dissociation of O5-H16 bond.

Proton released from PQQ binds with ammonia to form ammonium forming the fourth intermediate (Fig. 5.11). This is explained by the decrease in the N7-H16 distance from 2.50 Å to 2.21 Å and further reduces to 1.04 Å. Energy of the system shows that the fourth intermediate is 3.1 kcal/mol less stable when evaluated against completely reduced form of PQQ. The imaginary frequency equivalent to the transition state is 2611 cm^{-1} with an energy barrier of 7.8 kcal/mol.
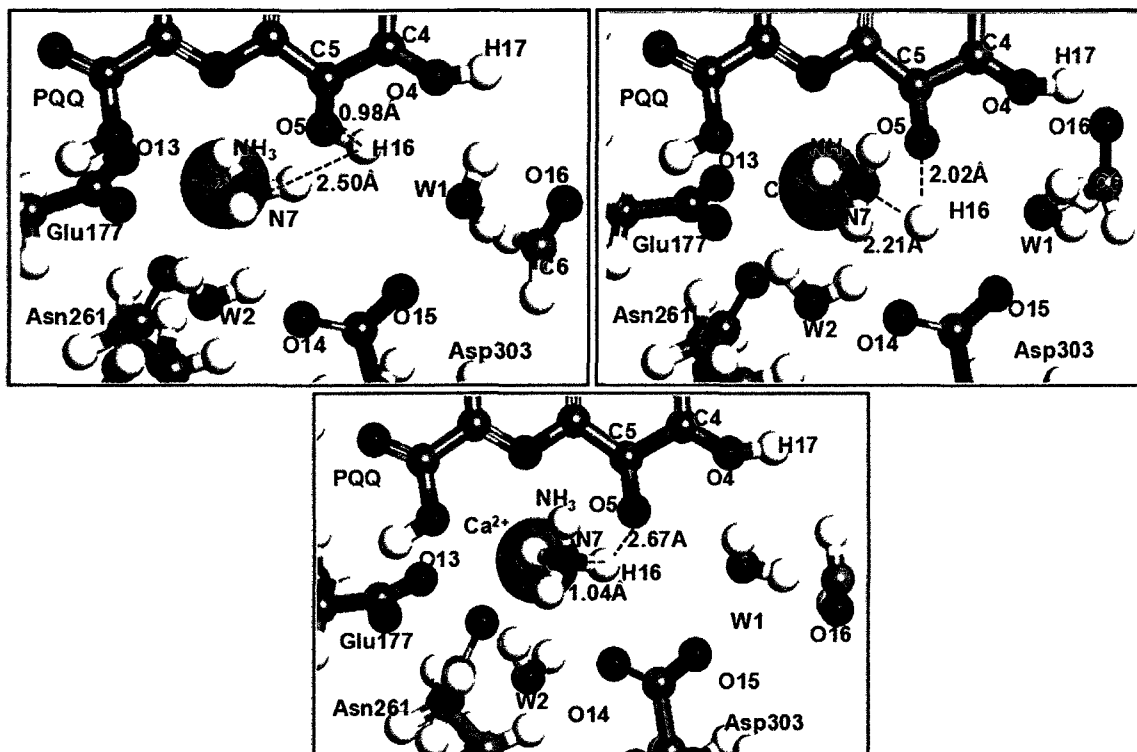
Figure 5.11: Figure shows orientation of third intermediate, Transition state 4 and fourth intermediate system.

5.5.5 Transfer of Hydride to Glu177

The fifth step involves detachment of H16 from ammonia and finally binding with O13 carboxylic oxygen of Glu177. Distance between N7 and H16 increases from 1.04 Å to 2.44 Å in the transition state indicating the dissociation of the bond between N7 and H16.

The distance further increases to 3.14 Å (Fig. 5.12). O13-H16 distance decreases from 3.77 Å to 2.45 Å in the transition state and finally reduces to 1.02 Å, signifying the bond formation. The energy barrier for the final step is 7.1 kcal/mol and the imaginary frequency associated with it is 573 cm^{-1}. The final semi-oxidized product is 3.8 kcal/mol more stable when weighed against the fourth intermediate and is 0.9 kcal/mol more stable compared to the reactant.
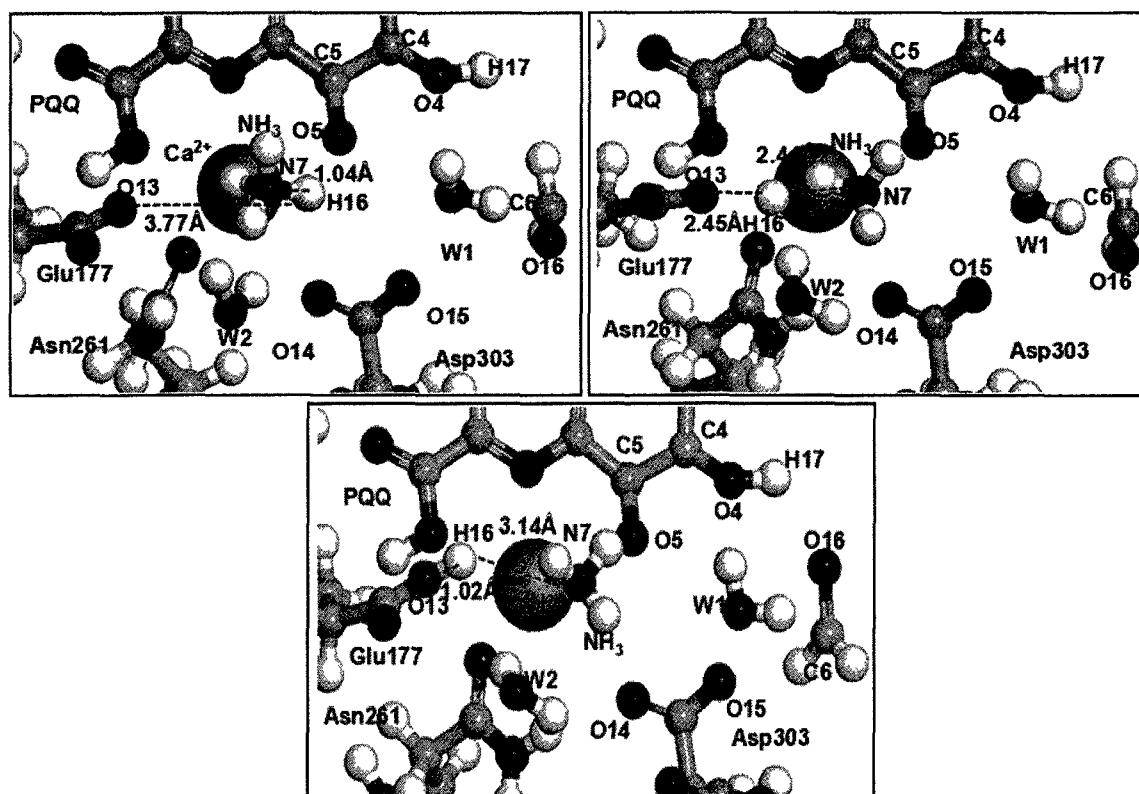
Figure 5.12: Figure shows orientation of fourth intermediate, Transition state 5 and product system.

5.6   Summary of Extended A-E Methanol Oxidation Mechanism

The dissociation of methanol in the first step and formation of hemiketal intermediate requires activation energy of 13.9 kcal/mol in Model 1 and 12.8 kcal/mol in Model 2 (Fig. 5.13). The energy barrier is lower by 1.0 kcal/mol in the case of Model 2. In the second step, H16 hydrogen is transferred from Asp303 to O5 of PQQ with an energy barrier of 7.8 kcal/mol and 7.2 kcal/mol in Models 1 and 2, respectively. The energy required for the complete reduction of PQQ and the release of formaldehyde is 8.2 kcal/mol in the case of Model 1 and 6.5 kcal/mol in Model 2. It is to be noted that the reduced form of PQQ is slightly more stable (0.2 kcal/mol) than the reactant in Model 2 and less stable (1.0 kcal/mol) in Model 1.
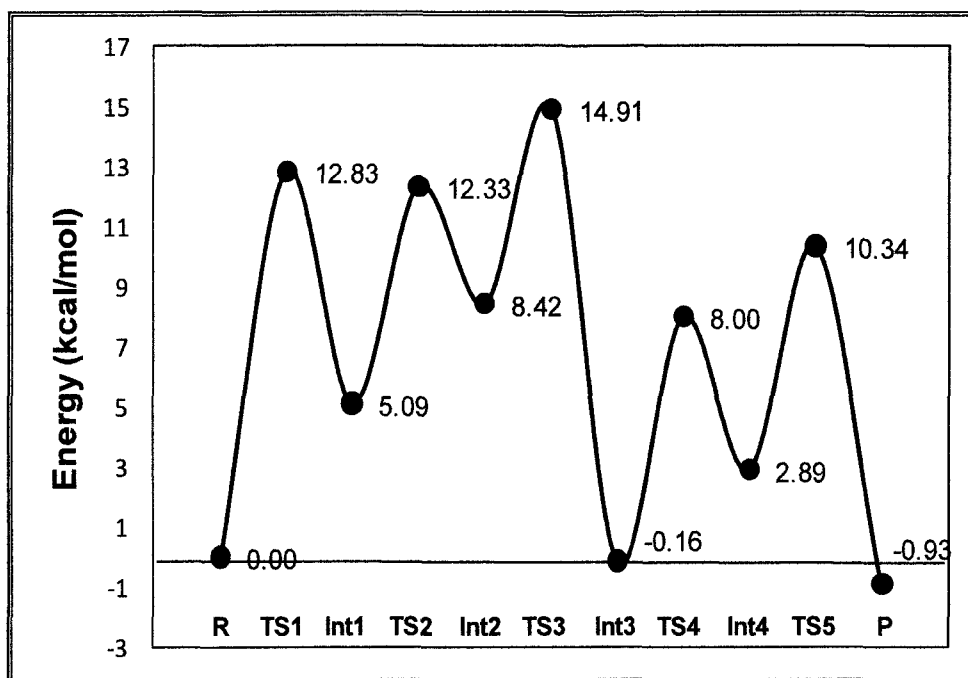
Figure 5.13: Energy profile of extended A-E reaction mechanism.

During the partial re-oxidation of PQQ, H16 hydrogen is transferred to ammonia which requires activation energy of 7.2 kcal/mol and 8.2 kcal/mol in Models 1 and 2, respectively. Both Model 1 and Model 2 show a similar trend in the reaction profile with slight variations in the distance measurements and energy values till this step. In the case of Model 1, it is observed that the final step is 3.9 kcal/mol less stable compared to the reactant. Model 2 consists of the fifth step in which hydride (H16) is transferred from ammonia to O13 atom of Glu177. Therefore, ammonia assists in the re-oxidation process of PQQ. This shows that the amino acid responsible for the abstraction of hydrogen from PQQ is Glu177. The final product in Model 2 is 0.9 kcal/mol more stable compared to the reactant.

Table 1 shows the distance measurements of active site components with respect to Ca^{2+}. When the values between reactant system of Model 1 and Model 2 are compared,

the distance measurements of Model 2 are comparatively closer to the experimental data compared to Model 1. For example, the variation of distance between Ca^{2+}-O10, Ca^{2+}-N6 and Ca^{2+}-O5 from the experimental data in Model 2 is between 0.06 Å to 0.14 Å, whereas the variation in Model 1 from experimental data is in the range of 0.05 Å to 0.35 Å. Distance between Ca^{2+} ion and O15 in Model 1 and Model 2 varies by 0.22 Å. This is because Model 2 includes two other amino acids, Glu177 and Asn261, and three water molecules.

The presence of the two amino acids and water molecules gives closer representation of active site of MDH because Ca^{2+} forms six co-ordinate bond, in which three bonds are with PQQ and the rest of them are with Glu177 and Asn261. Asn261 forms a hydrogen bond with Asp303 and hence stabilizes its position. This is the reason for Asp303 being closer to Ca^{2+} enzyme when compared to Model 1. During the reaction process, the amino acids are comparatively closer by 0.05 Å to 0.25 Å in Model 2 when compared with Model 1.

When we compare the reaction profile of Model 1 and Model 2, the reaction barrier in the case of Model 1 is comparatively higher than the reaction barriers in Model 2 except in Step 4 where it is the reverse (Fig. 5.14). The slight variation in the distance measurements in Model 1 and Model 2 causes variation in the energy barriers, too. By analyzing the role of ammonia, we find that ammonia does not form any complex with PQQ as proposed by Frank et al. [45]. The main role of ammonia is to assist in the re-oxidation of PQQ after the oxidation of methanol. Re-oxidation of PQQ makes it available for oxidation of methanol as a reduced form of PQQ cannot oxidize methanol.
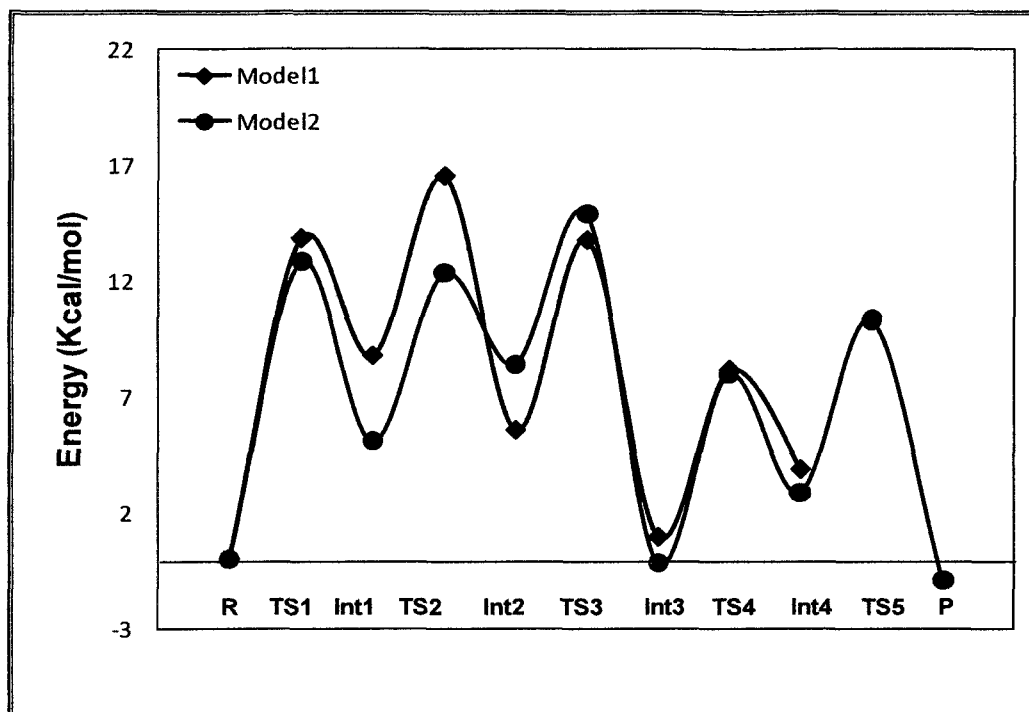
Figure 5.14: Figure compared reaction profile for Model 1 and Model 2.

Extraction of enzymes from the bacteria can cause structural changes in them which may hinder the re-oxidation of PQQ. Therefore, ammonia plays a very important role in attracting hydride from PQQ making it available of oxidation of the next methanol molecule. Another important role of ammonia is that it reduces the energy barrier for dissociation of methanol molecule in Step 2.

Idupulapati et al. did computational studies on A-E reaction in the absence of ammonia and the energy barrier for the first step was found to be 18.9 kcal/mol [36]. The presence of ammonia molecule has greatly reduced the energy barrier for dissociation of methanol to 12.8 kcal/mol in Model 2 and 13.9 kcal/mol in Model 1. The negative charge of N7 nitrogen of ammonia may assist in the abstraction of proton from the methanol towards Asp303. The presence of ammonia has reduced the energy of subsequent intermediates and transition states in the reaction profile with respect to reactant system.

The rate determining step in this reaction is the dissociation of methanol and the formation of hemiketal intermediate.

CHAPTER 6

EXTENDED HYDRIDE-TRANSFER
MECHANISM

6.1   Introduction

To investigate the most favorable mechanism for the oxidation of methanol,

Oubrie et al. and Zheng et al. investigated the structure of PQQ from methanol and

glucose dehydrogenases, using both experimental and computational methods [28, 40]. In

depth study on the conformation of PQQ reveals that, one of the carbonyl groups of PQQ

(C5) is most reactive due to presence of polarized charges. Therefore, C5 is the most

favorable site for the formation of a methanol complex, or direct transfer of hydride from

methanol [28]. Quantum mechanical and X-Ray crystallographic studies show variation

in the structure of PQQ. Computational calculations showed planarity in the semiquinone

form of PQQ, but higher resolution X-Ray crystallographic studies on MDH from

Methylophilus methylotrophus W3A1 showed contradictory results. The C5 position of

PQQ showed notable distortions from planarity and tetrahedral structure. PQQ and

methanol complex at C5 center can give a tetrahedral structure, but it is not compatible

with the electron density map. Zheng et al. conducted computational and experimental

studies, that favors the presence of hydride at the C5 position [40]. Therefore, a second

mechanism was proposed for the oxidation of methanol called Hydride-Transfer (H-T).

Experimental data from Dewanti et al. shows the breaking of C-H bond at the C5 center of PQQ. This suggests that there is no formation of hemiketal intermediate. Instead, a hydrogen is attached directly to C5 during the oxidation of the substrate [41]. Theoretical studies by Zheng et al. also showed that the transition state for the formation of PQQ-methanol adduct varies from that of direct hydride transfer from methanol. The transition state supports direct hydride transfer and the energy barrier for the same reaction was found to be 10 kcal/mol [26].

The H-T follows a four step mechanism. In the case of H-T mechanism, by-product formaldehyde is formed at the first step. Methanol dissociates in such a way that hydride H16 moves towards O14 atom of Asp303 and methyl hydride H17 attaches to C5 carbonyl group of PQQ leading to formation of formaldehyde. The second step involves transfer of hydride H16 from O14 of Asp303 to carbonyl oxygen O5 of PQQ. This leads to the formation of semiquinone or partially reduced form of PQQ. The third step is followed by the detachment of H17 from C5 of PQQ and association with O14 of Asp303. In the fourth step, PQQ is completely reduced by the transfer of H17 from Asp303 to O4 carbonyl oxygen of PQQ. Oxidation of methanol and reduction of PQQ is followed by re-oxidation of PQQ [40-41]. As proposed in Chapter 4, re-oxidation of PQQ is assisted by ammonia. After the completion of H-T mechanism, H16 hydride gets attracted towards ammonia molecule. The next step involves the transfer of Hydride H16 from ammonia to O13 oxygen atom of Glu177.

6.2   Modeling of Enzymes

As in the case of extended A-E reaction, we consider two models to explore the extended H-T mechanism. Model 1 consists of cofactor PQQ, probable catalytic base

Asp303 and Ca^{2+} ion. Model 2 includes two more amino acids Glu177 and Asn261 along with three water molecules (Figs. 5.1 and 5.2). Reactants, product and intermediates involved in the mechanism are built and optimized using MS 4.4.

6.3   Computational Method

Geometry optimization is carried out using GGA functional and BLYP/DNP level. The structure is optimized using a dielectric concentration of four, which corresponds to the enzyme environment [70]. Once the structures are optimized, the transition state for each step is determined by using synchronous transit method. The atoms in the reactant and product are matched using Equivalent Atoms Tools and a trajectory file is generated using Reaction Preview tool available in $DMOL^3$ module of MS4.4 [70]. The search for the transition state is done using combined LST/QST method. In this method, LST/Optimization and QST maximization calculation are conducted alternately till a stationary point is obtained. The Hessian associated with the structure is also generated simultaneously by requesting for frequency calculation. Once the transition state is obtained, the corresponding negative eigenvalue mode is selected and refined using TS optimization. It carries out Newton-Raphson search on the potential energy surface to search for energy maximum in a normal mode. The transition state is established by conducting a TS confirmation calculation where it follows an Intrinsic Reaction Path to confirm that there is no other minima apart from the reactant and the product.

6.4   Reaction Profile for Model 1

The components included in Model 1 are PQQ, Ca^{2+} and Asp303 as in the case of A-E reaction. To initiate the reaction mechanism, a methanol molecule is added to the

reactant system. Three different reactant systems were considered by varying the position of methanol. The most stable configuration was included in the reaction mechanism. A similar method was applied to the intermediate and product systems, also. The reaction mechanism consists of the Reactant, first intermediate to fourth intermediate and Product systems.

In order to see if there were any variations in the coordinates of the active site components, we compared the distance between Ca^{2+} ion, PQQ and Asp303 with that of X-Ray crystallographic data. The Ca^{2+}-O5, Ca^{2+}-N6 Ca^{2+}-O10 distance is 2.39 Å, 2.63 Å, and 2.69 Å, respectively, in the case of optimized structure, whereas experimental data shows that the inter atomic distance is 2.25 Å, 2.32 Å and 2.44 Å in the same order. Ca^{2+} ion forms coordinate bonds with these atoms of PQQ.

The distance between Ca^{2+} ion and O15 atom of Asp303 is 4.25 Å in the computational calculations whereas in the case of X-Ray crystallographic structure the distance between them is 4.6 Å [23-24]. The distances are in close agreement with the experimental results. There is a slight variation in the inter-atomic distance which ranges from 0.14 Å to 0.35 Å. Such deviations in the distance measurement can be because the entire enzyme is not included in the model. Since enzyme structures have thousands of atoms the entire enzyme cannot be included in DFT calculations.

The position of methanol in the active site model is in such a way that the distance between O15 atom of Asp303 and H16 atom of methanol is at a distance of 2.81 Å and the distance between O5 carbonyl oxygen of PQQ and O16 atom of methanol is 3.61 Å. The orientation of methanol is in such a way that H16 atom faces towards Asp303 and O16 towards PQQ.

6.4.1   Hydride Transfer and Formation of By-product

In the case of H-T mechanism, the methanol is completely oxidized at the first step itself. The hydrogen atom H16, which is closer to Asp303, binds with O15 oxygen atom of the same amino acid. In addition to this, a second hydrogen atom H17 is abstracted from methanol, which is transferred to C5 carbonyl atom of PQQ resulting in the release of formaldehyde. The distance between O15 and H16 decreases from 2.81 Å to 1.88 Å in the transition state (Fig. 6.1). The distance between them further reduces to 1.00 Å which shows the binding of O15 and H16 atoms. On the other hand, the distance between C5 and H17 reduces from 3.78 Å in the reactant to 2.31 Å in the transition state and finally settles at 1.13 Å, evidence of a formation of bond between them.
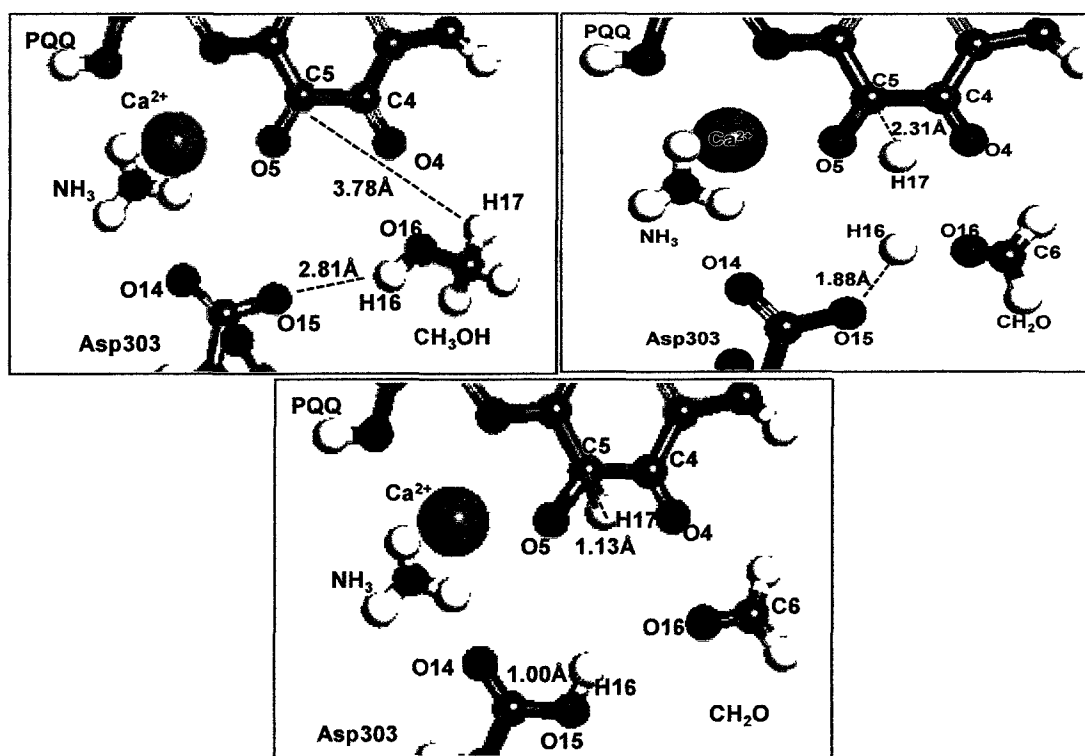
Figure 6.1: Figure shows orientation of Reactant, Transition state 1 and first intermediate system.

The energy barrier for the abstraction of hydrogen atoms from methanol are 14.3 kcal/mol with a single imaginary frequency of -1148 cm^{-1}. This negative frequency is due to the oscillation of C5-H17 bond. The first intermediate formed in this step is 7.1 kcal/mol less stable compared to that of the reactant system.

6.4.2   Hydride Transfer Between O14 and O5

Followed by the release of formaldehyde, we observe an increase in the O15 and H16 distance from 1.00 Å in the first intermediate to 2.70 Å in the transition state (Fig. 6.2).
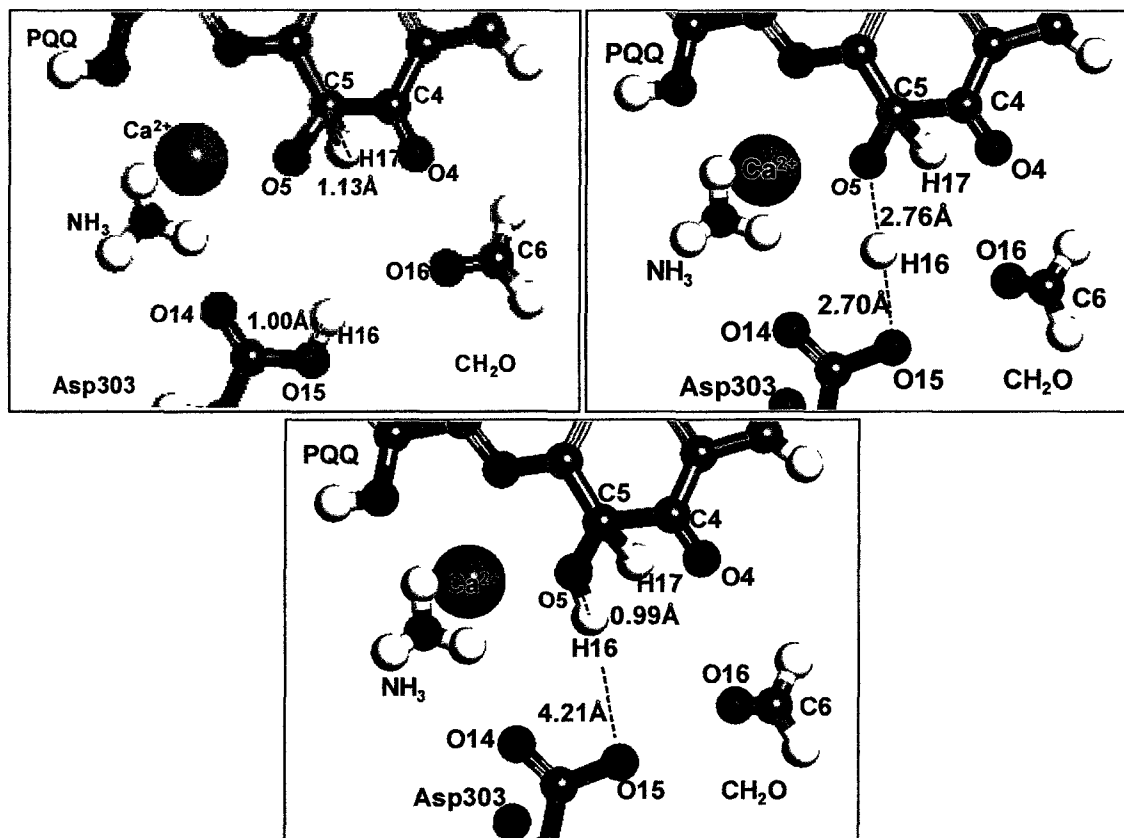
Figure 6.2: Figure shows orientation of first intermediate, Transition state 2 and second intermediate system.

The distance further increases to 4.21 Å in the second intermediate, indicating the breaking of O15-H16 bond. Simultaneously, the O5-H16 distance decreases from 3.22 Å to 2.76 Å in the transition state. H16 hydride binds with O5 as the distance between them reduces to 0.99 Å in the second intermediate. Therefore, in this step we observe a transfer of hydride from O14 oxygen atom of Asp303 to O5 carbonyl oxygen of PQQ.

The activation energy for this step is 10.1 kcal/mol. The single imaginary frequency involved in this step is 369 cm^{-1} which corresponds to the oscillation of O15-H16 bond. Due to the proximity of H16 hydride and O5 oxygen atoms, the energy required for the transfer of hydride is very low. The second transition state is 7.7 kcal/mol less stable when compared with the reactant. The energy of both first and second intermediate vary slightly by 0.7 kcal/mol with the first intermediate being more stable compared to the second intermediate.

6.4.3   Formation of Semiquinone PQQ

In the third step, PQQ forms a semiquinone structure which is nothing but the partially reduced from of PQQ. The hydrogen present at the C5 carbonyl carbon gets transferred to O14 oxygen of Asp303 (Fig. 6.3). C5-H17 distance increases from 1.11 Å in the second intermediate to 3.91 Å in the third transition state confirming the breaking of C—H17 bond (Fig. 6.3). The distance further increases to 4.90 Å in the case of third intermediate. The O15-H17 distance decreases from 5.30 Å to 2.58 Å during the transition state followed by the attachment of H17 hydride to O14 oxygen of Asp303. The distance between O15 and H17 is reduced to 0.98 Å in the bound state.
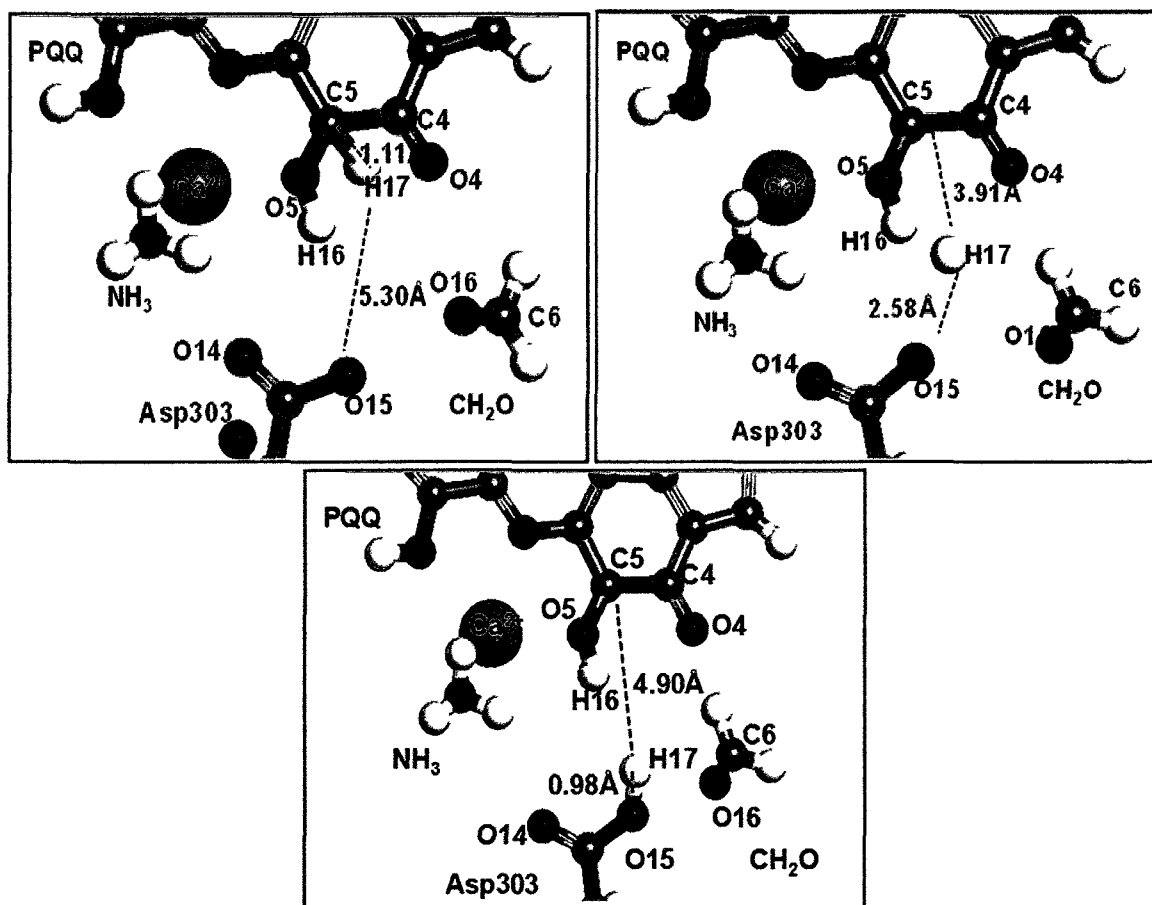
Figure 6.3: Figure shows orientation of second intermediate, Transition state 3 and third intermediate system

The third transition state is 1.4 kcal/mol more stable compared to the second intermediate; hence, the activation energy required for the hydride transfer to take place in this step is 8.7 kcal/mol. The imaginary frequency corresponding to this transition state is 877 cm^{-1}. The vibrational frequency corresponds to the oscillation of C5-H17 bond. The transition state is 6.3 kcal/mol less stable in relation to the reactant.

6.4.4 Complete Reduction of PQQ

The fourth step involves the complete reduction of PQQ by transfer of hydride from O14 oxygen atom of Asp303 to O4 carbonyl oxygen of PQQ. O15-H17 distance increases from 0.98 Å in the third intermediate to 3.48 Å in the transition state. Finally,

the distance increases to 5.32 Å when H16 binds with O4 carbonyl oxygen of PQQ (Fig. 6.4). At the same time, the O4-H17 distance reduces from 4.43 Å to 3.2 Å in the transition state. H17 hydride binds with O4 to reduce the distance between them to 0.98 Å, resulting in the complete reduction of PQQ.
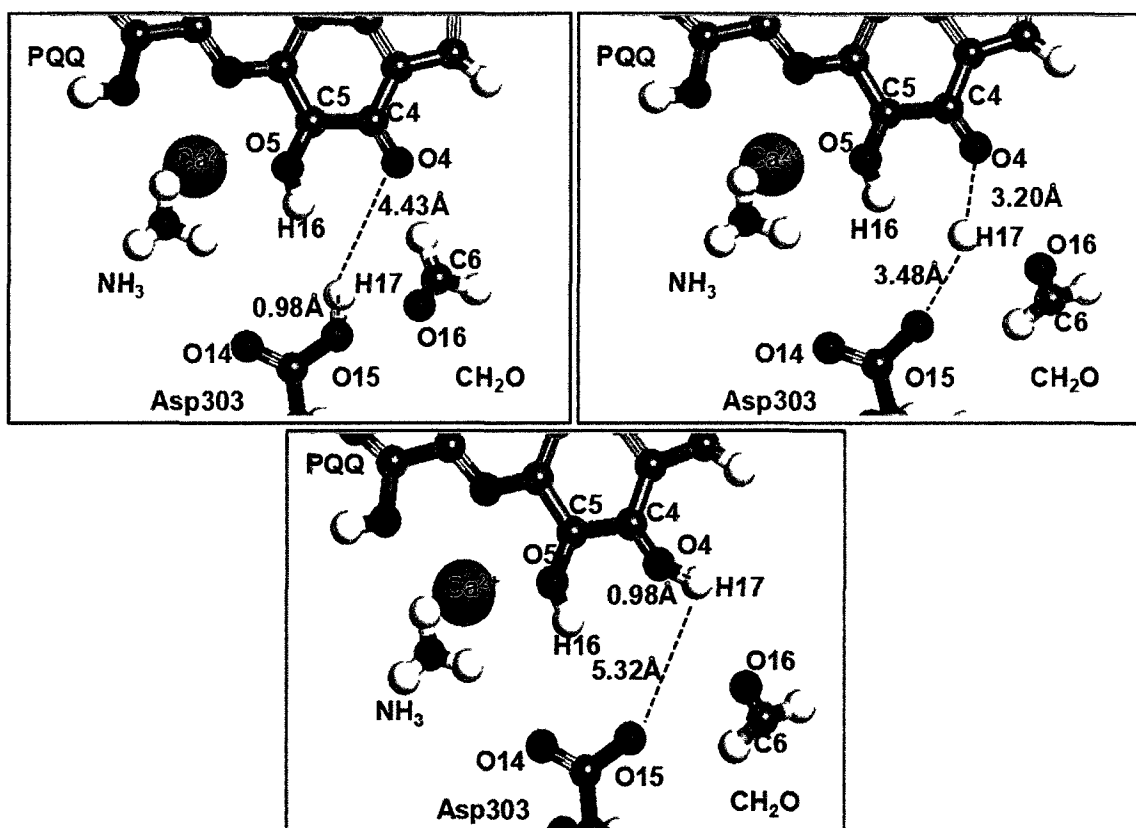
Figure 6.4: Figure shows orientation of third intermediate, Transition state 4 and fourth intermediate system.

The energy barrier corresponding to this step is 5.3 kcal/mol with a single imaginary frequency of 829 cm^{-1}. The imaginary frequency is due to the wavering of O15-H17 bond. The transition state is 11.6 kcal/mol less stable compared to that of the reactant molecule. The completely reduced form of PQQ system has very similar energy with respect to the reactant. The energy of the reduced PQQ system is similar to the reactant system and 4.8 kcal/mol more stable than the semi-reduced system.

6.4.5   Re-oxidation of PQQ

The final step consists of the partial re-oxidation of PQQ. The H16 hydride detaches from O5 carbonyl oxygen of PQQ and gets attracted to ammonia. The distance measurements show that O5-H16 distance increases from 0.98 Å in the fourth intermediate to 2.01 Å in the transition state confirming the breaking of the bond. In the final product, the distance increases to 3.27 Å (Fig. 6.5). The distance between N7 and H16 decreases from 3.65 Å to 2.13 Å in the transition state. The distance further reduces to 1.06 Å in the final product indicating the binding of N7 with H16.
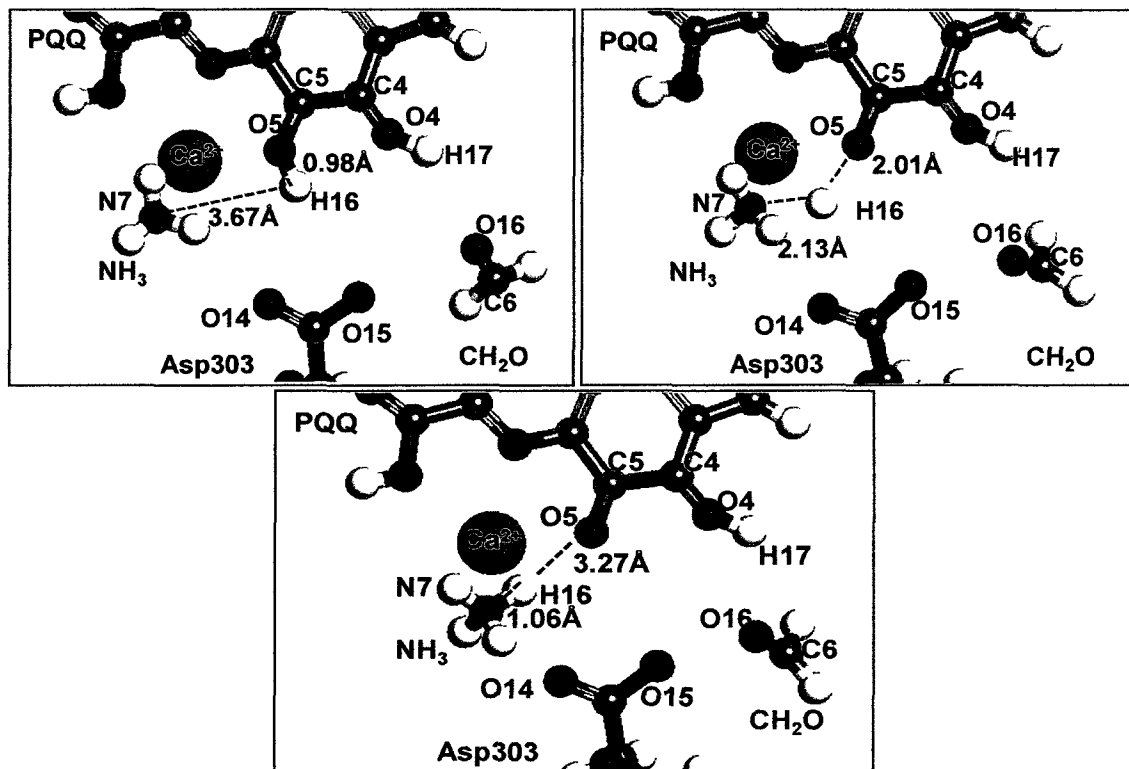
Figure 6.5: Figure shows orientation of fourth intermediate, Transition state 4 and product system.

The energy barrier for this step is 13.2 kcal/mol with a single imaginary frequency of 665 cm^{-1}. The imaginary frequency arises due to the bond oscillation between O5 and

H16 and also between N6 and H16. The final product consists of a partially re-oxidized PQQ, which is 7.6 kcal/mol less stable than the completely reduced PQQ system. The system is 7.7 kcal/mol less stable than the reactant with a fully oxidized form of PQQ. Figure 6.6 shows the complete reaction profile of the extended H-T mechanism. Rate limiting step is the partial re-oxidation of PQQ by abstraction of H16 hydrogen from O5 carbonyl oxygen of PQQ.
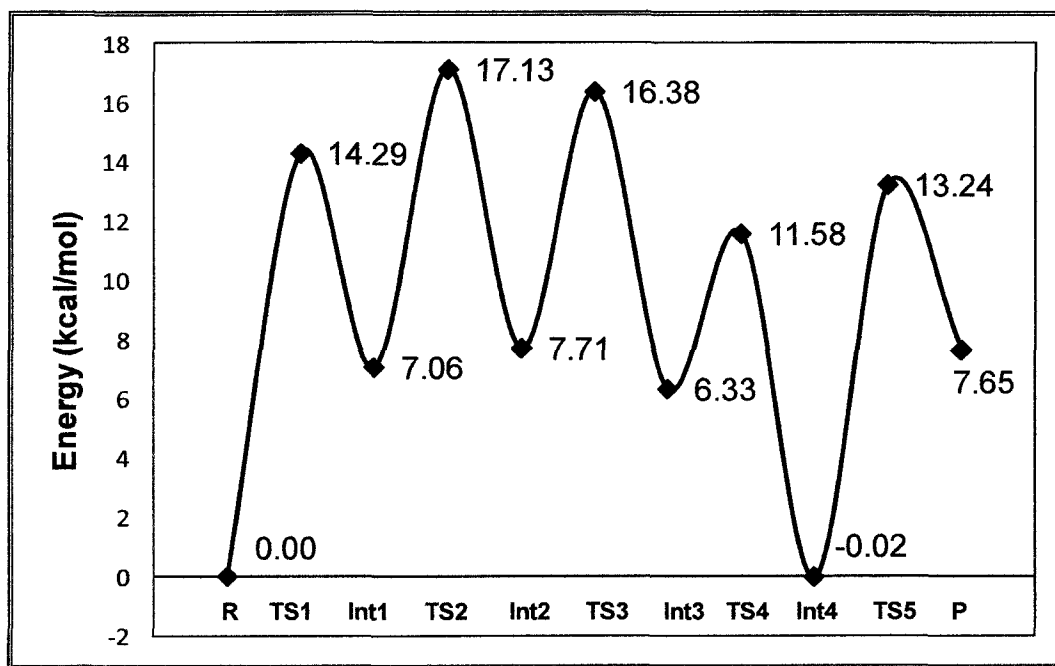
Figure 6.6: Reaction profile of extended H-T mechanism using Model 1.

6.5 Reaction Profile for Model 2

Model 2 consists of PQQ, Ca^{2+} ion, Asp303, Glu177, and Asn261 along with three water molecules similar to the system used in the A-E mechanism. A methanol molecule was added to this optimized active site model for oxidation. Multiple reactant systems were built by varying the position and orientation of methanol and the most stable configuration was chosen for further simulations of the transition states. The same

procedure was followed for all the other intermediate and product systems. The reaction mechanism consists of Reactant, five intermediates, and the final product.

The coordinates of the optimized reactant system are compared with the X-Ray crystallographic data. Ca^{2+} forms coordinate bond with three atoms of PQQ, which are O5, N6, and O10. Experimental data shows that the Ca^{2+}-O5, Ca^{2+}-N6 Ca^{2+}-O10 distance are 2.39 Å, 2.63 Å and 2.69 Å, respectively. The corresponding distance in the optimized model of the reactant is 2.43 Å, 2.72 Å and 2.55 Å, respectively. Ca^{2+} also forms coordinate bond with the O13 atom of Glu177 and O11 oxygen atom of Asn261.

Ca^{2+}-O11 and Ca^{2+}-O13 distance 3.21 Å and 2.56 Å respectively in the optimized system. X-Ray crystallographic results show that the corresponding distance is 3.13 Å and 2.81 Å in the same order. It is observed that the distance measurements are in close agreement with the experimental values. The distance between Ca^{2+} and the O15 atom of catalytic base Asp303 is 4.14 Å. The variation in the distance measurement ranges from 0.04 Å to 0.25 Å. This slight variation is due to the fact that the complete enzyme model of the enzyme is not considered. Instead, the components playing an important role in the oxidation of methanol is considered in our models.

6.5.1   Hydride Transfer and Formation of By-product

In the case of hydride transfer reaction, methanol is reduced to formaldehyde right at the first step. The orientation of methanol in the active site is such a way that H16 hydrogen faces towards Asp303 and O16 towards PQQ. The distance between H16 and O14 oxygen atom of Asp303 is 2.70 Å and the O16-C5 distance is 3.40 Å (Fig. 6.7). In the first step, H16 hydrogen moves towards O14 oxygen atom of Asp303 and binds with it. Simultaneously, H17 hydrogen gets detached from methanol and binds with C5 carbonyl group of PQQ resulting in the formation of formaldehyde. O16-H16 distance

increases from 0.98 Å to 3.39 Å in the transition state leading to the breaking of O16-H16

bond. The distance increases to 3.97 Å in the first intermediate.
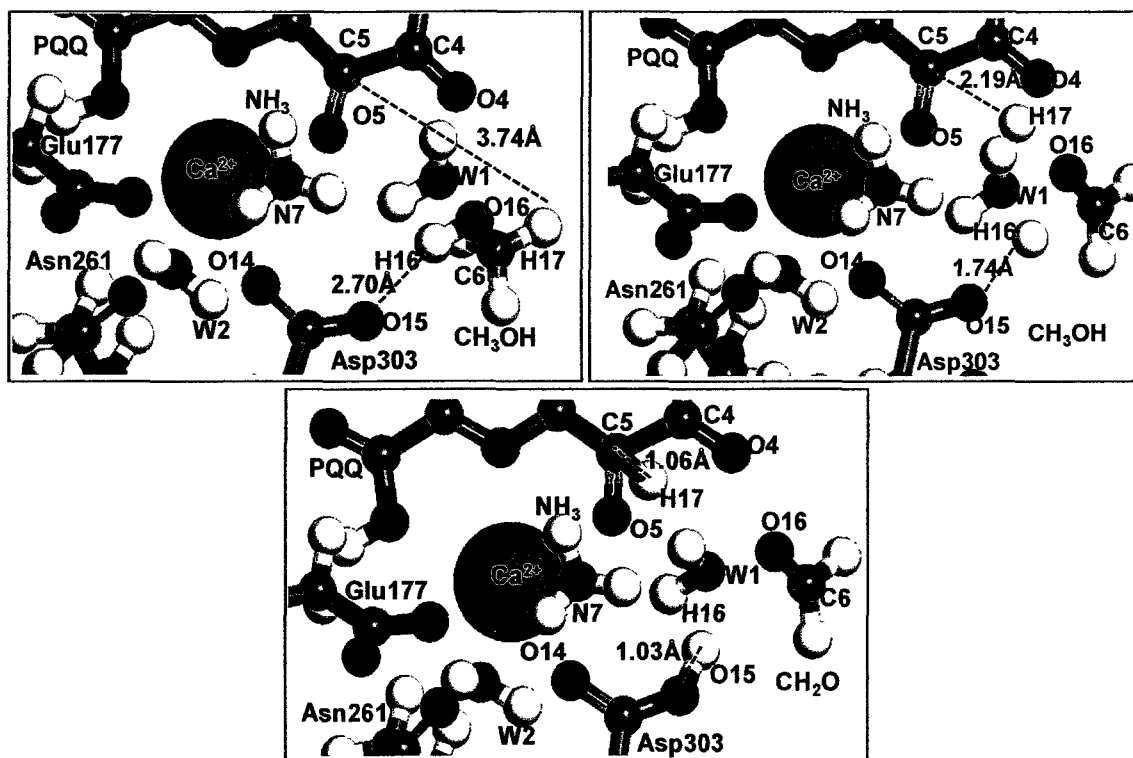
Figure 6.7: Figure shows orientation of Reactant, Transition state 1 and first intermediate system.

The distance between O14 and H16 reduces from 2.70Å in the reactant to 1.74Å

in the first transition state. The distance further reduces to 1.03Å indicating a formation

of bond between O14 and H16. At the same time C6-H17 distance increases from 1.10 Å

to 3.37 Å and further to 4.82 Å causing the detachment of the bond between them. C5-

H17 distance reduces from 3.74 Å to 2.19 Å in the transition state. Finally, the distance

between them reduces to 1.06 Å, resulting in the binding of C5 and H17.

The energy barrier for this step is 13.2 kcal/mole. The single point energy of the

first intermediate formed is 3.7 kcal/mol less stable than the reactant. The imaginary

frequency corresponding to this step is 1817 cm^{-1}, which is due to the stretching and contraction of O16-H16 and C6-H17 bond.

6.5.2   Hydride Transfer from O14 to O5

In the second step, H16 hydrogen gets attracted towards O5 carbonyl oxygen of PQQ and hence moves from O14 of Asp303 towards O5 of PQQ. The distance between O14 and H16 increases from 1.03 Å in the first intermediate to 2.39 Å in the transition state, evidence of detachment of O15-H16 bond (Fig. 6.8).
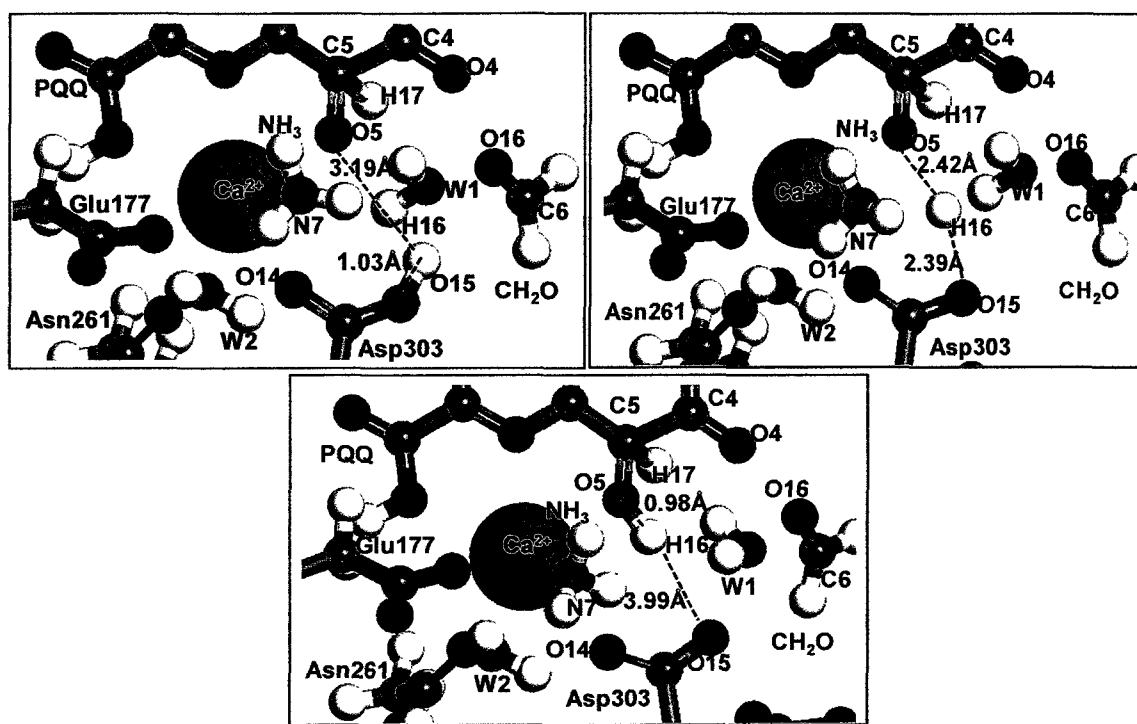
Figure 6.8: Figure shows orientation of first intermediate, Transition state 2 and second intermediate system.

The distance between them further increases to 3.99 Å. Simultaneously, the distance between O5 and H16 reduces from 3.19 Å in the first intermediate to 2.42 Å in the transition state. H16 binds with O5 as the distance reduces from 2.42 Å to 0.98 Å in the second intermediate.

The activation energy for the transfer of hydride from O15 of Asp303 to O5

carbonyl oxygen of PQQ is 9.5 kcal/mol. The imaginary frequency corresponding to this

step is 391 cm^{-1}, which represents the bond oscillation between O15 and H16 atoms. The

energy of the transition state is 13.17 kcal/mol less stable compared to the reactant

system. When we compare the energy between the first and second intermediate, the

latter is 1.5 kcal/mol less stable than the former.

6.5.3   Formation of Semiquinone form of PQQ

In the third step, H17 hydrogen from C5 carbonyl group moves towards O15 atom

of Asp303. This leads to the formation of semiquinone or a partially reduced (PQQH)

form of PQQ (Fig. 6.9).
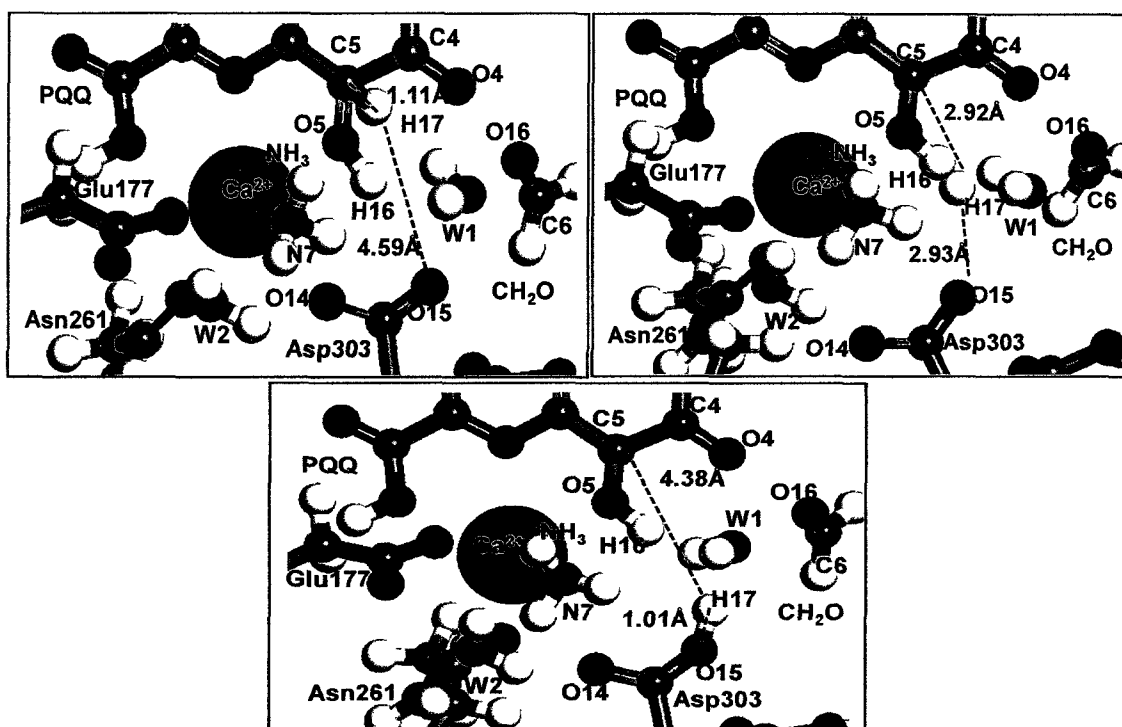
Figure 6.9: Figure shows orientation of second intermediate, Transition state 3 and third intermediate system.

The distance measurements show that the H17 moves away from C5 as the distance between them increases from 1.11 Å to 2.92 Å. This indicates the breaking of C5-H17 bond. The hydride moves further away, increasing the distance between them to 4.38 Å. On the other hand, O15-H17 distance decreases from 4.59 Å to 2.93 Å as the hydride moves towards O14 of Asp303. The distance finally reduces to 1.01 Å, supporting the formation of O15-H17 bond.

The activation energy for this step is 9.6 kcal/mol with the imaginary frequency of 2913 cm^{-1}. The frequency corresponds to the stretching of the bond between C5 carbonyl of PQQ and H17. The system with semiquinone form of PQQ is 5.5 kcal/mol less stable compared to the reactant system and 0.4 kcal/mol less stable when compared to the second intermediate.

6.5.4   Complete Reduction of PQQ

The fourth step involves complete reduction of PQQ. Asp303 transfers H17 hydrogen from O15 oxygen to O4 carbonyl oxygen of PQQ. This leads to the complete reduction of PQQ to PQQH$_2$. The distance measurements show that O15-H17 distance increases from 1.01 Å to 5.15 Å in the transition state confirming the breaking of the bond between them. The distance settles at 5.23 Å in the fourth intermediate.

It is also observed that the distance between O4 and H17 decreases from 3.96 Å in the third intermediate to 2.51 Å in the transition state. The distance eventually reduces to 0.98 Å, evidencing the formation of O4-H17 bond (Fig. 6.10). Energy barrier for this step is 5.3 kcal/mol with an imaginary frequency of 531 cm^{-1}. The imaginary frequency of this step corresponds to the oscillation of O15-H17 and O4-H17 bonds. The transition state is 10.8 kcal/mol less stable than the reactant. The system with a completely reduced from of

PQQ is 5.5 kcal/mol more stable than the system with partially reduced PQQ. Also, the reduced system is 0.1 kcal/mol less stable than the initial reactant system.
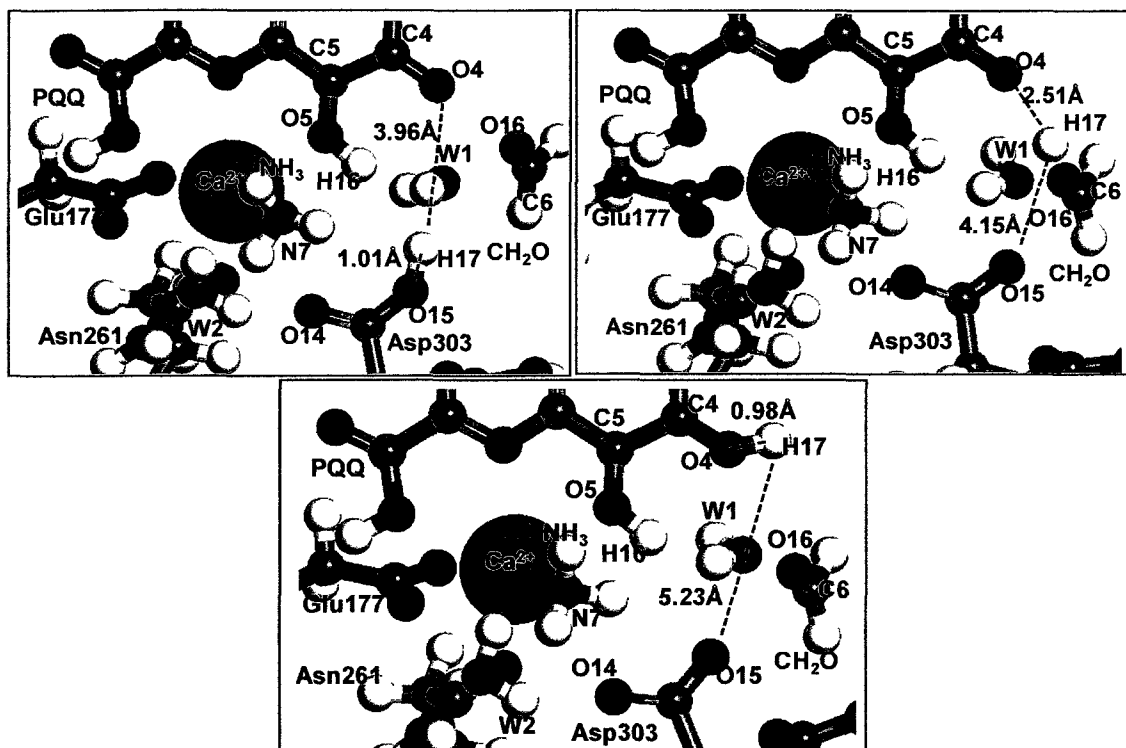
Figure 6.10: Figure shows orientation of third intermediate, Transition state 4 and fourth intermediate system.

6.5.5   Re-oxidation of PQQ

Once the PQQ is reduced, it returns to its oxidized state by transferring the hydrides to the surface of the enzyme by the process of re-oxidation. Ammonia plays a very important role in the re-oxidation of PQQ. It attracts H16 hydrogen from O5 carbonyl oxygen of PQQ. Therefore, in the fifth step we observe the transfer of hydride from O5 carbonyl oxygen to N7 nitrogen of ammonia molecule. The O5-H16 distance increases from 0.98 Å in the fourth intermediate to 2.40 Å in the transition state, indicating the detachment of the bond (Fig. 6.11). The distance further increases to 2.60 Å in the fifth intermediate. The distance between N7 and H16 decreases from 3.51 Å to

2.25 Å in the transition state. H16 finally binds with N7 nitrogen of ammonia molecule, which is indicated by the reduction of the distance between them to 1.12 Å.
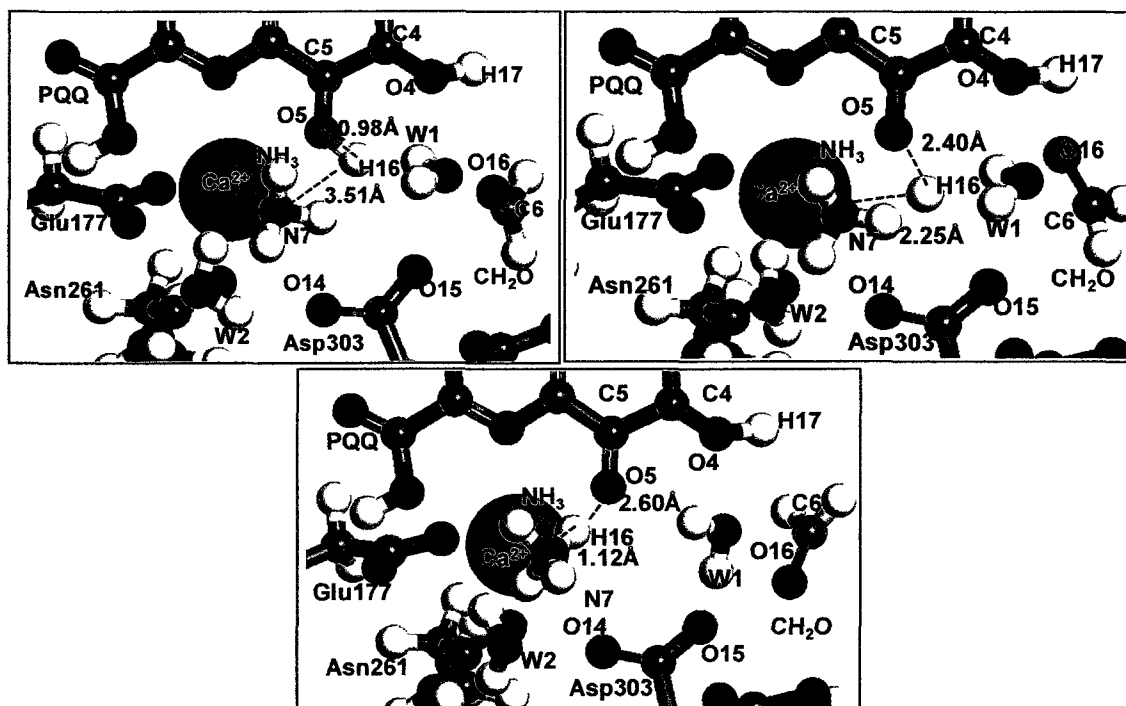
Figure 6.11: Figure shows orientation of fourth intermediate, Transition state 5 and fifth intermediate system.

The energy barrier for this step is 10.1 kcal/mol with an imaginary frequency of 1729 cm^{-1}, which corresponds to the stretching and contraction of bond between O5 and H16 atom. The partially oxidized PQQ system is 4.8 kcal/mol less stable than the system with completely reduced PQQ. Transition state involved in this step is 10.2 kcal/mol less stable than the reactant system.

6.5.6   Transfer of Hydride from Ammonia to Glu177

The final step of this mechanism involves the transfer of H16 hydrogen from ammonia to O13 oxygen atom of Glu177. This transfer of atom is indicated by the distance measurements N7 and H16 (Fig. 6.12).
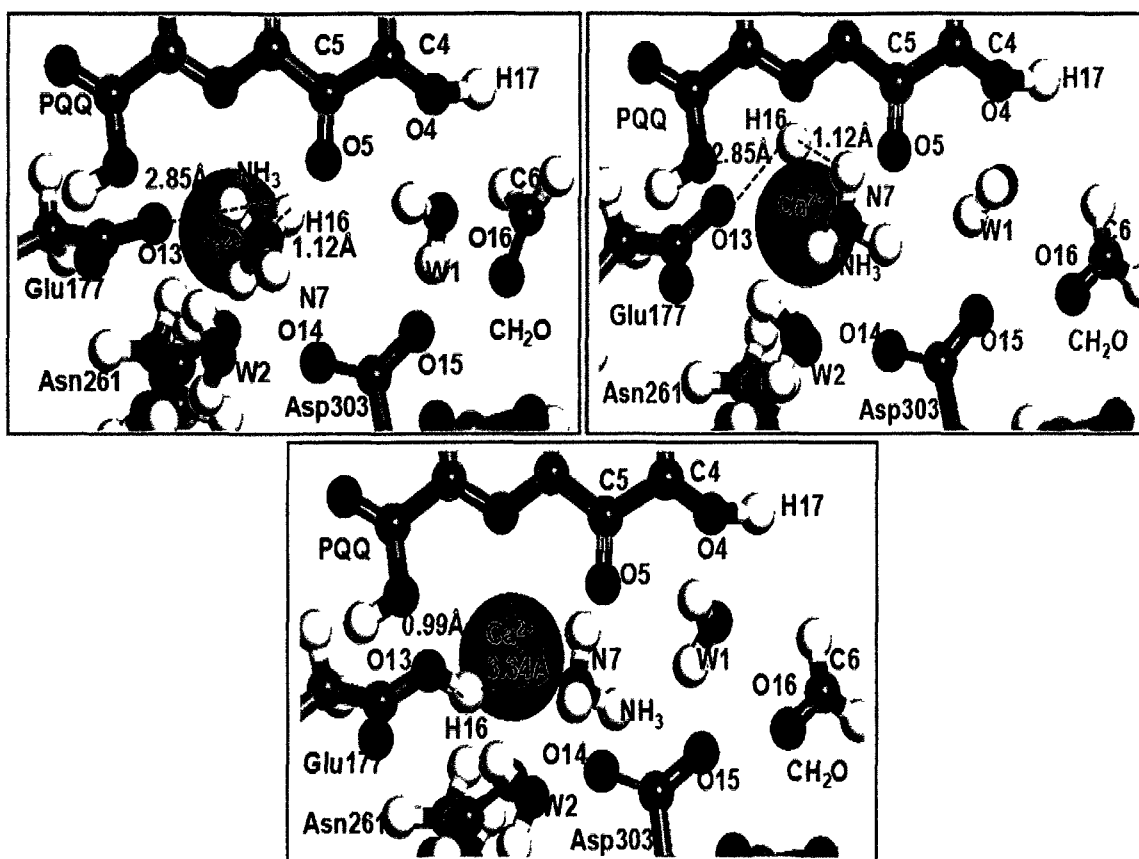
Figure 6.12: Figure shows orientation of fifth intermediate, transition state 6 and product system.

N7-H16 bond distance increases from 1.12 Å in the fifth intermediate to 2.32 Å in the transition state verifying the detachment of the bond. This distance increases to 3.34 Å in the final product.Concurrently, the distance between O13 oxygen of Glu177 and H16 atom decreases from 2.85 Å to 2.10 Å in the transition state. The distance between them finally reduces to 0.99 Å, indicating the binding of H16 with O13. Energy barrier for the transfer of hydride is 4.2 kcal/mol with an imaginary frequency of 159 cm^{-1}, which corresponds to the stretching of the bond between N7 and H16. The final product is 5.3k cal/mol more stable compared to the fifth intermediate and 0.5kcal/mol more stable compared to the reactant system.

The system is 0.4 kcal/mol more stable compared to the reduced form of the PQQ system (fourth intermediate). Figure 6.13 shows the reaction profile of the extended H-T reaction using Model 2.
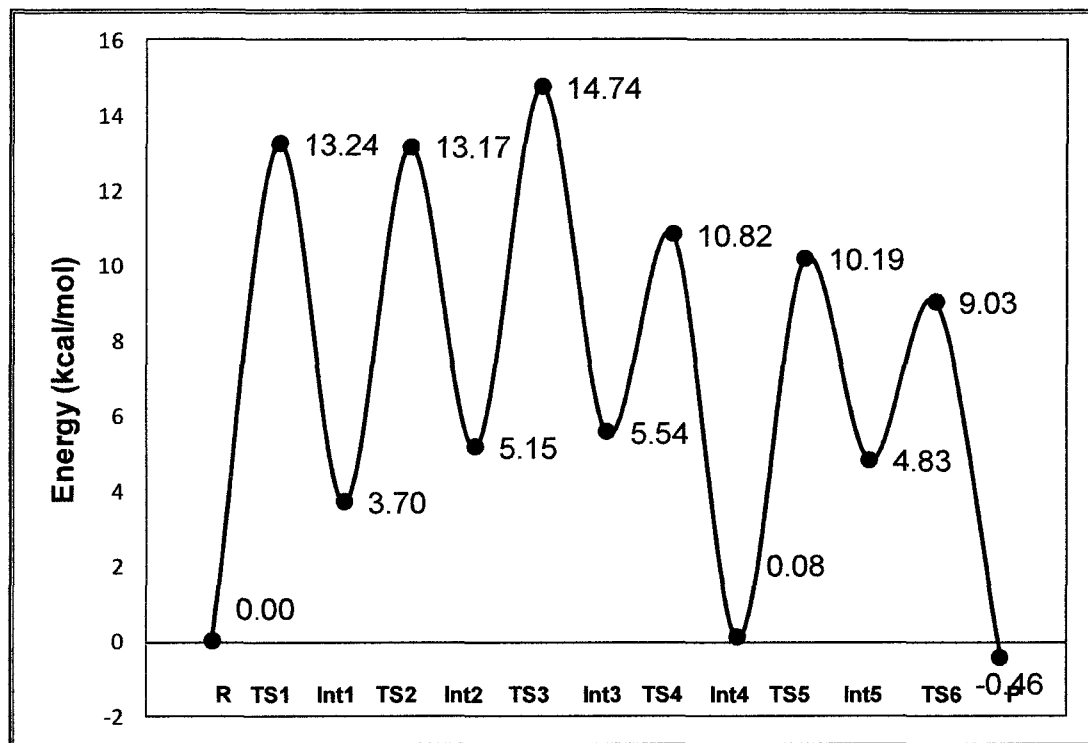
Figure 6.13: Reaction profile for extended Hydride-Transfer reaction using Model 2.

The rate limiting step is Step 5, which involves partial re-oxidation of PQQ by abstraction of H16 proton from O5 carbonyl oxygen of PQQ.

6.6   Summary of Extended H-T Methanol Oxidation Mechanism

The oxidation of methanol in the first step and formation of by-product formaldehyde requires activation energy of 14.3 kcal/mol in Model 1 and 13.2 kcal/mol in Model 2 (Fig. 6.14). The energy barrier is lower by 1.1 kcal/mol in the case of Model 2. In the second step, H16 hydrogen is transferred from Asp303 to O5 of PQQ with an energy barrier of 10.1 kcal/mol and 9.5 kcal/mol in Models 1 and 2, respectively. The

energy required for the transfer of hydride H17 from C5 of PQQ to O15 is 8.7 kcal/mol in the case of Model 1 and 9.6 kcal/mol in Model 2. Step 4 involves the complete reduction of PQQ and the energy barrier for this step is 5.3 kcal/mol in both Models 1 and 2. It is to be noted that the energy of the reduced form of PQQ is similar to the reactant.
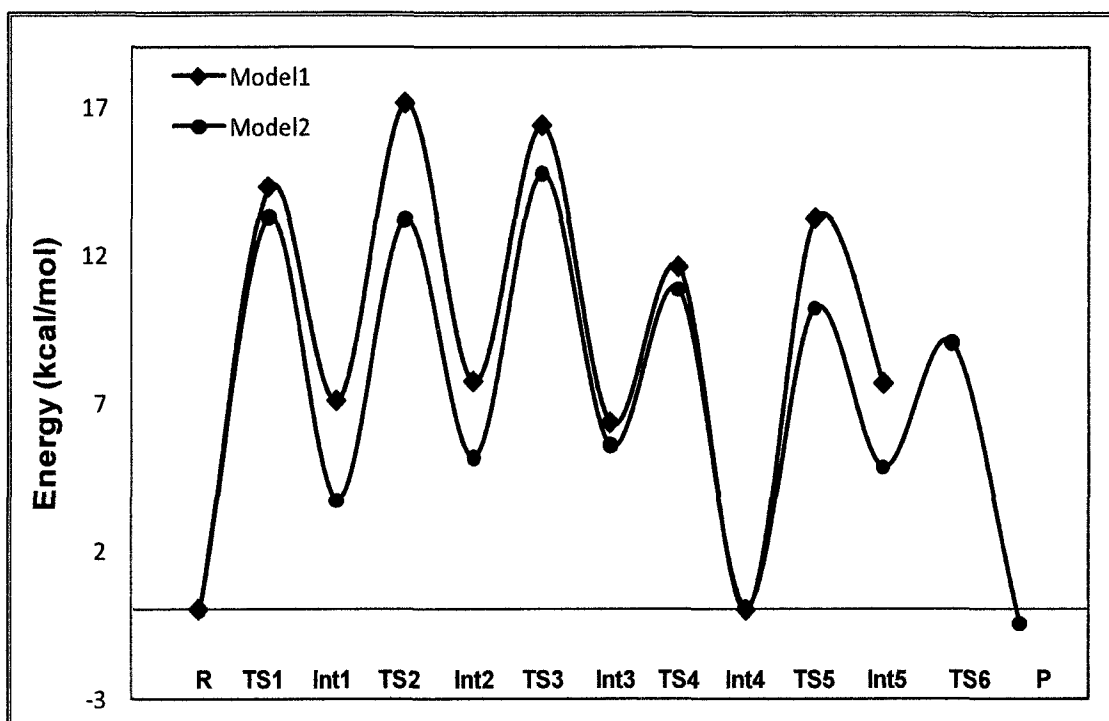
Figure 6.14: Figure compares the reaction profile of extended H-T mechanism of Model 1 and Model 2.

During the partial re-oxidation of PQQ H16, hydrogen is transferred to ammonia which requires activation energy of 13.2 kcal/mol and 10.2 kcal/mol in Models 1 and 2, respectively. Both Model 1 and Model 2 show similar trend in the reaction profile with slight variation in the distance measurements and energy values till this step. In case of Model 1, it is observed that the final step is 7.6 kcal/mol less stable compared to the reactant. Model 2 consists of the sixth step in which hydride (H16) is transferred from ammonia to O13 atom of Glu177. Therefore, ammonia assists in the re-oxidation process

of PQQ. This shows that the amino acid responsible for the abstraction of hydrogen from PQQ is Glu177. The final product in Model 2 is 0.5 kcal/mol more stable compared to the reactant.

Though ammonia does not form any complex with any of the active site components of MDH, it assists in the transfer of hydride from PQQ to Glu177 (Step 5). The negative charge of N7 nitrogen atom of ammonia attracts H16 proton from O5 carbonyl oxygen of PQQ. The resulting ammonium is unstable and transfers the hydrogen to Glu177. Therefore, ammonia assists in the re-oxidation of PQQ. Re-oxidation of PQQ is very important as the reduced from of PQQ will not be able to oxidize methanol substrate. Once PQQ is completely re-oxidized it will be able to oxidize the next available methanol substrate.

From the reaction profile, we can infer that the rate limiting step for this reaction is the dissociation of methanol and formation of formaldehyde (Step 1). The energy barriers in Model 2 were lower than the energy barrier in Model 1 except in Step 3. Activation energy required in the rate limiting step in Model 1 is 1.0 kcal/mol more than that of Model 2. The distance measurements of the optimized reactant of Model 1 vary in the range of 0.14 Å to 0.35 Å. The deviation in the case of Model 2 is from 0.04 Å to 0.25 Å. Therefore, when Model 1 and Model 2 are compared, the latter shows better representation of the active site of MDH.

Rate limiting step for the oxidation of methanol using H-T mechanism in the absence of ammonia was 19.7 kcal/mol. Both the models show a decrease in the energy barrier in the presence of ammonia. Therefore, ammonia also assists in reducing the energy barriers for the oxidation of methanol. The orientation and negative charge of

ammonia may assists in the abstraction of proton from methanol to Asp303, which in turn reduces the energy barrier of the rate limiting step.

CHAPTER 7

CONCLUSION AND FUTRURE WORK

7.1 Conclusions

The main objective of this research was to investigate the role of ammonia in the activation of Methanol dehydrogenase enzyme. Initially, we investigated the role of ammonia in the docking of MDH and its natural electron acceptor Cytochrome c_L. The entire enzyme structures of MDH and C_L were minimized using molecular mechanics and docked using Adsorption Locator module of MS4.4 [70]. After looking into the binding of MDH and C_L, the affect of ammonia in the active site was explored using reduced enzyme models of the same enzymes. The enzyme structures were reduced in such a way that the active site of the enzyme and the amino acids surrounding the active site were considered for our calculations. MM and MD calculations were used to explore the effect and position of ammonia in the active site of MDH.

Based on the results obtained from the mechanics and dynamics calculations, the position of ammonia was determined and used for further analysis on methanol oxidation mechanism. Two most debated mechanisms were used for the oxidation of methanol in MDH, which are Addition-Elimination reaction and the Hydride-Transfer mechanism. Role of ammonia during the oxidation of methanol was investigated using transition state calculations. Extended A-E and H-T mechanisms were proposed to show how ammonia

104

affects the reaction mechanism. Therefore, analysis using various computational techniques concludes that:

- Ammonia affects both the surface and active site characteristics of MDH.

- The docking of MDH and its natural electron acceptor C_L in the presence and absence of ammonia shows that, as we increase the concentration of ammonia, the interaction energy between the enzymes becomes more negative. The negative interaction energy shows that the enzymes are feasible to bind with each other. This shows that ammonia may interact with surface amino acids of both these enzymes and help in their binding.

- Going further in the active site of the enzyme, we find that the addition of NH_3 at a concentration of 5.54 mM does increase the overall stability of the system by 165.7 Kcal/mol compared to that of no NH_3. The system becomes more stable as we raise the concentration of NH_3. The system is most stable at a concentration of 33.24 mM of NH_3. Further increase in the concentration decreases the stability of the system.

- While comparing the orientation of active site residues with the energy of the system at the same concentration, it is observed that at a concentration of 33.24 mM the distance between Ca^{2+} and O15 oxygen atom of Asp303 are closest. Further increase in concentration of NH_3 decreases the stability of the system. In addition to that, an increase in the distance between Ca^{2+} and Asn261/Asp303 is observed. When the concentration of ammonia is increased to 55.39 mM, the system becomes 1273.62 kcal/mol less stable than the system with no ammonia molecules.

- An excess of ammonia concentration can cause an increase in the number of ammonia molecules in the active site which disrupts the orientation of Ca^{2+} ion. Ca^{2+} ion is coordinated to O10, N6, O5 atoms of PQQ, O12, O13 atoms of Glu177 and O11 atoms of Asn261. Therefore, deviation in the position of Ca^{2+} causes large variations in the positions of the active site amino acids.

- As we increase the concentration of NH_3, the diffusivity of Ca^{2+} and ammonia molecule closest to the active site increases. The increase is less prominent at low NH_3 concentrations, but rises rapidly at high concentration of NH_3. A similar trend is seen in the case active site amino acids such as Asn261, Asp303, and Glu177.

- Ca^{2+} ion has the least magnitude of diffusivity coefficient when compared to other amino acids present in the active site. A slight variation in the position of Ca^{2+} can cause larger variations in the position of the active site amino acids. Ca^{2+} ion is coordinated to O10, N6, O5 atoms of PQQ, O12, O13 atoms of Glu177 and O11 atoms of Asn261. Therefore, a small deviation in the position of Ca^{2+} causes large variations in the positions of active site amino acids.

- Asp303 has the highest and Glu177 has the least diffusivity coefficient. The possible reason for this variation is because Glu177 has two coordinate bonds with Ca^{2+} ions which restrict its mobility. Asn261 is bound to Ca^{2+} through a single coordinate bond which also stabilizes the position of Asn261, but the stability is less than that of Glu177. Asp303

does not form any coordinate bond with Ca^{2+} ion. This allows Asp303 to have less structural restrictions compared to Asn261 and Glu177.

- Due to this reason, the presence of the hydrogen bond between Asn261 and Asp303 is very important to stabilize the position of Asp303 during the oxidation of methanol.

The oxidation of methanol in the presence of ammonia was analyzed using two reaction mechanisms, namely, Addition-Elimination and Hydride-Transfer reaction. The analysis was done using two Models, a smaller Model 1 and larger Model 2. In the case of A-E reaction mechanism:

- Both Model 1 and Model 2 show a similar trend in the reaction profile, but there were slight variation in the distance measurements and energy values.

- The distance measurements of Model 2 are comparatively closer to the experimental data compared to Model 1. This is because Model 2 includes two other amino acids Glu177 and Asn261 and three water molecules. The presence of the two amino acids and water molecules gives closer representation of the active site of MDH because Ca^{2+} forms six co-ordinate bonds, in which three bonds are with PQQ and the rest of them are with Glu177 and Asn261. Asn261 forms hydrogen bond with Asp303 and hence stabilizes its position. This is the reason for Asp303 being closer to Ca^{2+} enzyme when compared to Model 1. During the reaction process, the amino acids are comparatively closer by 0.05 Å to 0.25 Å in Model 2 when compared with Model 1.

- When we compare the reaction profile of Model 1 and Model 2, the reaction barrier in the case of Model 1 is comparatively higher than the reaction barriers in Model 2 except in Step 4 where it is the reverse. The variation in the distance measurements in Model 1 and Model 2 causes variations in the energy barriers too.

- By analyzing the role of ammonia, we find that ammonia does not form any complex with PQQ as proposed by Frank et al. [45]. The main role of ammonia is to assist in the re-oxidation of PQQ after the oxidation of methanol. Re-oxidation of PQQ makes it available for oxidation of methanol as reduced form of PQQ cannot oxidize methanol.

- Extraction of enzymes from the bacteria can cause structural changes in them which may hinder the re-oxidation of PQQ. Therefore, ammonia plays a very important role in attracting hydride from PQQ making it available of oxidation for the next methanol molecule.

- Another important role of ammonia is that it reduces the energy barrier for dissociation of methanol molecule in Step 1. Computational studies on A-E reaction in the absence of ammonia show the energy barrier for the rate step was 18.9 kcal/mol [36]. The presence of ammonia molecule has significantly reduced the energy barrier for dissociation of methanol to 12.8 kcal/mol in Model 2 and 13.9 kcal/mol in Model1.

- The negative charge of N7 nitrogen of ammonia may assist in the abstraction of proton from the methanol towards Asp303. The presence of

ammonia has reduced the energy of subsequent intermediates and transition states in the reaction profile with respect to the reactant system.

A similar trend was seen in the case of Hydride-Transfer mechanism of methanol oxidation:

- Ammonia does not form any complex with any of the active site components of MDH it assists in the transfer of hydride from PQQ to Glu177 (Step 5). The negative charge of N7 nitrogen atom of ammonia attracts H16 proton from O5 carbonyl oxygen of PQQ.

- Rate limiting step for the oxidation of methanol using H-T mechanism in the absence of ammonia was 19.7 kcal/mol [36]. Both the models show a decrease in the energy barrier in the presence of ammonia. Therefore, ammonia also assists in reducing the energy barriers for the oxidation of methanol. The orientation and negative charge of ammonia may assists in the abstraction of proton from methanol to Asp303, which in turn reduces the energy barrier of the rate limiting the step. When we compare Model 1 and Model 2, the latter shows better representation of the active site of MDH. The distance measurements of the optimized reactant of Model 1 vary in the range of 0.14 Å to 0.35 Å. The deviation in the case of Model 2 is from 0.04 Å to 0.25 Å.

- Addition of Glu177 and Asn261 along with three water molecules has added stability to the system. This is because Ca^{2+} forms six coordinate bonds with the active site components of MDH. Three of the coordinate bonds are with PQQ, two with oxygen atoms of Glu177 and one with

oxygen atom of Asn261 in turn forms a hydrogen bond with Asp303 and stabilizes its position.

7.2 Future Work

7.2.1 Surface Characteristic of the Enzyme

MM and MD calculations can be used to study the surface characteristics of the entire MDH and C_L enzyme. Using Monte Carlo based adsorption calculations, we were able to explore the binding orientation of MDH/C_L. It was also detected that the ammonia concentrates at the interface between MDH and C_L and assists in their binding. By running dynamics calculation with the ammonia molecules, we will be able to analyze the characteristics of surface amino acids of these enzymes and their interaction with each other in the presence of ammonia. This will give insight about the amino acids responsible for binding with natural or artificial electron acceptors.

7.2.2 Re-oxidation of PQQ

From the transition state calculations, we were able to find that ammonia played a very important role in the partial re-oxidation of PQQ by attracting protons from O5 carbonyl oxygen of PQQ and transferring it to Glu177. In our MM and MD calculations, we were able to detect that the active site of MDH can accommodate two ammonia molecules. The transition state calculations showed that ammonia does not form complexes with any of the amino acids or PQQ during the oxidation of methanol. Using this information, complete re-oxidation mechanism can be obtained by investigating the mechanism using a bigger model. The key components of the active site model are PQQ, Ca^{2+} ion, catalytic base Asp303, Glu177, disulphide bridge (Cys103-104), two ammonia, and three water molecules based on the orientations obtained from MM/MD calculations.

In the partial re-oxidation of PQQ, we were able to detect that one of the proton (H16) is transferred to Glu177. This is because O5 oxygen is closer to Glu177, but the distance between O4 and Glu177 is larger. Therefore, a disulphide bridge is incorporated to investigate the complete re-oxidation of PQQ. Re-oxidation of PQQ is important for it to be able to oxidize subsequent methanol molecules. In addition to that, QMMR techniques can be used to explore the transfer of electrons using the same model.

This idea can be incorporated in the design of artificial bio-catalysts, bio-sensors and bio-fuel cells. In the oxidation of methanol, we observe that the main role is played by the co-factor PQQ with Ca^{2+}, catalytic base Asp303, ammonia, and a proton or electron acceptor. Layer-by-layer technique can be used to assemble the co-factor, catalytic base, and amino acid responsible for the abstraction of proton and electron at favorable pH conditions. Substrate can be added in the presence of the activator, which initiates the redox reaction, thus leading to the transfer of protons and electrons which can be used for generating power, fasten chemical reactions, or devising efficient bio-sensors.

REFERENCES

[1]   Walsh, C., *Enabling the chemistry of life.* Nature, 2001. **409**(6817): p. 226-231.

[2]   Arnold, F.H., *Combinatorial and computational challenges for biocatalyst design.* Nature, 2001. **409**(6817): p. 253-257.

[3]   Fessner, W.D., *Biocatalysis : from discovery to application.* 2000, Berlin; New York: Springer.

[4]   Koeller, K.M. and C.H. Wong, *Enzymes for chemical synthesis.* Nature, 2001. **409**(6817): p. 232-240.

[5]   Schmid, A., J. S. Dordick, B. Hauer, A. Kiener, M. Wubbolts and B. Witholt, *Industrial biocatalysis today and tomorrow.* Nature, 2001. **409**(6817): p. 258-268.

[6]   Rechnitz, G.A., *Bioanalysis with potentiometric membrane electrodes.* Analytical Chemistry, 1982. **54**(11): p. 1194A-1200A.

[7]   Richard, J.A., Y. Meyer, V. Jolivel, M. Massonneau, R. Dumeunier, D. Vaudry, H. Vaudry, P. Y. Renard and A. Romieu, *Latent fluorophores based on a self-immolative linker strategy and suitable for protease sensing.* Bioconjugate Chemistry, 2008. **19**(8): p. 1707-1718.

[8]   Benjamin, S. and A. Pandey, *Isolation and characterization of three distinct forms of lipases from candida rugosa produced in solid state fermentation.* Brazilian Archives of Biology and Technology, 2001. **44**(2): p. 213-221.

[9]   Jose, J. and T.F. Meyer, *The autodisplay story, from discovery to biotechnical and biomedical applications.* Microbiology and Molecular Biology Reviews, 2007. **71**(4): p. 600-619.

[10]   Rao, N.N., S. Lütz, K. Würges and D. Minör, *Continuous Biocatalytic Processes.* Organic Process Research & Development, 2009. **13**(3): p. 607-616.

[11]   Inamori, Y., C. Muro, E. Sajima, M. Katagiri, Y. Okamoto, H. Tanaka, Y. Sakagami and H. Tsujibo, *Biological Activity of Purpurogallin.* Bioscience, Biotechnology, and Biochemistry, 1997. **61**(5): p. 890-892.

[12]   Johnston, W., N. Maynard, B. Y. Liaw and M. J. Cooney, *In situ measurement of activity and mass transfer effects in enzyme immobilized electrodes.* Enzyme and Microbial Technology, 2006. **39**(1): p. 131-140.

[13]   Goode, D.R., R. K. Totten, J. T. Heeres and P. J. Hergenrother, *Identification of Promiscuous Small Molecule Activators in High-Throughput Enzyme Activation Screens.* Journal of Medicinal Chemistry, 2008. **51**(8): p. 2346-2349.

[14]   Patel, R.N. and A. Felix, *Microbial oxidation of methane and methanol: crystallization and properties of methanol dehydrogenase from Methylosinus sporium.* Journal of Bacteriology, 1976. **128**(1): p. 413-424.

[15]   Jorgenson, A.K., *Global Warming and the Neglected Greenhouse Gas: A Cross-National Study of the Social Causes of Methane Emissions Intensity, 1995.* Social Forces, 2006. **84**(3): p. 1779-1798.

[16]   Stanley, S.H., S. D. Prior, D. J. Leak, and H. Dalton, *Copper stress underlies the fundamental change in intracellular location of methane mono-oxygenase in methane-oxidizing organisms: Studies in batch and continuous cultures.* Biotechnology Letters, 1983. **5**(7): p. 487-492.

[17]   Felipo, V. and R.F. Butterworth, *Neurobiology of ammonia.* Progress in Neurobiology, 2002. **67**(4): p. 259-279.

[18]   Zhang, X.-C., A. Ranta, and A. Halme, *Direct methanol biocatalytic fuel cell-Considerations of restraints on electron transfer.* Biosensors and Bioelectronics, 2006. (21): p. 2052-2057.

[19]   Hektor, H.J., H. Kloosterman, and L. Dijkhuizen, *Nicotinoprotein methanol dehydrogenase enzymes in Gram-positive methylotrophic bacteria.* Journal of Molecular Catalysis - B Enzymatic, 2000. **8**(1-3): p. 103-109.

[20]   Duine, J.A., J. Frank, and P.E. Verwiel, *Structure and activity of the prosthetic group of methanol dehydrogenase.* European Journal of Biochemistry, 1980. **108**(1): p. 187-192.

[21]   Guo, X. and M.E. Lidstrom, *Physiological analysis of Methylobacterium extorquens AM1 grown in continuous and batch cultures.* Archives of Microbiology, 2006. **186**(2): p. 139-149.

[22]   Choi, Y.J., L. Morel, D. Bourque, A. Mullick, B. Massie and C. B. Míguez *Bestowing inducibility on the cloned methanol dehydrogenase promoter (PmxaF) of Methylobacterium extorquens by applying regulatory elements of Pseudomonas putida F1.* Applied and Environmental Microbiology, 2006. **72**(12): p. 7723-7729.

[23]   Ghosh, M., C. Anthony, K. Harlos, M. G. Goodwin and C. Blake, *The refined structure of the quinoprotein methanol dehydrogenase from Methylobacterium extorquens at 1.94 Å.* Structure, 1995. **3**(2): p. 177-187.

[24]   Williams, P.A., L. Coates, F. Mohammed, R. Gill, P. T. Erskine, A. Coker, S. P. Wood, C. Anthony and J. B. Cooper, *The atomic resolution structure of methanol dehydrogenase from Methylobacterium extorquens.* Acta Crystallographica Section D: Biological Crystallography, 2005. **61**(1): p. 75-79.

[25]   Afolabi, P.R., F. Mohammed, K. Amaratunga, O. Majekodunmi, S. L. Dales, R. Gill, D. Thompson, J. B. Cooper, S. P. Wood, P. M. Goodwin and C. Anthony, *Site-directed mutagenesis and X-ray crystallography of the PQQ-containing quinoprotein methanol dehydrogenase and its electron acceptor, cytochrome cL.* Biochemistry, 2001. **40**(33): p. 9799-9809.

[26]   Zheng, Y.J. and T.C. Bruice, *Conformation of coenzyme pyrroloquinoline quinone and role of Ca^{2+} in the catalytic mechanism of quinoprotein methanol dehydrogenase.* Proceedings of the National Academy of Sciences of the United States of America, 1997. **94**(22): p. 11881-11886.

[27]   Duine, J.A., *Quinoproteins: Enzymes containing the quinonoid cofactor pyrroloquinoline quinone, topaquinone or tryptophan-tryptophan quinone.* European Journal of Biochemistry, 1991. **200**(2): p. 271-284.

[28]   Oubrie, A., H.J. Rozeboom, and B.W. Dijkstra, *Active-site structure of the soluble quinoprotein glucose dehydrogenase complexed with methylhydrazine: A covalent cofactor-inhibitor complex.* Proceedings of the National Academy of Sciences of the United States of America, 1999. **96**(21): p. 11787-11791.

[29]   Itoh, S., H. Kawakami, and S. Fukuzumi, *Development of the active site model for calcium-containing quinoprotein alcohol dehydrogenases.* Journal of Molecular Catalysis - B Enzymatic, 2000. **8**(1-3): p. 85-94.

[30]   Itoh, S., H. Kawakami, and S. Fukuzumi, *Model studies on calcium-containing quinoprotein alcohol dehydrogenases. Catalytic role of Ca^{2+} for the oxidation of alcohols by coenzyme PQQ (4,5-dihydro-4,5-dioxo-1H-pyrrolo[2,3-f]quinoline-2,7,9-tricarboxylic acid).* Biochemistry, 1998. **37**(18): p. 6562-6571.

[31]   Goodwin, M.G. and C. Anthony, *Characterization of a novel methanol dehydrogenase containing a Ba^{2+} ion at the active site.* Biochemical Journal, 1996. **318**(2): p. 673-679.

[32]   Richardson, I.W. and C. Anthony, *Characterization of mutant forms of the quinoprotein methanol dehydrogenase lacking an essential calcium ion.* Biochemical Journal, 1992. **287**(3): p. 709-715.

[33]   Reddy, S.Y. and T.C. Bruice, *Mechanism of Glucose Oxidation by Quinoprotein Soluble Glucose Dehydrogenase: Insights from Molecular Dynamics Studies.* Journal of the American Chemical Society, 2004. **126**(8): p. 2431-2438.

[34]   Reddy, S.Y. and T.C. Bruice, *In silico studies of the mechanism of methanol oxidation by quinoprotein methanol dehydrogenase.* Journal of the American Chemical Society, 2003. **125**(27): p. 8141-8150.

[35]   Xia, Z.X., Y. N. He, W. W. Dai, S. A. White, G. D. Boyd and F. S. Mathews, *Detailed active site configuration of a new crystal form of methanol dehydrogenase from Methylophilus W3A1 at 1.9 Å resolution.* Biochemistry, 1999. **38**(4): p. 1214-1220.

[36]   Idupulapati, N.B. and D.S. Mainardi, *Quantum Chemical Modeling of Methanol Oxidation Mechanisms by Methanol Dehydrogenase Enzyme: Effect of Substitution of Calcium by Barium in the Active Site.* The Journal of Physical Chemistry A, 2010. **114**(4): p. 1887-1896.

[37]   Anthony, C. and P. Williams, *The structure and mechanism of methanol dehydrogenase.* Biochimica et Biophysica Acta - Proteins and Proteomics, 2003. **1647**(1-2): p. 18-23.

[38]   Leopoldini, M., N. Russo, and M. Toscano, *The Preferred Reaction Path for the Oxidation of Methanol by PQQ-Containing Methanol Dehydrogenase: Addition-- Elimination versus Hydride-Transfer Mechanism.* Chemistry – A European Journal, 2007. **13**(7): p. 2109-2117.

[39]   Zhang, X., S.Y. Reddy, and T.C. Bruice, *Mechanism of methanol oxidation by quinoprotein methanol dehydrogenase.* Proceedings of the National Academy of Sciences of the United States of America, 2007. **104**(3): p. 745-749.

[40]   Zheng, Y.J., Z. X. Xia, Z. W. Chen, F. S. Mathews and T. C. Bruice *Catalytic mechanism of quinoprotein methanol dehydrogenase: A theoretical and x-ray crystallographic investigation.* Proceedings of the National Academy of Sciences of the United States of America, 2001. **98**(2): p. 432-434.

[41]   Dewanti, A.R. and J.A. Duine, *Ca2+-assisted, direct hydride transfer, and rate- determining tautomerization of C5-reduced PQQ to PQQH2, in the oxidation of β-D-glucose by soluble, quinoprotein glucose dehydrogenase.* Biochemistry, 2000. **39**(31): p. 9384-9392.

[42]   Duine, J.A. and J. Frank Jr, *Studies on methanol dehydrogenase from Hyphomicrobium X. Isolation of an oxidized form of the enzyme.* Biochemical Journal, 1980. **187**(1): p. 213-219.

[43]   Williams, P., L. Coates, F. Mohammed, R. Gill, P. Erskine, D. Bourgeois, S. P. Wood, C. Anthony and J. B. Cooper, *The 1.6 Å X-ray structure of the unusual c- type cytochrome, cytochrome cL, from the methylotrophic bacterium*

Methylobacterium extorquens. Journal of Molecular Biology, 2006. **357**(1): p. 151-162.

[44]   Harris, T.K. and V.L. Davidson, *A new kinetic model for the steady-state reactions of the quinoprotein methanol dehydrogenase from Paracoccus denitrificans.* Biochemistry, 1993. **32**(16): p. 4362-4368.

[45]   Frank Jzn, J., M. Dijkstra, J. A. Duine and C. Balny, *Kinetic and spectral studies on the redox forms of methanol dehydrogenase from Hyphomicrobium X.* European Journal of Biochemistry, 1988. **174**(2): p. 331-338.

[46]   Leach, A.R., *Molecular Modelling 2nd ed.* Principles and Applications, 2001.

[47]   Horn, A.H.C., *Essentials of Computational Chemistry, Theories and Models By Christopher J. Cramer. Wiley: Chichester, England. 2002. 562 pp.* Journal of Chemical Information and Computer Sciences, 2003. **43**(5): p. 1720-1721.

[48]   Stanton, J.F., *A Chemist's Guide to Density Functional Theory By Wolfram Koch (German Chemical Society, Frankfurt am Main) and Max C. Holthausen (Humbolt University Berlin). Wiley-VCH: Weinheim. 2000.* Journal of the American Chemical Society, 2001. **123**(11): p. 2701-2701.

[49]   Bushmaker, A.W., V. V. Deshpande, S. Hsieh, M. W. Boekrath and S. B. Cronin, *Direct observation of born - Oppenheimer approximation breakdown in carbon nanotubes.* Nano Letters, 2009. **9**(2): p. 607-611.

[50]   W. Koch and M. C. Holthausen, *A Chemist's Guide to Density Functional Theory.* Second ed. 2001: Wiley-CVH.

[51]   W. J. Hehre , L. Radom, P. V. Schleyer and J. Pople, *Ab Initio Molecular Orbital Theory.* 1986, Newyork: John Wiley & Sons.

[52]   P. Hohenberg and W. Kohn, *Inhomogeneous electron gas.* Physical Review B, 1964. 136: p. 864-871.

[53]   J. P. Perdew, *Electronic Structure of Solids,* ed. Ziesche and H. Eschrig. 1991, Berlin: Akademie Verlag.

[54]   J. P.Perdew , J. A. Chevary, S. H. Vosko, K. A. Jackson, M. R. Pederson, D. J. Singh and C. Fiolhais, *Atoms, molecules, solids, and surfaces: applications of the generalized gradient approximation for exchange and correlation.* Physical Review B, 1992. 46: p. 6671-6687.

[55]   R. M. Dreialer and E. K. U. Gross, *Density Functional Theory: An Approach to Quantum Many Body Problem.* 1990, Berlin: Springer.

[56]   Y. Wang, *Accurate and simple analytic representation of the electron-gas correlation energy.* Physical Review B, 1992. 45: p. 13244-13249.

[57]   C. Lee, W. Yang, and R. Parr, *Accurate and simple analytic representation of the electron-gas correlation energy.* Physical Review B., 1998. 37: p. 786.

[58]   F. Jensen, *Introduction to Computational Chemistry.* 2002: Wiley&Sons.

[59]   Accelrys, *Materials Studio.* 2006.

[60]   Accelrys Inc., *DMOL³ User Guide* 2003: San Diego.

[61]   E. lewars, *Introduction to the Theory and Applications of Molecular and Quantum Mechanics.* 2003, Norwell: Kluwer Academic Publications.

[62]   C. J. Cramer, *Essentials of Computational Chemistry : Theories and Models.* 2004, West Sussex: John Wiley & Sons.

[63]   J. B. Foresman and A. Frisch, *Exploring Chemistry with Electronic Structure Methods.* Vol. 2. 1996, Pittsburgh, PA: Gaussian,Inc.

[64]   M.E Grillo, J. W. Andzelm, N. Govind, G. Fitzgerald and K. B. Stark, *Computational Material Science with Materials Studio: Applications in Catalysis.* Lecture Notes in Physics, 2004. 642: p. 202-227.

[65]   N. Govind, M. Petersen, G. Fitzgerald, D. King-Smith and J. Andzelm, *A generalized synchronous transit method for transition state location.* Computational Material Science, 2003. **28**(2): p. 250-258.

[66]   Cerný, V., *A thermodynamical approach to the travelling salesman problem: an efficient simulation algorithm.* J. Optim. Theor. Appl., 1985. 45: p. 41-51.

[67]   Kirkpatrick, S., C.D. Gelatt, and M.P. Vecchi, *Optimization by Simulated Annealing.* Science, 1983. **220**(4598): p. 671-680.

[68]   Mohanty, S.R., P.L.E. Bodelier, and R. Conrad, *Effect of temperature on composition of themethanotrophic community in rice field and forest soil.* FEMS Microbiol Ecol, 2007. **62**: p. 24-31.

[69]   Leach, A.R., *Molecular Modelling Principles and Applications.* 1999, Harlow: Pearson Education Limited.

[70]   *Material Studio Software Package.* 2008, Accelrys Inc.: San Diego, CA.

[71]   Yang, J., Y. Ren, A. M. Tian and H. Sun, *COMPASS Force Field for 14 Inorganic Molecules, He, Ne, Ar, Kr, Xe, H₂, O₂, N₂, NO, CO, CO₂, NO₂, CS₂,*

and SO₂, in Liquid Phases. Journal of Physical Chemistry B, 2000. **104**(20): p. 4951-4957.

[72]   Pérez-Aparicio, R., F. Alvarez, A. Arbe, L. Willner, D. Richter, P. Falus and J. Colmenero, *Chain dynamics of unentangled poly(ethylene-alt-propylene) melts by means of neutron scattering and fully atomistic molecular dynamics simulations.* Macromolecules, 2011. **44**(8): p. 3129-3139.

[73]   Steinmetz, H.L., *Using The Method Of Steepest Descent.* Industrial and Engineering Chemistry, 1966. **58**(1): p. 33-39.

[74]   Li, K.P., D.L. Duewer, and R.S. Juvet Jr, *Kinetics of chromatographic processes with application of the steepest descent approximation method.* Analytical Chemistry, 1974. **46**(9): p. 1209-1214.

[75]   Kästner, J., J. M. Carr, T. W. Keal, W. Thiel, A. Wander and P. Sherwood, *DL-FIND: An open-source geometry optimizer for atomistic simulations*.* Journal of Physical Chemistry A, 2009. **113**(43): p. 11856-11865.

[76]   D. Marx and J. Hutter, *Ab initio molecular dynamics: Theory and Implementation.* Modern Methods and Algorithms of Quantum Chemistry, 2000. 1: p. 301-449.

[77]   A.R. Leach, *Molecular Modeling: principles and applications.* 2nd ed. 2001, London: Prentice Hall.

[78]   Patel, R.N., C.T. Hou, and A. Felix, *Microbial oxidation of methane and methanol: Isolation of methane-utilizing bacteria and characterization of a facultative methane-utilizing isolate.* Journal of Bacteriology, 1978. **136**(1): p. 352-358.

[79]   Anthony, C. and L.J. Zatman, *The microbial oxidation of methanol. 2. The methanol-oxidizing enzyme of Pseudomonas sp. M 27.* Biochemical Journal, 1964. **92**(3): p. 614-621.

[80]   Berman, H., K. Henrick, H. Nakamura and J. L. Markley, *The worldwide Protein Data Bank (wwPDB): Ensuring a single, uniform archive of PDB data.* Nucleic Acids Research, 2007. **35**(1): p. D301-D303.

[81]   Fleys, M., R.W. Thompson, and J.C. MacDonald, *Comparison of the behavior of water in silicalite and dealuminated zeolite y at different temperatures by molecular dynamic simulations.* Journal of Physical Chemistry B, 2004. **108**(32): p. 12197-12203.

[82]   Anthony, C., *The quinoprotein dehydrogenases for methanol and glucose.* Archives of Biochemistry and Biophysics, 2004. **428**(1): p. 2-9.

[83]   Suye, S.I., Y. Nakamura, S. Inuta, T. Ikeda and M. Senda *Mediated amperometric determination of ammonia with a methanol dehydrogenase from Pseudomonas sp. AM-1 immobilized carbon paste electrode.* Biosensors and Bioelectronics, 1996. **11**(5): p. 529-534.

[84]   Inada, Y. and H. Orita, *Efficiency of numerical basis sets for predicting the binding energies of hydrogen bonded complexes: Evidence of small basis set superposition error compared to Gaussian basis sets.* Journal of Computational Chemistry, 2008. **29**(2): p. 225-232.